1958 JAN. 17.

EK

PERIODICA POLYTECHNICA

ELECTRICAL ENGINEERING — ELEKTROTECHNIK

VOL. 1 * NO. 3 * 1957

POLYTECHNICAL UNIVERSITY
TECHNISCHE UNIVERSITÄT
BUDAPEST

PERIODICA POLYTECHNICA

Contributions to international technical sciences published by the Polytechnical University, Budapest (Hungary)	Originalbeiträge zur internationalen technischen Wissenschaft, veröffentlicht von der Technischen Universität, Budapest (Ungarn)

PERIODICA POLYTECHNICA

includes the following series	enthält folgende Serien
Engineering	*Maschinen- und Bauwesen*
Electrical Engineering including Applied Physics	*Elektrotechnik und angewandte Physik*
Chemical Engineering	*Chemisches Ingenieurwesen*
The issues of each series appear at quarterly intervals	Einzelnummern der genannten Serien erscheinen vierteljährlich

CHAIRMAN OF THE EDITORIAL BOARD — HAUPTSCHRIFTLEITER

Z. CSŰRÖS

EDITORIAL BOARD — SCHRIFTLEITUNG

O. BENEDIKT, S. BORBÉLY, L. GILLEMOT, P. GOMBÁS, L. HELLER, K. P. KOVÁCS, J. PROSZT, G. SCHAY, I. VÖRÖS

EXECUTIVE EDITOR — SCHRIFTLEITER

J. KLÁR

The rate of subscription to a series is $ 4,00 a year. For subscription or exchange copies please write to	*Jahresabonnement pro Serie: $ 4,00. Bestellungen und Anträge für Tauschverbindungen sind zu richten an:*

PERIODICA POLYTECHNICA

BUDAPEST 62, POSTAFIÓK 440

TRANSIENTE VORGÄNGE IN DOPPELKÄFIGMOTOREN
I. TEIL

I. Rácz
Lehrstuhl für Betriebslehre elektrischer Maschinen der Technischen Universität, Budapest

(Eingegangen am 10. April 1957)

1. Einleitung

Die Hochleistungs-Drehstrom-Asynchronmotoren mit Kurzschlußläufer werden zwecks Verbesserung der Anlaufeigenschaften mit Spezialläufer erzeugt. Von diesen werden hier die Maschinen mit Doppelkäfigläufer behandelt, jedoch sind einige Ergebnisse auch für den Tiefnutläufer gültig. In der Praxis ist vor allem die Kenntnis folgender transienter Vorgänge wichtig.

a) Beim Anlassen eines Motors aus dem Stillstand, die Höhe des Einschaltstromstoßes und des Momentenstoßes. Die Wichtigkeit dieser Frage steigt fortwährend, da das Anlassen mit Zuschaltung auf volle Spannung immer häufiger angewendet wird. Die auftretenden elektromagnetischen transienten Vorgänge spielen sich binnen einer bis zwei Perioden ab, weshalb bei den Untersuchungen einfachheitshalber angenommen wird, daß der Motor eine Weile im Ruhezustand bleibt. Mit der späteren Periode des Anlassens, wo die Beschleunigung des Motors transiente Erscheinungen von geringerer Bedeutung hervorruft, werden wir uns nicht befassen.

b) Die beim Kurzschluß oder Umschaltung des mit Betriebsdrehzahl laufenden Motors auftretenden Strom- und Momentenstöße. Die Umschaltungen erfolgen z. B. am Ende des Anlaßvorganges (Anlassen mit Stern-Dreieck-Umschalter, Transformator, Drosselspule) oder beim Umschalten des Motors im Betrieb auf eine andere Stromquelle (z. B. automatische Umschaltung in den Hilfsbetrieben von Kraftwerken). Auch hier wird angenommen, daß während der elektromagnetischen transienten Vorgänge die Drehzahl des Motors noch konstant bleibt. Mit dieser Voraussetzung können die Umschaltungen mit Hilfe des Superpositionsprinzips auf den Fall der Spannungsanlegung an einen laufenden Motor zurückgeführt werden.

Bei den Berechnungen werden die Eisensättigung, der Skineffekt, die Eisenverluste und die Oberharmonischen am Umfang vernachlässigt. Die Ständerspannung U_s des Motors wird als symmetrische Dreiphasenspannung (mitlaufende) mit konstantem Wert angenommen. Ändert sich die Klemmenspannung infolge des an den Netzelementen vor dem Motor (z. B. Kabel, Transformator usw.) auftretenden Spannungsabfalles, wird die Spannung vor diesen Elementen als die Klemmenspannung des Motors betrachtet, wobei die resultierende Netzimpedanz in jene der Motorständerwicklung einbezogen wird. Es wird angenommen, daß der Motor bezüglich Aufbaues der drei Phasen vollkommen symmetrisch, ferner, im Falle eines Motors in Sternschaltung kein Nulleiter vorhanden ist, und somit keine Ströme des Nullsystems auftreten können.

2. Berechnungsmethode

Die elektrischen bzw. magnetischen Größen der drei Phasen werden zu einem einzigen Vektor zusammengefaßt, z. B. der aus den drei Ständerströmen (i_{sa}, i_{sb}, i_{sc}) gebildete Vektor, der Vektor der Ständerströme $\bar{i}_s$ (s. Abb. 1):

$$\bar{i}_s = \frac{2}{3}\left(i_{sa} + \bar{a} i_{sb} + \bar{a}^2 i_{sc}\right),$$

wo $\bar{a} = e^{j\frac{2\pi}{3}}$. Die Projektionen auf die Phasenachsen a, b, c des Vektors $\bar{i}_s$ ergeben die Momentanwerte der Phasenströme. Ähnliche Vektoren werden aus den Spannungen, Flussen, Läuferströmen usw. gebildet. Den Voraussetzungen gemäß können keine Ströme des Nullsystems auftreten und somit sind diese Vektoren vollkommen für die elektrischen und magnetischen Daten der drei Phasen

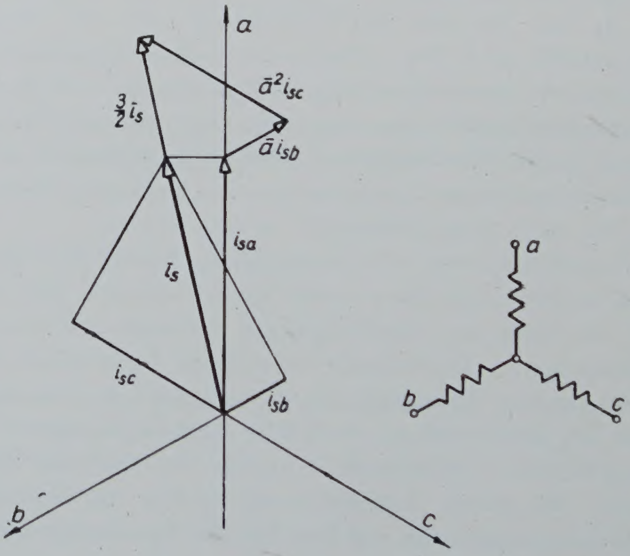

Abb. 1

bei jedwedem zeitlichen Verlauf kennzeichnend. In Abb. 1 deckt sich die Realachsrichtung des Koordinatensystems mit der Richtung der Phasenachse *a* des Ständers, es kann aber auch rotierendes Koordinatensystem angewendet werden.

Mit diesen Vektoren können für die drei Phasen dieselben Spannungs- oder Stromgleichungen aufgeschrieben werden, wie sie für eine Phase der Maschine auf die Momentanwerte bezogen aufzuschreiben sind. Somit kann die übliche Einphasen-Ersatzschaltung angewendet werden, wobei die Läufergrößen auf die Windungs- und Phasenzahlen des Ständers umgerechnet werden (Abb. 2). Zur Untersuchung des stationären Betriebes wird diese Schaltung im allgemeinen der Abb. 3 entsprechend umgeformt, wobei die hier vorkommenden Reaktanzen und Wirkwiderstände mittels folgender Gleichungen aus Abb. 2 berechnet werden können:

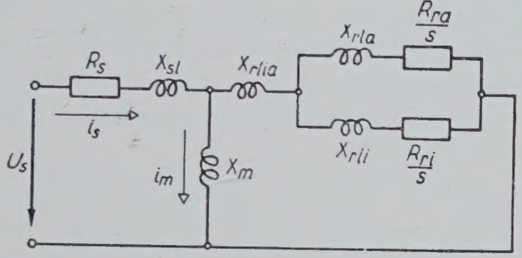

Abb. 2

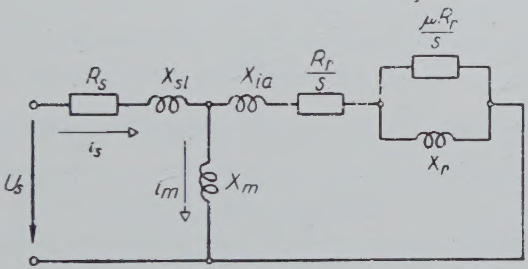

Abb. 3

$$\mu = \frac{R_{ra}}{R_{ri}}, \qquad R_r = \frac{R_{ra} R_{ri}}{R_{ra} + R_{ri}},$$

$$X_{ia} = X_{rlia} + \frac{X_{rla} \quad X_{rli}}{X_{rla} + X_{rli}}, \qquad X_r = \frac{X_{rla} + \mu^2 X_{rli}}{(1+\mu)^2} - \frac{X_{rla} \quad X_{rli}}{X_{rlia} + X_{rli}}$$

Im überwiegenden Teil der praktisch vorkommenden Fälle kann X_{rla} vernachlässigt werden, d. h. $X_{rla} \approx 0$, und somit werden obige Gleichungen noch einfacher:

$$X_{ia} = X_{rlia} \; ; \; X_r = \frac{\mu^2}{(1+\mu)^2} X_{rli} \; .$$

Die Umformung ist für jede Frequenz richtig, so daß Abb. 3 auch zur Untersuchung der transienten Erscheinungen als Grundlage dienen kann. In der vorliegenden Abhandlung wird stets auf Abb. 3 Bezug genommen, doch wird selbstverständlich in Betracht gezogen, daß es sich um keine stationären Erscheinungen handelt. Deswegen wird anstatt der Reaktanzen $X = \omega_1 L$ mit den Induktivitäten L gearbeitet und bei den Wirkwiderständen der Läuferkreise entfällt der Teiler s. Das Rotieren der Maschine ist bei der Aufschreibung der Spannungsgleichungen in Betracht zu ziehen.

In der Studie wird die LAPLACEsche Transformation (Operatorenrechnung) der Definitionsformel

$$L\{f(t)\} = p \int_0^\infty e^{-pt} f(t)\, dt$$

entsprechend angewendet. Einfachheitshalber werden die Zeitfunktion und die Operatorenform (LAPLACE-Transformierte) mit demselben Buchstaben bezeichnet. Eine der Induktivität L entsprechende operatorische Impendanz ist pL, die vielmehr in der Form $\frac{p}{\omega_1}\omega_1 L = \varrho X$ angewendet wird, wo

$$\varrho = \frac{p}{\omega_1} \; . \tag{1}$$

Die in der Studie vorkommenden Operatorenformen stellen die gebrochenen rationalen Funktionen von ϱ bzw. p dar:

$$f(\varrho) = \frac{P(\varrho)}{Q(\varrho)} \; . \tag{2a}$$

Hieraus erhalten wir die Zeitfunktion mit dem Entwicklungssatz:

$$f(t) = \frac{P(0)}{Q(0)} + \sum_{k=1}^{n} \frac{P(\varrho_k)}{\varrho_k \left(\frac{dQ}{d\varrho}\right)_{\varrho=\varrho_k}} e^{\varrho_k \omega_1 t} \; , \tag{2}$$

wo ϱ_k die Wurzeln der Gleichung n-ten Grades $Q(\varrho) = 0$ sind ($k = 1, 2 \ldots n$). Diese Form des Entwicklungssatzes ist nur in dem Falle gültig, wenn keine mehrfache Wurzeln vorhanden sind und auch $\varrho = 0$ keine Wurzel ist. Im vorliegenden Falle werden diese Bedingungen erfüllt.

Die einzelnen Ergebnisse werden auch an Zahlenbeispielen veranschaulicht. Sämtliche Zahlenbeispiele beziehen sich auf denselben Motor: 10poliger Drehstrommotor in Sternschaltung mit folgenden Nennwerten:

Leistung (an der Welle gemessen)	$P_N = 660$ kW ;
Spannung	$U_N = 3$ kV ;
Strom	$I_N = 160$ A ;
Leistungsfaktor	$\cos \varphi_N = 0{,}85$;
Wirkungsgrad	$\eta_N = 93{,}5$ % ;
Scheinleistung	$S_N = \sqrt{3}\, U_N I_N = 831$ kVA ;
Nennimpedanz	$Z_N = U_N/(\sqrt{3}\, I_N) = U_N^2/S_N = 10{,}82$ Ohm ;
Nennschlupf	$s_N = 1{,}75$ %.

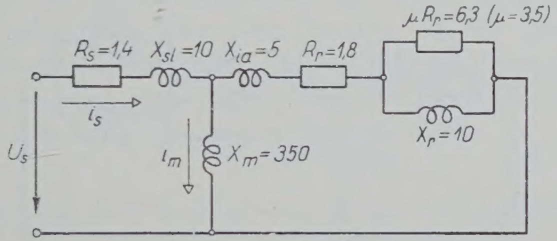

Abb. 4

Die Reaktanzen und Widerstände des Motors sind in Abb. 4 dargestellt. Die eingeschriebenen Zahlen bedeuten den Prozentwert der Nennimpedanz. Die Berechnungen werden in Relativeinheiten durchgeführt.

Die Grundeinheit des Momentes ist der aus der Nennscheinleistung mit der Synchronwinkelgeschwindigkeit berechnete Wert:

$$M_{Gr} = \frac{S_N}{\omega_1} .$$

Das Nennmoment beträgt

$$M_N = \frac{P_N}{(1 - s_N)\,\omega_1} .$$

Wenn also die in Grundeinheiten bestimmten Momentenwerte in Nennmomente umgerechnet werden sollen, ist mit dem Korrektionsfaktor

$$\frac{M_{Gr}}{M_N} = \frac{S_N}{P_N}(1 - s_N) = \frac{1 - s_N}{\eta_N \cos \varphi_N} = 1{,}24$$

zu multiplizieren.

3. Einschaltung des stillstehenden Motors

Das Ersatzschaltbild des Motors im Stillstand ist in Abb. 5 dargestellt. An Stelle der Induktivitäten wurden die operatorischen Impedanzen ϱX angeführt. An den Ständer wird im Moment $t = 0$ eine symmetrische Dreiphasenspannung gelegt, deren Vektor

$$\overline{u}_s = U_s e^{j\omega_1 t} , \tag{3}$$

und Laplace-Transformierte (Operatorenform)

$$\overline{u}_s = U_s \frac{p}{p - j\omega_1} = U_s \frac{\varrho}{\varrho - j} \tag{4}$$

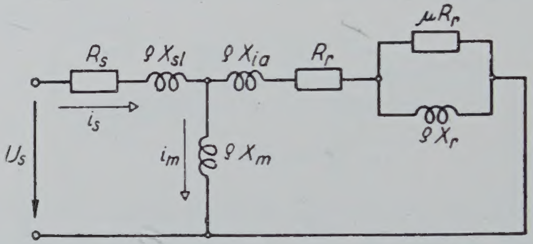

Abb. 5

ist.

Die Operatorenform der Vektoren der Ständerströme erhält man durch Division der Operatorenform $\overline{u}_s$ mit der auf die Ständerklemmen bezüglichen resultierenden operatorischen Impedanz $Z(\varrho)$. Die Impedanz $Z(\varrho)$ kann aus Abb. 5 berechnet werden:

$$Z(\varrho) = R_s + \varrho X_{sl} + \frac{\varrho X_m \left[R_r + \varrho X_{ia} + \dfrac{\mu R_r \varrho X_r}{\mu R_r + \varrho X_r} \right]}{\varrho X_m + R_r + \varrho X_{ia} + \dfrac{\mu R_r \varrho X_r}{\mu R_r + \varrho X_r}} = \frac{N(\varrho)}{S(\varrho)} . \tag{5}$$

Demnach ergibt sich der Vektor der Ständerströme durch Vereinfachung zu:

$$\overline{i}_s = \frac{\overline{u}_s}{Z(\varrho)} = U_s \frac{\varrho}{\varrho - j} \frac{S(\varrho)}{N(\varrho)} , \tag{6}$$

wo

$N(\varrho) = a_3 \varrho^3 + a_2 \varrho^2 + a_1 \varrho + a_0$;

$S(\varrho) = b_2 \varrho^2 + b_1 \varrho + b_0$;

$$
\begin{aligned}
a_3 &= X_r\,(X_{sl}\,X_m + X_{ia}\,X_m + X_{sl}X_{ia}) \;; \\
a_2 &= \mu\,R_r^2\,(X_{sl} + X_m) + R_s\,\mu\,R_r\,(X_m + X_{ia} + X_r) + R_s\,R_r\,X_r \;; \\
a_1 &= R_s\,(X_m + X_{ia})\,X_r + R_r\,X_r\,(X_{sl} + X_m) + \mu\,R_r\,[X_m\,(X_{sl} + X_{ia} + X_r) + \\
&\quad + X_{sl}\,(X_{ia} + X_r)] \,; \\
a_0 &= R_s\,\mu\,R_r^2 \;; \\
b_2 &= X_r\,(X_m + X_{ia}) \;; \qquad\qquad (6a) \\
b_1 &= \mu\,R_r\,(X_m + X_{ia} + X_r) + R_r\,X_r \;; \\
b_0 &= \mu\,R_r^2 \,.
\end{aligned}
$$

Den Ständerstrom in der Funktion der Zeit erhalten wir aus Gleichung (6) durch Anwendung des Entwicklungssatzes (2). Dieser wird aus vier Gliedern bestehen, deren jedes einer Wurzel des Nenners von (6) entspricht. Die dem Faktor $\varrho - j$ beigeordnete Wurzel ist : $\varrho_4 = j$, und die Wurzeln der Gleichung $N(\varrho) = 0$ sind ϱ_1, ϱ_2, ϱ_3, wobei letztere negative Realzahlen darstellen. Somit erhalten wir mit dem Entwicklungssatz folgende Form :

$$
\overline{i}_s(t) = \overline{A}_4\; e^{j\omega_1 t} + \overline{A}_1\; e^{\varrho_1\omega_1 t} + \overline{A}_2\; e^{\varrho_2\omega_1 t} + \overline{A}_3\; e^{\varrho_3\omega_1 t} \,, \qquad (7)
$$

wo

$$
\overline{A}_4 = U_s \frac{S(j)}{N(j)} \qquad (7a)
$$

und

$$
\overline{A}_k = U_s \frac{1}{\varrho_k - j} \frac{S(\varrho_k)}{N'(\varrho_k)} \;, \quad k = 1, 2, 3. \qquad (7b)
$$

Das erste Glied ist der stationäre Strom, d. h. der dem Punkt $s = 1$ im gewöhnlichen Stromvektordiagramm zugeordnete Kurzschlußstrom $\overline{I}_K$, $\overline{A}_4 = \overline{I}_K$.

Die folgenden drei Komponenten sind transiente Gleichströme, die exponential abklingen. Nachdem

$$
e^{\varrho_k \omega_1 t} = e^{-\frac{t}{1/\varrho_k \omega_1}} = e^{-\frac{t}{T_k}} \,,
$$

wird sich die Zeitkonstante der transienten Komponenten zu

$$
T_k = -\frac{1}{\varrho_k\,\omega_1} \qquad (8)
$$

ergeben.

A) *Zeitkonstanten*

Die Werte ϱ_k sind die Wurzeln der Gleichung dritten Grades $N(\varrho) = 0$. Anstatt der langwierigen Lösung der Gleichung können bei den in der Praxis vorkommenden Größenordnungen einfache Annäherungsformeln angewendet werden. Dies wird dadurch ermöglicht, daß die Größenordnungen der drei Wurzeln voneinander wesentlich abweichen. So kann die Wurzel von kleinstem Absolutwert der Gleichung $N(\varrho) = a_3\varrho^3 + a_2\varrho^2 + a_1\varrho + a_0 = 0$ mit der Annäherung bestimmt werden, daß die Glieder mit ϱ^3 und ϱ^2 vernachlässigt werden. Demnach erhalten wir

$$\varrho_1 \approx -\frac{a_0}{a_1}$$

und somit ergibt sich

$$T_1 = -\frac{1}{\omega_1 \varrho_1} \approx \frac{a_1}{a_0}\,\frac{1}{\omega_1}\,.$$

Unter Berücksichtigung der Gleichungen (6a) erhalten wir

$$T_1 \approx \left[\frac{X_{sl} + X_m}{R_s} + \frac{X_m + X_{ia} + X_r}{R_r} + \frac{X_r}{\mu R_r}\right]\frac{1}{\omega_1}\,. \tag{9}$$

Nachdem neben X_m die übrigen Reaktanzen vernachlässigt werden können, kann T_1 auch mittels folgender Formel berechnet werden:

$$T_1 \approx \frac{X_m}{\omega_1}\left[\frac{1}{R_s} + \frac{1}{R_r}\right] = \frac{X_m}{\omega_1}\left[\frac{1}{R_s} + \frac{1}{R_{ri}} + \frac{1}{R_{ra}}\right]. \tag{10}$$

Mit den Angaben unseres Zahlenbeispiels erhalten wir:

$$T_1 \approx \frac{350}{314}\left[\frac{1}{1{,}4} + \frac{1}{1{,}8}\right] = \frac{444}{314} = 1{,}414\ \text{s}.$$

Aus der Gleichung dritten Grades ergibt sich auf Grund der genauen Wurzel $T_1 = -\frac{452{,}2}{314} = 1{,}44\ s$.

Das Abklingen des dieser Wurzel zugeordneten freien Stromes $\overline{A}_1\, e^{\varrho\,\omega\cdot t}$ ist das langsamste. Für die Zeitkonstante T_1 kann auf Grund der Beziehung (10), aus Abb. 2 oder Abb. 3 ausgehend, eine Ersatzschaltung aufgezeichnet werden, die an der Stelle der Ständerklemmen kurzgeschlossen ist (da es sich um freie Ströme handelt) und in der die Streureaktanzen vernachlässigt sind (Abb. 6).

Das Verhältnis der mit derselben Zeitkonstante abklingenden Läuferströme zu den Ständerströmen ist ebenfalls der Ersatzschaltung entsprechend. Diese freien Ströme fließen im Ständer und in den beiden Käfigen in einer Richtung bei welcher ihre Erregungen sich addieren, so daß sie in erster Reihe den Hauptfluß erregen. Die Zeitkonstante T_1 ist daher eigentlich die Zeitkonstante der Änderung des Hauptflusses. Nachdem sogar der Hauptfluß von der Nenngröße durch einen verhältnismäßig kleinen Strom aufrechterhalten werden kann und im Stillstand die stationäre Komponente des Hauptflusses kleiner als der Nennfluß ist, sind die mit der Zeitkonstante T_1 behafteten freien Ströme im Vergleich zu den Kurzschlußströmen sehr klein. Aus diesem Grunde können sie sogar aus einem Oszillogramm nicht ausgewertet werden. Trotzdem sind sie von sehr großer Bedeutung mit Rücksicht auf die Entfaltung des Hauptflusses und des Momentes der Maschine. Mit den Angaben unseres Zahlenbeispiels wird der stationäre Kurzschlußstrom $\overline{I}_K = \overline{A}_1 = (2{,}01—j4{,}78)\ I_N$, wobei die mit Zeitkonstante T_1 behaftete Komponente des Einschaltständerstromes vom Anfangswert $\overline{A}_1 = j\ 0{,}09\ I_N$ ausgeht.

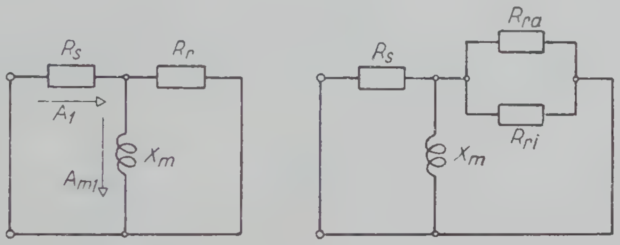

a) b)

Abb. 6

Die schneller abklingenden freien Komponenten erzeugen hauptsächlich nur Streuflusse, weshalb bei der Bestimmung von ϱ_2 und ϱ_3 in der Ersatzschaltung der Magnetisierungszweig vernachlässigt werden kann ($X_m \to \infty$). Bei der annähernden Berechnung der Wurzel von größtem Absolutwert ϱ_3 kann in $N(\varrho)$ der Ausdruck $a_1\varrho + a_0$ vernachlässigt werden; somit wird

$$\varrho_3 \approx -\frac{a_2}{a_3}$$

bzw. mit Vernachlässigung des Magnetisierungszweiges:

$$\varrho_3 \approx -\lim_{X_m \to \infty} \frac{a_2}{a_3} = -\left[\frac{R_s + R_r}{X_{sl} + X_{ia}} + \frac{R_r}{\dfrac{X_r\,(X_{sl} + X_{ia})}{X_r + X_{sl} + X_{ia}}}\right] \tag{11}$$

und

$$T_3 = -\frac{1}{\varrho_3\,\omega_1}\,. \tag{11}$$

Ähnlicherweise kann ϱ_2 und T_2 berechnet werden :

$$\varrho_2 = -\frac{1}{T_2\,\omega_1}$$

und

$$T_2 = -\frac{1}{\varrho_2\,\omega_1} \approx \lim_{x_m \to \infty} \frac{a_2}{a_1}\,\frac{1}{\omega_1} = \left[\frac{X_r}{\mu R_r} + \frac{X_{sl} + X_{ia} + X_r}{R_s + R_r}\right]\frac{1}{\omega_1}\,. \tag{12}$$

Zur Beurteilung der Güte der Annäherungen wurden in Tab. I die Werte der Zeitkonstanten der drei Gleichstromkomponenten zusammengestellt, die einerseits mit den Näherungsformeln (10), (11) und (12), andererseits durch Lösung der Gleichung dritten Grades von $N(\varrho) = 0$ (6a) bestimmt wurden.

Tabelle 1

	T_1, s	T_2, s	T_3, s
Näherungswerte	1,414	0,0300	0,00252
Genaue Werte	1,440	0,0272	0,00276

Wie ersichtlich, sind die Näherungsformeln für die Praxis vollkommen entsprechend. In der Wirklichkeit sind auch die »genauen« Wurzeln nicht ganz genau, da beispielsweise die Auswirkung der Sättigung größere Fehler verursachen kann. Weiterhin kann festgestellt werden, daß die Gleichstromkomponente mit der Zeitkonstante T_3 von keiner praktischen Bedeutung ist, da ihre Zeitkonstante etwa 1/7 Periode ausmacht und somit zur Zeit des größten Einschaltstromstoßes sozusagen vollkommen verschwindet.

B) Einschaltströme

Die Einschaltströme können mit Operatorenrechnung bei Anwendung der Formeln (7) berechnet werden. Jedoch können gute Näherungswerte mittels folgenden Verfahrens einfacher erhalten werden.

Die stationäre Komponente von $\overline{A}_4\,e^{j\omega t}$ ist uns aus der Untersuchung des stationären Betriebes bekannt, das ist der Kurzschlußstrom :

$$\overline{A}_4 = \overline{I}_K = \frac{U_s}{\overline{Z}_K}\,, \tag{13}$$

wo $\bar{Z}_K$ die resultierende Impedanz aus Abb. 3 für den Fall $s = 1$, d. h. die Kurzschlußimpedanz des Motors bedeutet.

Der Anfangswert $\bar{A}_1$ der Gleichstromkomponente $A_1\, e^{\varrho_1 \omega_1 t}$ kann aus Formel (7b) durch Substitution von $\varrho_k = \varrho_1$ berechnet werden. Mit den bei den vorkommenden Ordnungsgrößen zugelassenen Annäherungen erhalten wir die folgende Formel:

$$\bar{A}_1 \approx j \frac{U_s}{X_m + X_{sl}} \cdot \frac{R_r^2}{(R_r + R_s)^2} \tag{14}$$

Zur Bestimmung der Gleichstromkomponenten mit Anfangswerten $\bar{A}_2$ und A_3 kann die Tatsache ausgenutzt werden, daß der Motor vor der Einschaltung stromlos war und infolge der Induktivitäten die Größe des Ständerstromes im Zeitpunkt $t = 0$ noch Null bleibt. Deswegen wird auf Grund der Formeln (7):

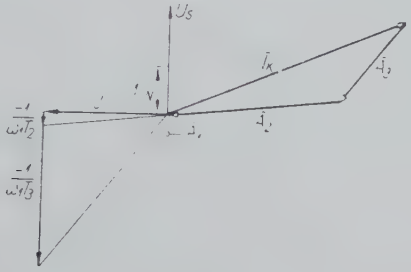

Abb. 7

$$0 = I_K + \bar{A}_1 + \bar{A}_2 + A_3 .$$

Außerdem ist auch die Richtung von $\bar{A}_2$ und A_3 bekannt. Auf der rechten Seite der Formel (7b) ist nämlich nur der Faktor $\frac{1}{\varrho_k - j}$ ein komplexer Wert, die übrigen stellen Realwerte dar. Nachdem

$$\frac{1}{\varrho_k - j} = \frac{\varrho_k + j}{\varrho_k^2 + 1} = \frac{-\frac{1}{\omega_1 T_k} + j}{\varrho_k^2 + 1} ,$$

kann die Konstruktion laut Abb. 7 zur Bestimmung von A_2 und $\bar{A}_3$ angewendet werden. Zuerst werden die mit Formel (13) bzw. (14) berechneten Vektoren $\bar{I}_K$ und $\bar{A}_1$ der Abbildung entsprechend ausgemessen. Danach werden aus dem Endpunkt von j die mit Formel (11) bzw. (12) berechneten Werte $-\frac{1}{\omega_1 T_2}$ und

$-\frac{1}{\omega_1 T_3}$ ausgemessen und mit den erhaltenen Richtungen Parallelen aus dem Anfangspunkt von $\overline{A}_1$ bzw. Endpunkt von $\overline{I}_K$ gezogen. Auf diese Weise werden die Vektoren $\overline{A}_2$ und $\overline{A}_3$ ausgeschnitten.

Mit den Angaben des Zahlenbeispieles ergibt sich:

$$\overline{I}_K = (2{,}01 - j\,4{,}78)\,I_N\,,\ \overline{A}_1 = j\,0{,}09\,I_N\,,\ \frac{1}{\omega_1 T_2} = 0{,}106$$

und $\frac{1}{\omega_1 T_3} = 1{,}263$. Nach Durchführung der Konstruktion erhalten wir die Werte von $\overline{A}_2$ und $\overline{A}_3$: $\overline{A}_2 = (-0{,}36 + j\,3{,}38)\ I_N$ und $\overline{A}_3 = (-1{,}65 + j\,1{,}31)\ I_N$. Bei genauer Anwendung des Entwicklungssatzes ergibt sich: $\overline{A}_2 = (-0{,}38 + j\,3{,}28)\ I_N$ und $\overline{A}_3 = (-1{,}63 + j\,1{,}41)\ I_N$.

Für den Wert der Komponente $\overline{A}_2$ kann eine gute Näherungsformel erhalten werden, indem der Näherungswert (12) von ϱ_2 in die Formel (7b) substituiert und der Magnetisierungszweig ($X_m \to \infty$) vernachlässigt wird. Somit ergibt sich:

$$\overline{A}_2 \approx \frac{1}{\varrho_2 - j}\ \frac{\overline{U}_s}{X_{sl} + X_{ia} + X_r} \times$$
$$\times \frac{1}{1 + \left[\dfrac{X_r}{X_{sl} + X_{ia} + X_r}\ \dfrac{R_s + R_r}{\mu R_r}\right]^2 \left[1 + 2\,\dfrac{\mu R_r}{R_s + R_r}\right]}\,. \tag{15}$$

Hier kann im ersten Faktor neben $-j$ auch ϱ_2 vernachlässigt werden.

Mit den Angaben des Zahlenbeispiels erhalten wir auf diese Weise den Wert $\overline{A}_2 = j\,3.32\ I_N$ [der genaue Wert ergibt sich zu $(-0.38 + j\,3{,}28)\ I_N$].

Der zeitliche Verlauf des Vektors i_s der Einschaltständerströme kann auf Grund der Formeln (7) berechnet oder konstruiert werden. In Abb. 8 ist die Kurve $i_s\,(t)$ für zwei Perioden aufgezeichnet. Die Ziffern in der Abbildung bedeuten die Zahl der vom Augenblick der Einschaltung verstrichenen Achtelperioden. Aus der Abbildung ist ersichtlich, daß der Vektor i_s sich rasch dem vom Kurzschlußstrom $\overline{I}_K$ beschriebenen Kreis (gestrichelte Linie) nähert. Der Ständerstrom ist nach einer nicht vollen Halbperiode am höchsten. Der Zeitpunkt des Maximums kann zu $t_m = \frac{\pi/2 + \varphi_K}{\omega_1}$ geschätzt werden.

Mit den Angaben des Zahlenbeispiels ergibt sich $\varphi_K = 67{,}2° = 1{,}17$ Radiane, d. h. $t_m = \frac{1{,}57 + 1{,}17}{314} = 0{,}00872\ s$. Zu diesem Zeitpunkt werden die Größen der einzelnen Stromkomponenten die folgenden sein :

$$\overline{I}_K e^{j\omega_1 t_m} = j I_K = j\,5{,}19\ ;$$

$$\overline{A}_1 e^{-\frac{t_m}{T_1}} = j\,0{,}09 \cdot 0{,}994 = j\,0{,}09\ ;$$

$$\overline{A}_2 e^{-\frac{t_m}{T_2}} = (-0{,}38 + j\,3{,}28)\,0{,}728 = -0{,}28 + j\,2{,}38\ ;$$

$$\overline{A}_3 e^{-\frac{t_m}{T_3}} = (-1{,}63 + j\,1{,}41)\,0{,}0426 = -0{,}07 + j\,0{,}06\,.$$

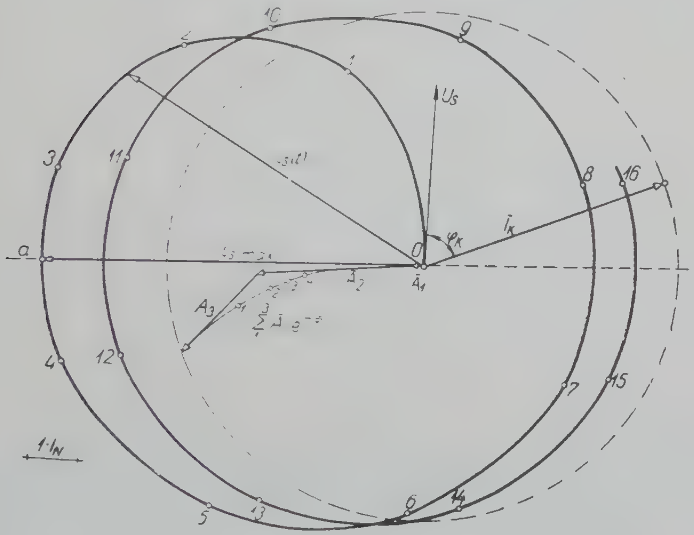

Abb. 8

Der Ständerstrom ergibt sich im Zeitpunkt t_m als die Summe der obigen Komponenten zu :

$$\overline{i}_{s\,\max} = (-0{,}35 + j\,7{,}72)\,I_N\,.$$

Der Absolutwert des Vektors beträgt 7,73 I_N, hier ist er mit dem Scheitelwert von I_N zu nehmen. Nachdem der stationäre Kurzschlußstrom 5,19 I_N beträgt, ist der Scheitelfaktor des Stromstoßes 7,73/5,19 = 1,49. Aus dem Wert der Gleichstromkomponenten ist ersichtlich, daß praktisch nur die Komponente mit der Zeitkonstante T_2 zum Kurzschlußstrom hinzukommt.

Der größte Stromstoß kann auf folgende Weise berechnet werden :

$$i_{s\,\max} = I_K + A_2\, e^{-\frac{\pi/2 + \varphi_K}{\omega_1 T_2}}\,. \tag{16}$$

Falls wir keine genauere Berechnung machen wollen, kann der Wert des Scheitelfaktors mit 1,5 angenommen werden oder bei kleineren Motoren mit 1,4. Bei den kleineren Motoren sind nämlich die Wirkwiderstände verhältnismäßig höher, weshalb auch das Abklingen schneller ist.

Die Phasenströme erhalten wir durch Projizierung auf die Phasenachsen aus Vektor i_s. Dementsprechend tritt der obige Höchststrom tatsächlich nur in dem Falle in einer Phase auf, wenn der Vektor i_s im Zeitpunkt t_m mit einer der Phasenachsen zusammenfällt. Dies hängt von der Lage der Spannung U_s im Zeitpunkt der Einschaltung ab, was mit der Verdrehung der ganzen Abbildung 8 in Verbindung steht. Anstatt dessen ist es viel bequemer, die Phasenachsen zu verdrehen. In Abb. 8 ist die Phasenachse a mit gestrichelter Linie so aufgezeichnet worden, daß der Höchststrom in Phase a auftrete. Diese Lage entsteht, wenn im Zeitpunkt des Einschaltens die Spannung U_s eben den Nullwert überschreitet. Der zeitliche Verlauf des Phasenstromes i_{sa} ist in Abb. 9 dargestellt. Der resultierende Gleichstrom ist in der Abbildung mit gestrichelter Linie angegeben.

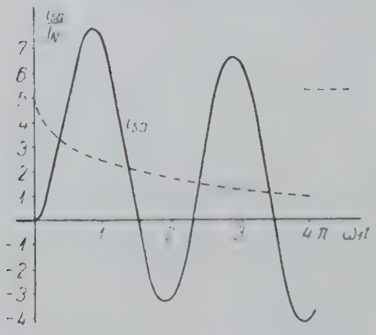

Abb. 9

C) *Einschalt-Momentenstoß*

Das gewöhnliche Anlaßmoment (Kurzschlußmoment) des stillstehenden Motors wird von den im Ständer und Läufer fließenden Strömen erzeugt. Infolge den nach der Einschaltung auftretenden Gleichströmen erscheinen auch transiente Momentenkomponente. Zur Berechnung des Momentes kann die auch für den transienten Zustand gültige Formel

$$M = \overline{\psi}_m \times \overline{i}_s = \mathrm{Im}\,[\widehat{\psi}_m\, \overline{i}_s] \tag{17}$$

gebraucht werden. Diese Beziehung ist in Relativeinheiten gültig. Der Hauptfluß ψ_m kann aus dem Magnetisierungsstrom berechnet werden:

$$\psi_m = L_m\, i_m\,.$$

Somit wird das Moment

$$M = L_m \bar{i}_m \times \bar{i}_s = L_m \operatorname{Im} [\hat{i}_m \bar{i}_s] \, . \tag{18}$$

Bei der Einschaltung enthält der Strom i_m auch Gleichstromkomponenten mit derselben Zeitkonstante wie der Ständerstrom.

Wie bei der Formel (7) gezeigt wurde, ist

$$\bar{i}_s = \bar{I}_K e^{j\omega_1 t} + \bar{A}_1 e^{-\frac{t}{T_1}} + \bar{A}_2 e^{-\frac{t}{T_2}} + \bar{A}_3 e^{-\frac{t}{T_3}} \tag{7'}$$

Der Magnetisierungsstrom kann in ähnlicher Form aufgeschrieben werden:

$$\bar{i}_m = \bar{I}_{mK} e^{j\omega_1 t} + \bar{A}_{m1} e^{-\frac{t}{T_1}} + \bar{A}_{m2} e^{-\frac{t}{T_2}} + \bar{A}_{m3} e^{-\frac{t}{T_3}} \, . \tag{19}$$

Die einzelnen Komponenten des Momentes werden durch das Vektorprodukt der einzelnen Glieder von (7') und (19) gegeben. Von den vielen Komponenten sind nur zwei in Betracht zu ziehen, da die Zeitkonstanten T_2 und T_3 so klein sind, daß diese Komponenten bis zum Zeitpunkt der Entwicklung des Momentenscheitels praktisch abklingen. Wie im Abschnitt *B)* gezeigt wurde, ist in der Formel des Ständerstromes auch $\bar{A}_1$ sehr gering, so daß die Annäherungen

$$\left.\begin{aligned} \bar{i}_s &\approx \bar{I}_K e^{j\omega_1 t} \\ \text{und} \qquad & \\ \bar{i}_m &\approx \bar{I}_{mK} e^{j\omega_1 t} + \bar{A}_{m1} e^{-\frac{t}{T_1}} \end{aligned}\right\} \tag{20}$$

benutzt werden können. Das Vektorprodukt der beiden $e^{j\omega_1 t}$ enthaltenden Glieder gibt das stationäre Anlaßmoment M_K, wogegen das Vektorprodukt aus dem Ständerstrom und der Gleichstromkomponente des Magnetisierungsstromes ein pulsierendes Moment (M_p) darstellt. Es wir daher

$$M = M_K + M_p \, , \tag{21}$$

wo

$$M_p = L_m \left(\bar{A}_{m1} e^{-\frac{t}{T_1}} \right) \times \left(\bar{I}_K e^{j\omega_1 t} \right) = L_m \operatorname{Im} \left\{ \hat{A}_{m1} e^{-\frac{t}{T_1}} \bar{I}_K e^{j\omega_1 t} \right\} \, . \tag{22}$$

$\bar{I}_K$ kann zweckmäßigerweise in der Form $I_K e^{-j\varphi_K}$ aufgeschrieben werden. Bei der Bestimmung von $\bar{A}_{m1}$ kann aus der Komponente $\bar{A}_1$ des Ständerstromes ausgegangen werden, die mittels Formel (14) berechnet werden kann. Auf Grund der Abb. 6a ist

$$\bar{A}_{m1} : \bar{A}_1 \approx (R_s + R_r) : R_r \, ,$$

woraus mit Berücksichtigung der Formel (14):

$$\bar{A}_{m1} \approx \bar{A}_1 \frac{R_s + R_r}{R_r} \approx j \frac{U_s}{X_{sl} + X_m} \frac{R_r}{R_r + R_s} \, . \tag{23}$$

Das pulsierende Moment wird daher auf Grund der Gleichung (22):

$$M_p \approx L_m \operatorname{Im} \left\{ -j \frac{U_s}{X_{sl} + X_m} \frac{R_r}{R_r + R_s} e^{-\frac{t}{T_1}} I_k \, e^{-j\varphi_K} \, e^{j\omega_1 t} \right\},$$

also

$$\begin{aligned} M_p &\approx -\frac{U_s I_K}{\omega_1} \frac{X_m}{X_{sl} + X_m} \frac{R_r}{R_r + R_s} e^{-\frac{t}{T_1}} \cos(\omega_1 t - \varphi_K) = \\ &= -M_{p\,\max} e^{-\frac{t}{T_1}} \cos(\omega_1 t - \varphi_K) \, , \end{aligned} \tag{24}$$

wo die Anfangsamplitude des pulsierenden Momentes:

$$M_{p\,\max} \approx \frac{U_s I_K}{\omega_1} \frac{X_m}{X_{sl} + X_m} \frac{R_r}{R_r + R_s} \, . \tag{25}$$

Die Amplitude des pulsierenden Momentes vermindert sich kaum in einigen ersten Perioden, da die Zeitkonstante T_1 eine Größenordnung von 50 bis 100 Perioden aufweist. Aus diesem Grunde kann der Höchstwert des Momentes

$$M_{\max} \approx M_K + M_{p\,\max} \tag{26}$$

erreichen. Bei der obigen Berechnung wurde vorausgesetzt, daß die Einschaltung der drei Phasen am Ständer des Motors völlig gleichzeitig erfolgt. Bei den Schaltern kann jedoch zwischen den Einschaltungen der einzelnen Phasen eine Abweichung von sogar $^1/_4$ Periode vorkommen. Wenn beispielsweise zuerst die Kontakte der Phasen *b* und *c* schließen, dann entwickelt sich im Motor in der resultierenden Richtung der Spulen *b* und *c* ein Hauptfluß, dessen mit der Zeitkonstante T_1 behaftete Komponente bei ungünstiger Einschaltphasenlage einen der Komponente $\bar{A}_{m1}$ entsprechenden Wert ereichen kann. Wenn nun Phase *a* um eine Viertelperiode später eingeschaltet wird, entwickelt sich auch in der Achsrichtung der Phasenspule *a* eine mit der Zeitkonstante T_1 behaftete Hauptfluß-Komponente gleicher Größe, so daß als Endergebnis ein $\sqrt{2}$ facher Wert auftreten kann. Infolgedessen kann bei ungünstigen Phasenlagen im Falle nicht gleichzeitiger

Einschaltung die Amplitude des pulsierenden Momentes den Wert $\sqrt{2}\, M_{p\max}$ erreichen und der Höchstwert des Momentes

$$M_{\max} \approx M_K + \sqrt{2}\, M_{p\,\max} \tag{27}$$

betragen.

Mit den Angaben des Zahlenbeispiels ergibt sich :

$$M_K = \mathrm{Re}\left[\hat{U}_s \bar{I}_K\right] - I_K^2 R_s = 2{,}01 - 5{,}19^2 \cdot 0{,}014 = 1{,}63\,;$$

$$M_{p\,\max} = \frac{1 \cdot 5{,}19}{1}\, \frac{3{,}5}{3{,}6}\, \frac{0{,}018}{0{,}018 + 0{,}014} = 2{,}83\,\cdot$$

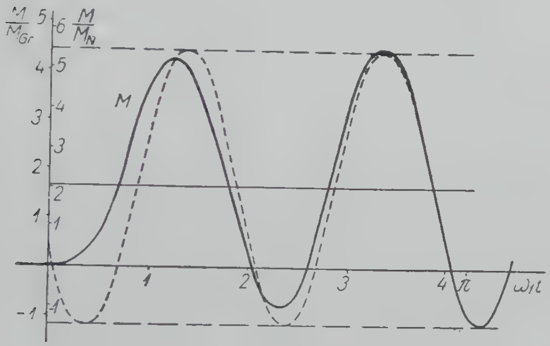

Abb. 10

Der Höchstwert des Momentes kann daher im Falle gleichzeitiger Einschaltung $1{,}63 + 2{,}83 = 4{,}46$ bzw. bei nicht gleichzeitiger Einschaltung im ungünstigen Falle $1{,}63 + \sqrt{2} \cdot 2{,}83 = 5{,}63$ betragen. Diese Zahlen beziehen sich auf das aus der Nennscheinleistung mit der Synchronwinkelgeschwindigkeit berechnete Grundmoment. Auf das Nennmoment M_N bezogen, das aus der Nennleistung an der Welle berechnet wird, ergeben sich 1,24fache Werte, so daß der höchstmögliche Wert des Momentes $1{,}24 \cdot 5{,}63\, M_N = 7\, M_N$ ausmachen kann.

In Abb. 10 ist der zeitliche Verlauf des Momentes bei gleichzeitiger Einschaltung dargestellt. Für den Fall des Zahlenbeispiels ergibt sich :

$$M = 1{,}63 + 2{,}83\; e^{-\frac{t}{T_1}} \cos\left(\omega_1 t - 67{,}2^0\right) \cdot$$

In den ersten ein bis zwei Perioden weicht das Moment von dieser Beziehung ab, weil zu dieser Zeit die Komponenten mit der Zeitkonstante T_2 und T_3 noch nicht abgeklungen sind. Diese wirken jedoch auf das Momentenmaximum nicht, sie vermindern das Moment nur in der ersten Periode. Das Moment soll nämlich im Zeitpunkt $t = 0$ von Null ausgehen, an dieser Stelle ist sogar auch der erste und zweite Differentialquotient nach der Zeit ebenfalls Null. In Abb. 10 sind bei der mit starker Linie gezogenen Momentenkurve sämtliche Komponenten berücksichtigt, während die Kurve mit gestrichelter Linie der obigen Näherungsformel entspricht.

Der obige hohe Wert des Momentenmaximums wird durch die Sättigung nicht in bedeutendem Masse vermindert, da der Wert von $\overline{A}_{m1} L_m$ 55% des Nennflusses und die Komponente mit der Kreisfrequenz ω_1 des Hauptflusses 50% beträgt ; die beiden ergeben auch summiert keine große Sättigung. Die Sättigung wirkt auf die Zeitkonstante in stärkerem Masse, jedoch ist die Zeitkonstante $T_1 = 1{,}4\ s$ nur insofern von Bedeutung, daß sie viel größer als die Periodenzeit ist. In der Praxis beschleunigt sich der Motor nach der Einschaltung, so daß die Zeitkonstante sich stark vermindern wird.

Zusammenfassung

Der erste Teil der Abhandlung befasst sich mit den elektromagnetischen transienten Erscheinungen des Doppelkäfigmotors im Ruhezustand. Es werden einfache Annäherungsformeln für die Einschaltströme, deren Zeitkonstanten, sowie für den Wert der Einschalt-Momentenstösse gegeben. Zur Veranschaulichung der Grössenordnungen dient ein Zahlenbeispiel. Die transienten Erscheinungen der mit Betriebsdrehzahl laufenden Maschine werden im zweiten Teil erörtert.

I. RÁCZ, Budapest, XI. Budafoki út 4—6, Ungarn

EFFECT OF THE SPARK-GAP WORKING TIME UPON THE SHORT-CIRCUIT CURRENTS IN CIRCUITS CONTAINING SERIES CAPACITOR*

F. Csáki
Department for Special Electrical Machines, Polytechnic University, Budapest

(Received April 16, 1957)

In a previous article [1] we examined in detail the short-circuit currents of the system containing a series capacitor, and estimated the value of overvoltages arising on the series capacitor. It was stated that the series capacitor must be protected in almost every case. The question arises, how fast the protective device must work to comply with this requirement, that the short-circuit current should not be greater in the compensated system, than in the noncompensated one. The present article deals with this question.

The problem will be examined in detail only for the most simple case. Again a symmetrical, three-phase short-circuit arising at no-load will be supposed. First we neglect the resistance of the short-circuit loop.

Expression of the short-circuit current in this case is (see expressions (7), (8) and (22) of [1]):

$$\bar{I}(t) = \frac{U_m e^{j\left(\psi - \frac{\pi}{2}\right)}}{X_L(1-k)} e^{j\omega t} -$$

$$- \frac{U_m e^{j\left(\psi - \frac{\pi}{2}\right)}}{X_L(1-k)} \cdot \left(\frac{1+\sqrt{k}}{2} e^{j\sqrt{k}\omega t} + \frac{1-\sqrt{k}}{2} e^{-j\sqrt{k}\omega t} \right). \qquad (1)$$

This solution is valid for a stationary co-ordinate system. The steady-state component is a vector of constant length rotating with an angular speed ω, the two transient components are also vectors of constant lengths rotating with angular velocities $+\sqrt{k}\omega$ and $-\sqrt{k}\omega$ resp. The resultant of the three vectors can be more simply designed, if the solution is written in synchronously, with angular speed ω rotating co-ordinate system. Therefore let us multiply both sides of (1) by $e^{-j\omega t}$:

---

* The present paper, as well as the previous one, was realized at the Department for Theory of Operation of Electrical Machninery, Polytechnic University, Budapest.

$$\overline{I}(t)\, e^{-j\omega t} = \frac{U_m\, e^{j\left(\psi - \frac{\pi}{2}\right)}}{X_L\,(1-k)} -$$

$$- \frac{U_m\, e^{j\left(\psi - \frac{\pi}{2}\right)}}{X_L\,(1-k)} \cdot \left[\frac{1+\sqrt{k}}{2}\, e^{+j(\sqrt{k}-1)\,\omega t} + \frac{1-\sqrt{k}}{2}\, e^{-j(\sqrt{k}+1)\,\omega t}\right] \cdot \qquad (2)$$

In this case the steady-state component is a stationary vector, while the transient components rotate with different angular speeds. The absolute value of all of three vectors is constant.

For the degree of compensation the values of

$$k = 0{,}25\,;\quad 0{,}562\,;\quad 1{,}5625\,;\quad 2{,}25$$

are chosen, as in this case

$$\sqrt{k} = 0{,}5\,;\quad 0{,}75\,;\quad 1{,}25\,;\quad 1{,}5$$

is a rational fracture further simplifying the solution of the problem.

Realization of the design itself may be seen on Figs. 1 a, b, c, d. In all cases the steady-state component is the vector $\overrightarrow{QO}$. (To simplify the design, this vector $\overrightarrow{QO}$ was taken of unit length.) Circle K_1 is the diagram of the first, K_2 that of the second transient component, the curve G is the diagram of the resultant vector.

The vector traced from point O to an arbitrary point P of curve G gives the resultant of the two transient components, while the vector drawn from point Q to point P gives the resultant $\overline{I}(t)\ e^{-j\omega t}$ of the steady-state and transient components.

Curve G was calibrated according to ωt expressed in degrees. By aid of this it may be stated for instance, that we got a resultant twice as large as the steady-state component in the first and fourth case at $\omega t = 360^\circ$, in the second and third case at $\omega t = 720^\circ$.

Suppose furthermore, that at a certain instant the series capacitor is short-circuited in all the three phases *at the same time*. The resistance of the by-pass circuit is then taken as zero.

The Laplace-transforme of the new short-circuit current is in this case

$$\overline{I}(p) = U_m e^{j\psi} \frac{p}{p - j\omega}\ \frac{1}{pL} + \overline{I}_0 \frac{pL}{pL}\ . \qquad (3)$$

where $\overline{I}_0$ is the current flowing through inductivity L at the instant when the

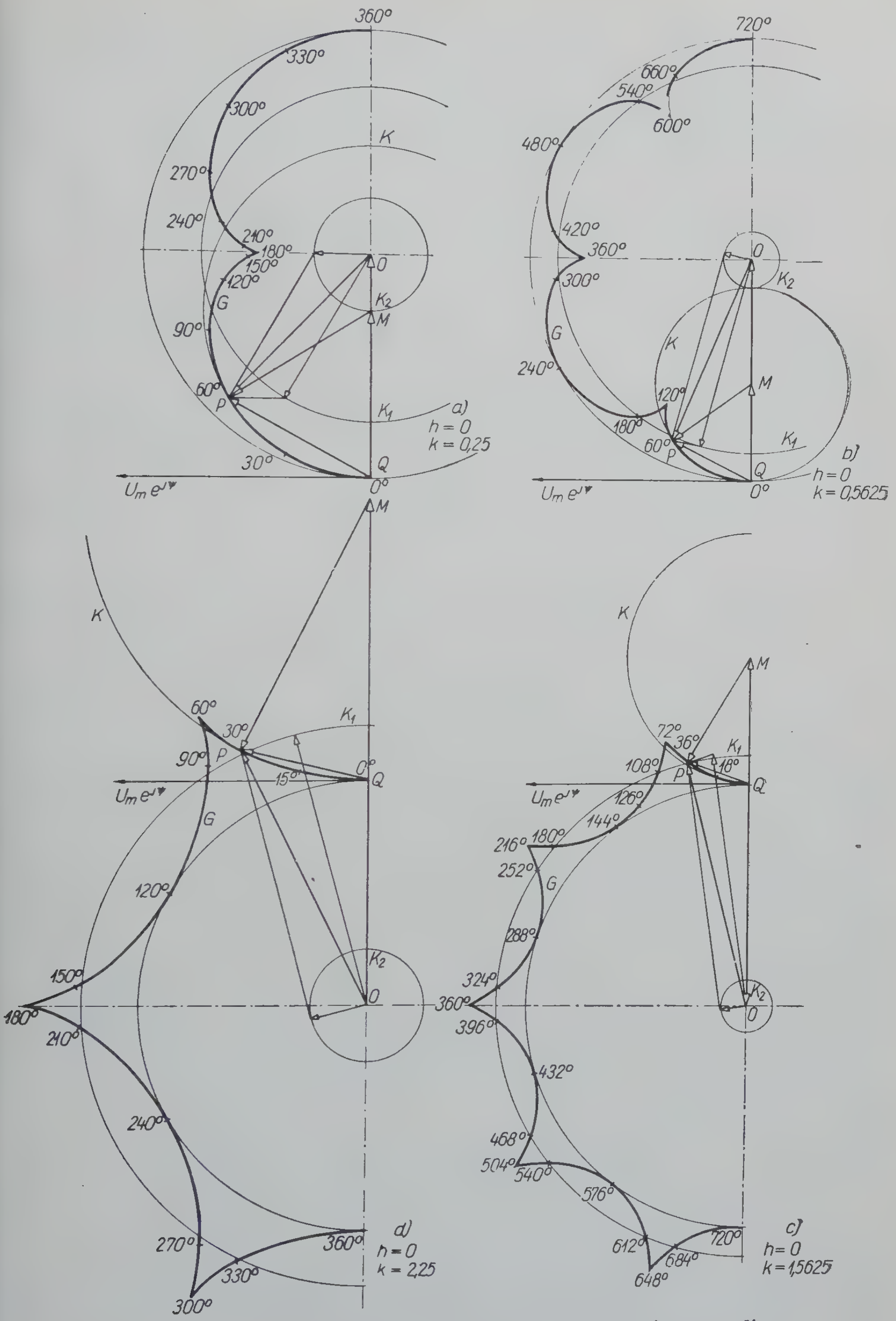

Fig. 1. Diagrams of short-circuit currents in synchronously rotating co-ordinate system. Resistance is neglected

series capacitor is by-passed. The current $\overline{I}_0$ is given by the vector $\overrightarrow{QP}$ of the previous design.

The time-function of the new short-circuit current is (with the aid of the generalized expansion theorem [2, 3]) :

$$\overline{I}(t) = \frac{U_m\, e^{j\left(\psi - \frac{\pi}{2}\right)}}{X_L}\, e^{j\omega t} - \left(\frac{U_m\, e^{j\left(\psi - \frac{\pi}{2}\right)}}{X_L} - \overline{I}_0 \right) \tag{4}$$

computing now the time t from the instant, when the series capacitor is bypassed.

The steady-state component is the same as it would be in a noncompensated system in the case of a short-circuit arising at no-load, but the transient component is different.

Let us again pass over on to the synchronously rotating co-ordinate system :

$$\overline{I}(t)\, e^{-j\omega t} = \frac{U_m\, e^{j\left(\psi - \frac{\pi}{2}\right)}}{X_L} - \left[\frac{U_m\, e^{j\left(\psi - \frac{\pi}{2}\right)}}{X_L} - \overline{I}_0 \right] e^{-j\omega t}\,. \tag{5}$$

The new steady-state component is shown by the stationary vector $\overrightarrow{QM}$ and the new transient component by vector $\overrightarrow{MP}$. Latter rotates with angular velocity $-\omega$.

Let us draw a circle from point M as a center with the absolute value of the steady-state component as a radius. As far as the final point of vector $\overrightarrow{MP}$ belonging to the transient component is within this circle K, the greatest peak-value of the short-circuit current will not be greater, than in the noncompensated case.

In point Q the circle K is exactly the circle of curvature of the curve G. Namely the velocity of the point moving on curve G equals the total velocity of the final point belonging to the two transient components. (Differentiating two times one after the other the expression (2), we get the velocity and the acceleration.) The velocity is :

$$\overline{v}(t) = -\frac{U_m\, e^{j\left(\psi - \frac{\pi}{2}\right)}}{X_L(1-k)} \left[\frac{1+\sqrt{k}}{2}\, j(\sqrt{k}-1)\,\omega\, e^{j(\sqrt{k}-1)\,\omega t} - \right.$$

$$\left. - \frac{1-\sqrt{k}}{2}\, j(\sqrt{k}+1)\,\omega\, e^{-j(\sqrt{k}+1)\,\omega t} \right]. \tag{6}$$

Accordingly, the acceleration is

$$\bar{a}(t) = -\frac{U_m e^{j\left(\psi-\frac{\pi}{2}\right)}}{X_L(1-k)}\left[-\frac{1+\sqrt{k}}{2}(\sqrt{k}-1)^2\omega^2 e^{j(\sqrt{k}-1)\omega t} - \right.$$

$$\left. -\frac{1-\sqrt{k}}{2}(\sqrt{k}+1)^2\omega^2 e^{-j(\sqrt{k}+1)\omega t}\right]. \qquad (7)$$

At the initial point of time:

$$\bar{v}(o) = \frac{U_m e^{j\left(\psi-\frac{\pi}{2}\right)}}{X_L} j\omega, \qquad (8)$$

and

$$\bar{a}(o) = \frac{U_m e^{j\left(\psi-\frac{\pi}{2}\right)}}{X_L}\omega^2. \qquad (9)$$

As $\bar{v}(o)$ is perpendicular to $\bar{a}(o)$, the radius of curvature is simply

$$r = \frac{v^2(o)}{a(o)} = \frac{U_m}{X_L}, \qquad (10)$$

where $v(o)$ and $a(o)$ are absolute values of $\bar{v}(o)$ and $\bar{a}(o)$. As the radius of curvature is unidirectional with the acceleration, the centre of curvature is just in point M.

Above it was shown that circle K is the circle of curvature of curve G. Circle K and curve G are near enough to each other in the initial section. If the by-pass of the capacitor takes place at the angle, or at the point of time belonging to this section, there will be no essential difference between the short-circuit currents of the compensated and noncompensated system. The values of the steady-state components are the same, these of the transient components are near to one another, only the initial angle formed by the vectors of the steady-state and transient component is different.

But an important deviation can be observed if the curve G already left the territory of circle K. So e. g. in case of $k = 0{,}562$ (Fig. 1b) if the by-pass of the capacitor takes place two cycles after the short-circuit, i. e. at $\omega t = 720°$, the transient component would be 3,5-times greater, than the steady-state component.

The transient component will be smaller, than the steady-state component, until curve G does not intersect circle K. It may be seen from Fig. 1, that greater security is served by taking the first peak-point of curve G, instead of the point of intersection. The time t, resp. the angle ωt of the by-pass belonging to the peak-point, can be easily computed. In the peak-point namely, the vector of the two transient components is of opposite direction, so the difference of angles made by the two vectors from the initial time is exactly 180° :

$$(\sqrt{k}-1)\,\omega\, t_0-[-(\sqrt{k}+1)\,\omega\, t_0]=2\sqrt{k}\,\omega\, t_0=\pi, \tag{11}$$

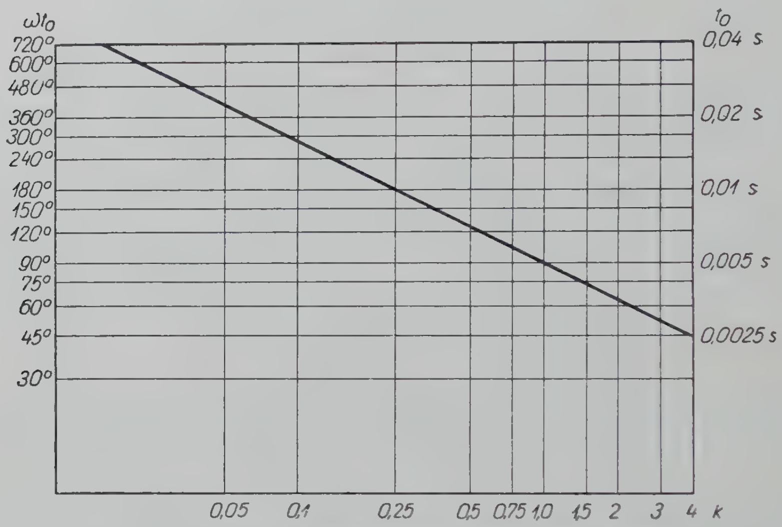

Fig. 2. Relation of the time-limit of the protective device and the degree of compensation

from which the time-limit of the protective device

$$t_0=\frac{\pi}{2\sqrt{k}\,\omega}, \tag{12}$$

or expressed in an angle

$$\omega\, t_0=\frac{\pi}{2\sqrt{k}}\ \text{radian}=\frac{180^\circ}{2\sqrt{k}}\,. \tag{13}$$

If the protective device works within this time-limit, the transient component of the short-circuit current will not be greater, than the steady-state component. The relation of the time-limit and the degree of compensation is shown on Fig. 2.

Until now resistance has been neglected. The question arises, whether consideration of the resistance does not alter the results obtained considerably.

To decide this, we drew up Figs. 3 a, b, c for case $h=0{,}2$; $0{,}4$; $0{,}6$ and $k=0{,}25$. The figures, similarly to Fig. 1. show the variation of the short-circuit current in a synchronously rotating co-ordinate system.

The diagram G of the resultant short-circuit current in the compensated system is given by the following expression :

$$\bar{I}(t) = \bar{I}_f \frac{1}{h + j(1-k)} - \bar{I}_f \frac{1}{h + j(1-k)} \cdot \frac{1}{2j\sqrt{k - \left(\frac{h}{2}\right)^2}} \times$$

$$\times \left\{ \left[-\frac{h}{2} + j\sqrt{k - \left(\frac{h}{2}\right)^2} + jk \right] e^{\left(-\frac{h}{2} - j\sqrt{k - \left(\frac{h}{2}\right)^2} - j\right)\omega t} - \right.$$

$$\left. - \left[-\frac{h}{2} - j\sqrt{k - \left(\frac{h}{2}\right)^2} + jk \right] e^{\left(-\frac{h}{2} - j\sqrt{k - \left(\frac{h}{2}\right)^1} - j\right)\omega t} \right\}, \tag{14}$$

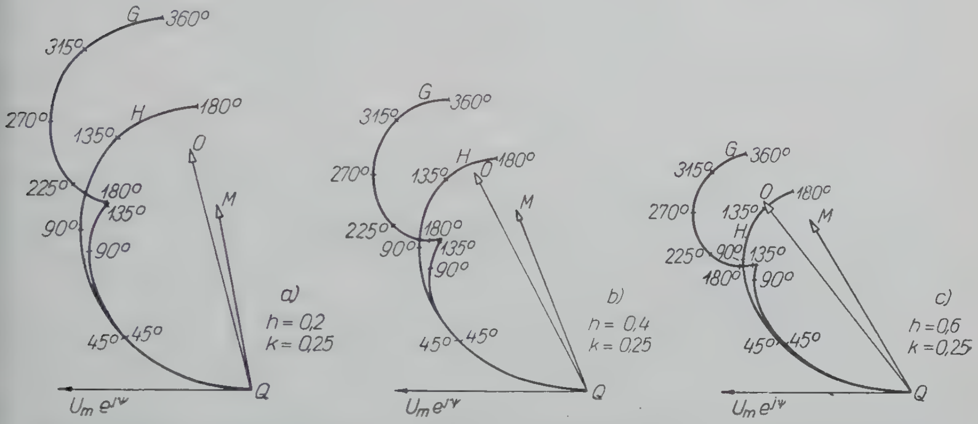

Fig. 3. Diagrams of short-circuit currents in synchronously rotating co-ordinate system. Resistance is taken in consideration

where

$$\bar{I}_f = \frac{U_m e^{j\psi}}{X_L}. \tag{15}$$

The diagram H of the short-circuit current in the noncompensated system is expressed as follows :

$$\bar{I}(t) = \bar{I}_f \frac{1}{h+j} - \bar{I}_f \frac{1}{h+j} e^{(-h-j)\omega t}. \tag{16}$$

Compared to the case of $h = 0$, the changes below may be observed : The vectors $\overrightarrow{QO}$ resp. $\overrightarrow{QM}$ of the steady-states short-circuit currents have not the same direction. The diagram G became deformed on account of damping. Furthermore, the circle K is substituted by a spiral H.

Nevertheless, it may be stated generally that in the initial point Q the circle of curvature of curves G and H are common.

The final point of the resultant current-vector of the noncompensated system moves with a velocity $\bar{v}(t)$ and with an acceleration $\bar{a}(t)$ along curve H. Differentiating twice one after the other the expression (16), we get

$$\bar{v}(t) = \bar{I}_f \frac{1}{h+j} (h+j)\, \omega\, e^{(-h-j)\,\omega t} \tag{17}$$

resp.

$$\bar{a}(t) = -\bar{I}_f \frac{1}{h+j} (h+j)^2 \omega^2 e^{(-h-j)\,\omega t} \; . \tag{18}$$

At the initial time

$$\bar{v}(o) = -\bar{I}_f\, \omega \tag{19}$$

and

$$\bar{a}(o) = -\bar{I}_f (h+j)\, \omega^2 \, . \tag{20}$$

Similarly, by differentiating expression (14) the velocity and acceleration of the final point of the vector moving on curve G can be computed for the initial time. Performing the computation we again obtain as a result, expressions (19) and (20) resp.

Consequently, the velocity, as well as the acceleration is of equal magnitude and direction in both cases. So curves G and H have a twofold contact with one another at the initial point of time. The velocity and so the tangent of curves G and H is unidirectional with vector $U_m e^{j\varphi}$. The result obtained may generally be put into words as follows : Connecting an alternating voltage to a series circuit R, L, C, with zero initial conditions, at the initial time the value of the short-circuit current, as well as its first and second differential quotient is of the same magnitude as in the case without capacitance ($C = \infty$). Therefore the initial sections of the current-curve of the compensated and noncompensated system are very near to one another.

Let us return to Figs. 3 a, b, c. With increasing resistances the curve H crosses the curve G always at smaller ωt values. So e. g. in case of $k = 0{,}25$, the point of intersection is at $\omega t = 230°$ if $h = 0$, and about at 175° if $h = 0{,}6$.

Consequently, with growing resistance the time-limit of the by-pass decreases. But as the time-limit of by-pass had been stated in case of $h = 0$ with a security (e. g. in case of $k = 0{,}25$ for 180°) the relations (12), (13) between the time-limit and the degree of compensation may be considered valid also for the cases $h \neq 0$. (Only at greater values of h must the time-limit be decreased.)

Up to now we examined the short-circuit current arising at no-load. How does the initial load current influence the results obtained? To decide this, we drew up Figs. 4a and 4b ($k = 0{,}25$, $h = 0{,}4$). In both cases the amplitude of the load current I_0 is — exaggerating — one fourth of the amplitude of the short-circuit current in the noncompensated system. In the first case the power factor is 1,0; in the second case 0,7. The diagram of the short-circuit current in the compensated system is G, in the noncompensated one H, resp. H_0. Curve H was drawn by taking in consideration the initial load current, curve H_0 refers to a short-circuit arising at no-load.

Already the tangent of curves G and H in point Q is not unidirectional. In the cases occuring in practice, at the initial section curve H runs farther in, than curve G, but the deviation is not important. If the by-pass of the series capacitor takes place quickly enough, the initial load will not cause a great difference between the short-circuit currents of the compensated and noncompensated systems.

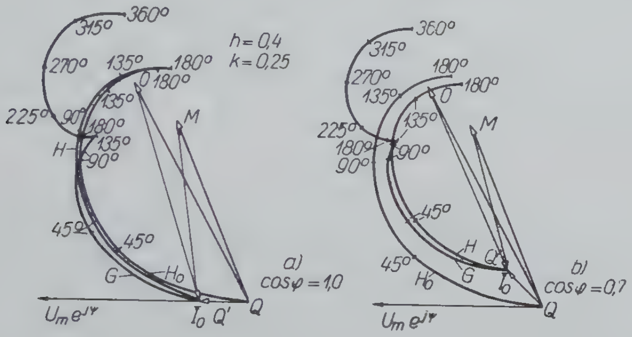

Fig. 4. **Influence of initial load current on the short-circuit currents**

Circumstances are even more favourable, when comparing curve G with curve H_0 (Fig. 4b). Curve G generally runs farther in, than curve H_0. The only exception is when the final point of the vector of the initial load current I_0 falls out of curve H_0 (Fig. 4a). But this only occurs at power factors very near to 1, which is an uncommon case in practice.

So it may be stated, that the time-limit of the by-pass is not considerably influenced, neither by the resistance of the short-circuit loop, nor by the initial load current, though strictly speaking the time-limit is not only a function of the degree of compensation, but also of these two factors.

Similarly to the reasoning in point 6 of [1], the results obtained may be generalized for the case of asymmetrical short-circuits too.

The gravest condition seems to be the obligation, that the series capacitor must be short-circuited in all phases at the same time. This cannot be realized by either of the protective devices known. But consideration of the different times of by-pass would complicate the calculations significantly.

Conclusion

In what has gone before we examined in detail, how fast the protective device of the series capacitor must work not to raise a greater short-circuit current in the compensated system, than in the noncompensated one. This question is important, not only from the point of view of short-circuit currents, but from that of the relay-protection. Neglecting the resistance of the short-circuit loop we stated a relation between the time-limit of by-pass and the degree of compensation (Fig. 2). The results obtained are not significantly influenced by consideration of the resistance and of the initial load current. For the time-limit of the by-pass we have got a relatively small value. While the spark-gap protection does not preceive the short-circuit current itself, but the overvoltage raising on the capacitor ; it is of high-speed operation, and so it may prevent the development of too great short-circuit currents, though it is not certain that the spark-gap will work in every case within the time-limit determined above.

References

1. Csáki, F. : Short-circuit Currents in Circuits Containing Series Capacitor. Periodica Polytechnica **1**, 155 (1957).
2. Wagner, K. W. : Operatorenrechnung und Laplacesche Transformation. Leipzig, 1950.
3. Kovács, K. P.—Rácz, I. : Transient Performance of Alternating-current Machines. Akadémiai Kiadó, Budapest, 1954.

Summary

Joining with a previous article, in this study it will be examined, how fast the protective device of the series capacitor must work to avoid a greater short-circuit current in the compensated system, than in the noncompensated one. A relation was found between the time-limit and the degree of compensation.

F. Csáki, Budapest XI. Budafoki út 4—6, Hungary

ABOUT THE STAR-LIKE FUSION REACTOR

K. Simonyi and M. Uzsoky
Institute for Theoretical Electricity, Polytechnic University, Budapest

(Received 20 April, 1957)

1. Energy balance

As is known from literature [1, 2, 3, 4], one of the most difficult problems in realizing thermonuclear reactors is that of confining the gas plasma of a temperature of about 10^8 °K, the only solution seems to be the generating of a sufficiently strong magnetic field, most conveniently by means of its own magnetic field of high intensity current flowing through the plasma, representing an electromagnetic wall. It cannot be envisaged to directly confine it into a vessel having any actual material wall; the idea has arisen to surround the central core of a several million degrees temperature by a very wide gas layer — similarly to the stars — to ensure heat isolation. The impossibility of this arrangement, because of the thermal conductivity of the plasma exceeding that of any metal, is pointed out in literature.

In the following we treat at least in principle quantitatively the dimensions for realising, a steady energy production in DT gas at constant pressure, confined in a spherical container having a wall of a high, but technically not impossible temperature; in other words we consider the behaviour of the isobar DT star.

This star has particular properties. As it is to be expected and subsequently verified, the phenomena of gravitation is of no importance, because of the small mass of the star. The Stefan-Boltzmann distribution law does not hold for the radiation, as it is a space radiation proportional to $\sqrt{T}$, as stated simultaneously in several places in literature [1, 3]. The radiation pressure term too, vanishes in the equilibrium equations. In contrast to the common stars, here we precisely know the composition of the star, and further the dependence of the fusion energy production upon density and temperature, is well known. Thus for the energy equilibrium an exact expression may be obtained.

We depart from the equation for this energy balance. The difference between the fusion power generated within a sphere of radius r and the radiated power is equal to the energy lost from the surface by conduction:

$$\int_0^r [p_f(T,\varrho) - p_r(T,\varrho)]\, 4\pi r^2\, dr = -4\pi r^2 \varkappa(T,r)\, \frac{dT}{dr} \qquad (1)$$

where p_f and p_r are the specific fusion and radiation powers, ϱ is the plasma-density; $\varkappa$ is the thermal conductivity.

For these quantities the functions are plotted as follows: The fusion energy production according to [1] is:

$$p_f = W_o N_D N_T (\sigma v_{DT})_{av}$$

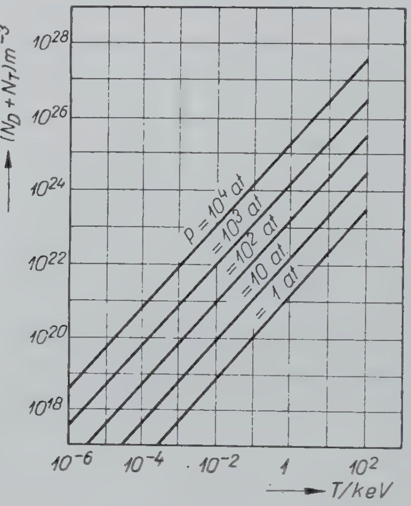

Fig. 1. Plasma-pressure dependence on temperature and density

where $W_0 = 0{,}2 \cdot 17$ MeV, is the fraction of energy released per reaction imparted to charged reaction products. Thus the energy of neutrons may be considered as lost in regards to heating effect. $(\sigma v_{DT})_{av}$ is the probability, that a particle will react and N_D and N_T are the densities of the deuterium and tritium nuclei, respectively. The value of $(\sigma v_{DT})_{av}$ can be obtained from the diagram.

According to [6] the thermonuclear power production may be expressed as:

$$p_f = a N^2 T^{-2/3} e^{-\beta T^{-1/3}}$$

A quantitative formula of this form is given by [5]

$$p_f = 1{,}88.10^{-24} (N_D + N_T)^2 T^{-2/3} e^{-3{,}9\, T^{-1/3}} \frac{W}{cm^3}$$

where differing from [5], T has to be substituted in keV. The formulas of [1] and [5] do not give the same results, the difference, however, does not essentially affect the result.

The radiation is the Bremsstrahlung of electrons. Its value obtained by [1] and [3] is identical, but in discrepancy with the numerical value given by [5] is

$$p_r = 0{,}54 \cdot 10^{-30} (N_D + N_T)^2 \, T^{1/2} \, \frac{W}{cm^3}$$

Here T has to be substituted in keV, and $N_D + N_T$ in cm^3.

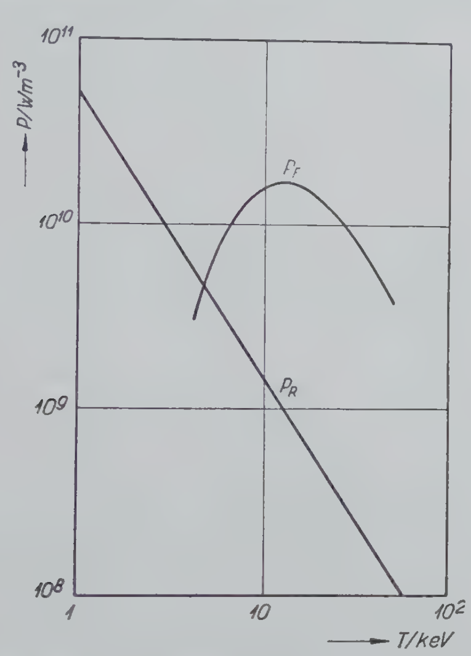

Fig. 2. Specific fusion and radiation energies at constant pressure $p = 1$ kat

Density and temperature are related through pressure. Considering that ions and electrons are involved equally in producing pressure, the equation for gas takes on the form:

$$p = (N_e + N_D + N_T) \frac{mc^2}{3} = (N_e + N_D + N_T) \, kT$$

If the pressure is measured in 1000 at (kat) and the temperature in keV, it becomes:

$$(N_D + N_T) = 3{,}06 \cdot 10^{23} \, p/T$$

Here the density is given in m^{-3}. This relationship is shown in Fig. 1.

The curve of the produced and that of the dissipated energy have both to be replotted against constant pressure instead of constant density. In the graph in Fig. 2 the curve plotted in [1] has been used. The radiation power is expressed by:

$$p_r(T,p) = 5 \cdot 10^{10} p^2 T^{-3/2} \qquad Wm^{-3}$$

This can also be seen in Fig. 2. At first the fact may seem surprising, that the radiated power decreases with increasing temperature; this only means the influence of the decrease in density to be dominant at constant pressure.

The thermal conduction coefficient may be evaluated in first approximation on basis of the equation for the kinetic gas theory:

$$\varkappa = \frac{k}{2} N_e \lambda v = \frac{k}{2} N_e \frac{v}{(N_D + N_T)\sigma}$$

where λ is the mean free path for electrons; v is the electron velocity; σ is the effective cross section for collision. The value of the latter is according to [1]:

$$\sigma = \frac{6 \cdot 10^{-19}}{W^2} cm^2$$

where W is the kinetic energy of electrons.

Thus for $\varkappa$ the following expression is obtained:

$$\varkappa = 1{,}68 \cdot 10^{13} T^{5/2} \frac{W}{m \cdot keV}$$

This relationship is shown by curve b, in Fig. 3. Here we have plotted the thermal conduction curve for the case of the effective collision cross section assumed to be constant, independently of the energy and to be just $r_0^2\pi$ where r_0 is the Bohr radius. It can be seen that at low temperatures the curve gives an extremely low conductivity.

For a as well as for b the conductivity is obtained as independent of density, and consequently of pressure: at low densities the small number of conducting electrons are compensated by a proportionally longer mean free path. According to the Spitzer—Härm theory [7] thermal conduction also depends even if in a smaller degree, on density.

We did not as yet consider the electric field due to the diffusion of electrons, which tends to decrease the diffusion and thus the thermal conductivity too. In general there is a flux of electric charges and also of current density. In the steady state the generated field just compensates for the excess diffusion of electrons, thus the current density becomes zero. For this case the thermal conduction expressed by SPITZER—HÄRM and calculated in units used by us, becomes:

$$\varkappa = \frac{6{,}43 \cdot 10^{13}}{\ln (qC^2)} T^{5/2} \frac{W}{m \cdot keV}$$

where

$$qC^2 = \frac{3}{\sqrt{\pi}} \frac{1}{e^3} \left(\frac{4 \pi \varepsilon_0}{2} \right)^3 \sqrt{\frac{1}{N_e}} T^{3/2} =$$

$$= 3{,}59 \cdot 10^{17} \frac{1}{\sqrt{N_e}} T^{3/2} = 6{,}51 \cdot 10^5 \sqrt{\frac{1}{p}} T^3$$

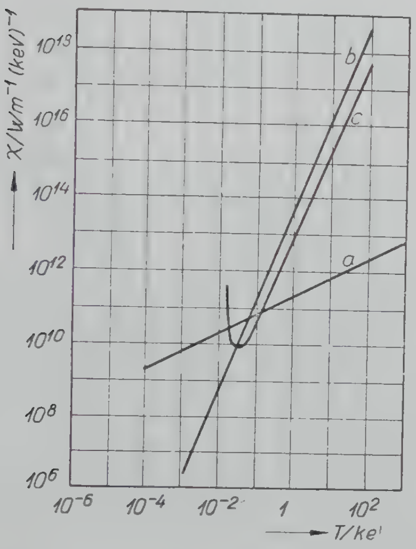

Fig. 3. The variation of thermal conductivity as a function of temperature

a) calculated according to the kinetic gas theory with the Bohr-radius as a radius for effective cross-section

b) calculated according to the kinetic gas theory, but with an effective cross-section, depending on the energy

c) calculated according to the Spitzer—Härm formula

where e is the electron charge; ε_0 is the dielectric constant in vacuum. For thermal conduction a relation almost similar to [7] is obtained, with the difference that by the expression $\ln (qC^2)$ density and pressure are also involved. The curve c, in Fig. 3 shows the value of $\varkappa$ evaluated for a pressure of $p = 1$ kat. As it can be seen the error is not too important, even if we calculate with the more simple curve b.

2. Transformation of the energy equation into an integral equation

Let us write our equation as follows :

$$\frac{1}{r^2}\int_0^r \{p_f\,[T(s),p] - p_r\,[T(s),p]\}\,s^2\,ds = \varkappa(T,p)\,\frac{dT}{dr}$$

By integrating both sides from 0 to r, that is from the corresponding temperature T_0 to temperature T.

$$\int_0^r \frac{1}{t^2}\int_0^t (p_f - p_r)\,s^2\,ds\,dt = -\int_{T_0}^{T} \varkappa\,\frac{dT}{dr}\,dr$$

The right hand side integrating by parts :

$$\left[-t^{-1}\int_0^t (p_f - p_r)\,s^2\,ds\right]_0^r + \int_0^r s\,(p_f - p_r)\,ds = \int_T^{T_0} \varkappa\,dT$$

Considering that

$$\lim_{t=0}\frac{1}{t}\int_0^t (p_f - p_r)\,s^2\,ds = 0$$

following integral equation is obtained :

$$\int_0^r s\left(1 - \frac{s}{r}\right)\left(p_f - p_r\right)ds = \int_T^{T_0} \varkappa\,dT$$

From this integral equation a simple law of similarity may be derived as a good approximation ; for approximation let us assume the value of $\varkappa$ to be independent of density.

Our equation may then be rewritten as follows :

$$\int_0^r sp\left(1 - \frac{sp}{rp}\right)\frac{(p_f - p_r)}{p^2}\,d(sp) = \int_T^{T_0} \varkappa\,dT$$

on the other hand

$$p_f(T,p) \equiv p^2 p_f^{*}(T)$$

$$p_r(T,p) \equiv p^2 p^{*}(T)$$

thus introducing the new variable $z = pr$

$$\int_0^z s\left(1 - \frac{s}{z}\right)\left[p_f^{*}(T) - p_r^{*}(T)\right]ds = \int_T^{T_0} \varkappa\,dT \qquad (2)$$

Consequently the relations depend only on the product pr and not separately on p and r, respectively.

Let us substitute for the temperature the new variable

$$y = \int_0^T \varkappa \, dT = \frac{2}{7} \cdot 1{,}68 \cdot 10^{13} \, T^{7/2} \tag{3}$$

by using above approximation. The right hand side of equation 2., then becomes:

$$\int_T^{T_0} \varkappa \, dT = \int_0^{T_0} \varkappa \, dT - \int_0^T \varkappa \, dT = y(o) - y(z)$$

Further, let us introduce the symbol:

$$p_f^*(T) - p_r^*(T) = F(y)$$

our integral equation may be written as:

$$y(z) + \int_0^z s \left(1 - \frac{s}{z}\right) F(y) \, ds = y(0) \tag{4}$$

In the case of calculating the thermal conduction by means of the SPITZER—HÄRM formula, y depends not only on T, but also on p, and thus the law of similarity does not strictly apply. Considering the portion of the function $\varkappa$ above the curve a. (Fig. 3) — incidentally it is also the condition at which the formula may be applied — the approximate value of y is:

$$y = \int_0^T \varkappa(T, p) \, dT \sim \frac{7{,}95 \cdot 10^{12}}{\ln (q C^2)} T^{7/2} \frac{W}{m}$$

3. Convergence of the integral equation iteration

The kernel of the equation being positive, for y following limit may be given:

$$y_m - y_0 - \frac{z^2}{6} \operatorname{Max} F(y) \leq y \leq y_0$$

As point of departure for the iteration let us assume the temperature to be constant:

$$y^0(z) \equiv y(o)$$

$$y^{(n+1)}(z) = y(o) - \int_0^z s \left(1 - \frac{s}{z}\right) F\left[y^{(n)}(s)\right] ds \quad (5)$$

For the error remaining after each step following limit may be given: As definition let it be that

$$M(z) = \operatorname*{Max}_{y_m \le y \le y_0} \left| \frac{dF(y)}{dy} \right|; \quad M(z) \text{ monotonous growing}$$

$$\left| y^{(n+1)}(z) - y^{(n)}(z) \right| = \left| \int_0^z s\left(1 - \frac{s}{z}\right) \left\{ F\left[y^{(n)}\right] - F\left[y^{(n-1)}\right] \right\} ds \right|$$

$$\le \int_0^z s\left(1 - \frac{s}{z}\right) \left| F\left[y^{(n)}\right] - F\left[y^{(n-1)}\right] \right| ds$$

$$\le \int_0^z s\left(1 - \frac{s}{z}\right) M(s) \left| y^{(n)}(s) - y^{(n-1)}(s) \right| ds$$

$$\le M(z) \int_0^z s\left(1 - \frac{s}{z}\right) \left| y^{(n)}(s) - y^{(n-1)}(s) \right| ds$$

By inserting the product $\delta^{(0)}(z, m)$

$$\delta^{(0)}(z, m) = \left| y^{(1)}(z) - y^{(0)}(z) \right| = \frac{z^2}{6} y_0 = \frac{z^2}{6} F_0$$

$$\delta^{(n+1)}(z, m) = M(m) \int_0^z s\left(1 - \frac{s}{z}\right) \delta^{(n)}(s, m)\, ds$$

it is evident that

$$\left| y^{(n+1)}(z) - y^{(n)}(z) \right| \le \delta^{(n)}(z, z)$$

by Laplace transformation with respect to the variable z

$$\overline{z\, \delta^{(n+1)}(z, m)} = \frac{M(m)}{p^2}\, \overline{z\, \delta^{(n)}(z, m)}$$

$$\overline{z\, \delta^{(n)}(z, m)} = \left(\frac{M(m)}{p^2} \right)^2 \overline{z\, \delta^{(0)}(zm)}$$

$$= \left(\frac{M(m)}{p^2} \right)^2 \overline{\frac{z^3}{6} F_0}$$

$$= \left(\frac{M(m)}{p^2} \right)^2 \frac{F_0}{p^4}$$

$$z\,\delta^{(n)}(z, m) = F_0 \left[M(m)\right]^n \frac{z^{2n+3}}{(2n+3)!}$$

$$\delta^{(n)}(z, z) = \frac{F_0}{z\left[M(z)\right]^{3/2}} \frac{\left[z\sqrt{M(z)}\,\right]^{2n+3}}{(2n+3)!}$$

$$|y - y^{(n)}| \leq \sum_{h=0}^{\infty} |y^{n+h} - y^{n+h+1}| \leq \sum_{h=0}^{\infty} \delta^{(n+h)}(z, z)$$

$$|y(z) - y^{(n)}(z)| \leq \frac{F_0}{z\left[M(z)\right]^{3/2}} \sum_{n-h}^{\infty} \frac{\left[z\sqrt{M(z)}\,\right]^{2h+3}}{(2h+3)!}$$

4. Quantitative discussion of the first order approximations

Let the temperature be constant in a zero order approximation

$$y^0(z) = y(0) = y_0$$

then according to equation (5) :

$$y(z) \equiv y^{(1)}(z) = y_0 - \frac{F_0 z^2}{6}$$

or in a somewhat rewritten form :

$$y(z) = y_0\left[1 - \left(\frac{z}{z_{kr}}\right)^2\right]$$

where as a definition :

$$z_{kr} = \sqrt{\frac{6\,y_0}{F_0}} = \sqrt{\frac{6\,y(T_0)}{p_f(T_0) - p_1(T_0)}}$$

and z_{kr} is called the characteristic radius.

Introducing the variable T from equation (3) :

$$T(z) = T_0\left[1 - \left(\frac{z}{z_{kr}}\right)^2\right]^{2/7}$$

For $z_{kr} = (pr)_{kr}$ the temperature falls to zero. The true value of (pr) which — let us say — at a temperature of $T \approx 2000°$ K is allowable, — is certainly smaller. The plot of $T(z)$ is shown in Fig. 4.

The value of the caracteristic radius depends — though in a small degree — also on the density given by the exact value of $\varkappa$. Further, again slightly, it depends on the value of T_0 taken at point $r = 0$. The following Table shows this dependence for 1 kat.

p	kat	1	1	1
T_0	keV	5	10	20
$N_D + N_T$	m^{-3}	$6{,}12 \cdot 10^{22}$	$3{,}06 \cdot 10^{22}$	$1{,}53 \cdot 10^{22}$
p_f	Wm^{-3}	$5{,}1 \cdot 10^{9}$	$1{,}6 \cdot 10^{10}$	$1{,}26 \cdot 10^{10}$
p_r	Wm^{-3}	$4 \cdot 10^{9}$	$1{,}6 \cdot 10^{9}$	$5 \cdot 10^{8}$
$p_f - p_r$	Wm^{-3}	$1{,}1 \cdot 10^{9}$	$1{,}1 \cdot 10^{10}$	$1{,}2 \cdot 10^{10}$
y	Wm^{-1}	$2{,}8 \cdot 10^{14}$	$2{,}85 \cdot 10^{15}$	$2{,}9 \cdot 10^{16}$
r_{kr}	m	1250	1250	3850

It can be seen that even by choosing a pressure of 1 kat, the radius will still be of the order of magnitude of km. s. At lower pressures this value obtained would be proportionally greater.

The high power production too, is due to the great size. In zero order approximation will be :

$$P_f = \frac{4\pi r_a^3}{3} p_f(T_0)$$

for $T_0 = 10$ keV and $p = 1$ kat it is given as

$$P_f = 3{,}68 \cdot 10^{16}\, W$$

The radiation power in first approximation is :

$$P_r = \int_0^{r_k} 4\pi r^2 p_r(r)\, dr \approx 4\pi r_k^3 p_r(T_0) \int_0^1 \frac{r}{r_k} \left(\frac{T_0}{T}\right)^{3/2} d\left(\frac{r}{r_k}\right) =$$

$$= \frac{3}{2} B\left(\frac{3}{2}; \frac{4}{7}\right) \frac{4\pi}{3} r_k^3 p_r(T_0) = 2{,}01 \frac{4\pi}{3} r_k^3 p_r(T_0)$$

where

$$B(x, y) = \frac{\Gamma(x).\Gamma(y)}{\Gamma(x+y)}$$

and it becomes by substituting the foregoing values :

$$P_r = 3{,}7 \cdot 10^{16}\, W$$

About 10% of the total power production leaves in the form of radiation, the rest by thermal conduction.

The energies here involved are rendered useless from a technical point of view by their order of magnitude. Taking into account, that a power plant of 200 MW is considered to be a large one, we can see what technical problems would have to be solved, in order to remove an output of 1000 MW from every m^2 of the surface of a sphere with 1 km radius. It has to be noted that also the neutron energy is to be considered.

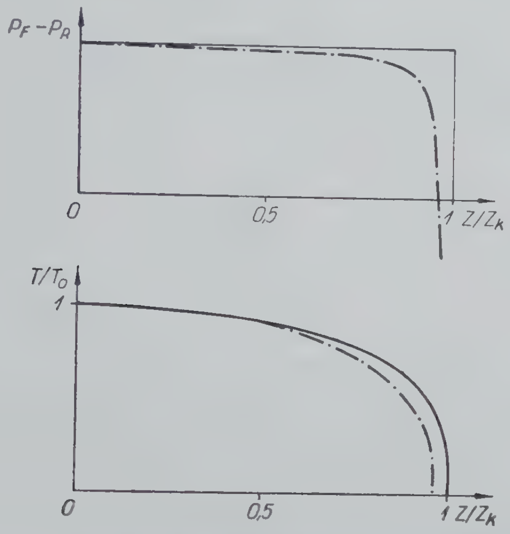

Fig. 4. Curves plotted for the first order approximation. The relative position of the exact curve is shown by the dashed line

Even if the conduction of 1000 MW could be realized — though with great difficulties — how and for what uses could the remaining energy be disposed of? This seems impossible on an earthly scale.

The conditions calculated at the first approximation do not essentially alter by further approximations. In Fig. 1 we have plotted the difference $p_f - p_r$, obtained by the first approximation. It can be seen that it is constant excepted in a thin shell; thus further iteration does not lead to a decisive alteration. For the exact solution the curve runs somewhat below the curve obtained for the first approximation (Fig. 4).

The value of the voltage taken at the center of the sphere and the point z_{kr} can be simply determined. According to Spitzer—Härm following relation may be written for current density j:

$$\mathbf{j} = 0 = \sigma E + \alpha \Delta T = -\sigma \frac{dU}{dr} + \alpha \frac{dT}{dr}$$

From this

$$U = -\int_0^{T_0} \frac{\alpha}{\sigma} \, dT = 0{,}72 \, \frac{k T_0}{e}$$

Let be $T_0 = 10$ keV then $V = 7{,}2$ kV.

This is a good value from a technical point of view : the tension of high power generators being of the same order of magnitude. In principle, if we could introduce an electrode in the center of the high temperature core, energy could be taken out of it as from a galvanic cell working according to diffusion law. A tension of the same character would occur at the steady state operation of a plasma surrounded by an electromagnetic wall, due to the small temperature-gradient.

5. Control of assumptions

Our speculations were based on the following assumptions :

a) The composition of the gas does not change.

b) The gas is in plasma state.

c) There is a Maxwellian distribution of velocity.

d) The radiation absorption being negligible, the plasma is transparent.

e) The pressure is constant.

f) The mean free path is so short that the thermal conduction may be calculated by applying the formula.

g) The reaction products reach an equilibrium with the gas at the place of their origin.

ad *a)* Let us examine the consumption time of the total amount of gas in the case of constantly producing the initial energy.

$$\Theta = \frac{\dfrac{N_D + N_T}{2}}{N_D N_T (\sigma v_{DT})_{av}} = \frac{2}{(N_D + N_T)(\sigma v_{DT})_{av}} = 0{,}67 \text{ sec}$$

From this it can be seen that our assumption is valid for only a fews msecs at the most. At a lower energy production an equilibrium is reached, owing to the increasing radiation effects of the reaction products at a smaller temperature gradient, thus the critical radius will increase.

ad *b)* The gas is at such a high temperature in the major part of the volume, that the plasma state is maintained. The conditions are uncertain in the neighbourhood of the external wall, where at a few thousand degrees, also neutral particles may be found. Of course, this effects the thermal conductivity.

The events here occuring may somewhat enlargen the shell, at the same time, however, neither the dimensions, nor the produced energy will undergo any essential alteration.

ad *c)* The essential difference from the Maxwellian distribution is the following: many reactions occur per unit time resulting in a great number of high energy reaction products. By transferring their energies to the D and T nuclei, the distribution density will be shifted towards higher energies. As the temperature T_0 is chosen for the sake of stability near to the temperature for the maximum energy production, no appreciably higher production will be obtained, thus the decreasing in size cannot be expected.

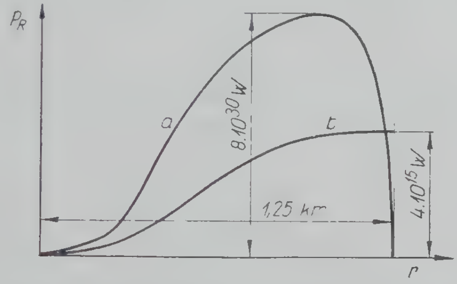

Fig. 5. The total radiated power *a)* according to the Stefan—Boltzmann law; *b)* according to the law of space radiation

ad *d)* In Fig. 5 we have plotted the total radiated power as evaluated according to the Stefan—Boltzmann law and on basis of the space radiation, respectively. It can be seen that our sphere is extremely transparent: the Stefan—Boltzmann formula giving a value that is higher by several orders of magnitude. Thus the absorption may again be neglected, except for a thin shell. The two radiation curves show an intersection at $T = 14$ eV.

ad *e)* For some ten tons of material, obviously, the gravitation effects may be neglected. In order to estimate the radiation pressure let us suppose the total energy to be absorbed in the external wall. Thus

$$\Delta p < \frac{2}{c} \frac{P_r}{4 \pi r_k^2} \sim 0{,}093\,at$$

which may be completely neglected, as compared to 1000 at.

ad *f)* The thermal conduction law is only valid, as long as the relative change per unit mean free path is small, that is:

$$\left| \lambda \frac{d(\ln T)}{dr} \right| \ll 1$$

By determining the value of λ from [1] this condition may be written as :

$$\left| \lambda \frac{d(\ln T)}{dr} \right| = \left| p\lambda \frac{d(\ln T)}{dz} \right| = \frac{T_0^3}{z_k} \frac{z}{z_k} \left[1 - \left(\frac{z}{z_k} \right)^2 \right]^{-1/7} =$$

$$= 2{,}97 \cdot 10^{-12} \left[1 - \left(\frac{T}{T_0} \right)^2 \right]^{1/2} \left(\frac{T_0}{T} \right)^{1/2}$$

for $T_0 = 20$ keV.

This value will be the unity for a temperature of 18 eV, thus immediately next to the wall, anywhere else it will be considerably smaller.

ad *g)* Similarly the reaction products, except for neutrons, will be stopped in the major part of the space on a path along which T does not appreciably change.

The mean free path of the reaction product $_2He^4$ is, in fact, of the order of several 10 meters. Approximation holds here only for a smaller fraction of space.

6. Conclusions

It can be seen that our assumptions hold, and that the results obtained for dimensions and power production may be considered true as regards to the order of magnitude. An improvement towards the approach of more real values cannot be expected from further refinement of calculations. By letting our imagination run loose, we may suggest the possibility of an artificial star, besides the artificial planet to be realised in the near future. In principle, thus a "black" wall temperature and radius might be found at which the total power output will be dissipated, and the problem of removing such an extremely large power does not arise. For the present, however, the resulting wall temperature makes the realisation quite illusory, even in the case of a sudden improvement in the heat resistivity of materials.

Summary

The possibility of the steady state of a deuterium tritium plasma-mixture, confined at constant pressure in a spherical container, is considered.

The temperature chosen for the plasma sphere center is in the vicinity of the temperature belonging to the maximum of thermonuclear energy production ; the temperature of the external wall being fixed at about a few thousand degrees. Although the dimensions obtained are on an earthly scale, technically the realization of a fusion reactor of this type is found to be impossible.

References

1. Post, R. F.: Controlled Fusion Research. An Application of the Physics of High Temperature Plasmas. Rev. Mod. Phys. **28**, 338 (1956).
2. Teller, E.: General Problems of the Controlled Thermonuclear Process. Nucl. Sci. and Eng. **1**, 313 (1956).
3. Kálmán, G., Pócs, L., Schmidt, G. and Simonyi, K.: On the Possibility of Controlled Power Production Using Thermonuclear Fusion. Periodica Polytechnica **1**, 53 (1957).
4. Thompson, W. B.: Thermonuclear Power. A Theoretical Introduction. Nature, **179**, 886 (1957).
5. Linhard, I. G.: Power from Thermonuclear Reactions. Nucl. Energy **2/11**, 60 (1957).
6. Gamow, G.—Critchfield, C. L.: Theory of Atomic Nucleus and Nuclear Energy Sources. Oxford, Clarendon Press, 1949.
7. Spitzer, L., Härm, R. Ir.: Phys. Rev. **89**, 977 (1953).

Professor K. Simonyi, Budapest XI. Budafoki út 4—6, Hungary.

CONTINUOUS IMAGE-FORMING SYSTEMS OF LARGE FIELD OF VISION (TELESCOPES)

N. Bárány

Institute for Instrumental Design and Precision Mechanics, Polytechnic University,
Budapest

(Received May 30, 1957)

I

It is not the aim of the present paper to give a detailed specification of telescopes. Our investigations are chiefly concerned with the geometrical relations of the *field of vision*. The field of vision of the telescope is in close correlation with magnification which, according to Fig. 1, is the quotient of the focal length f for the objective, and f_1 for the eye-piece, or

$$N = f : f_1 .$$

If the telescope is adjusted to infinity, the image lies in the focal plane of the objective. The angle included between the lines connecting points A and C of the image with the centre 0 of the objective is the *real* field of vision viewed through the eye-piece 3 at an angle α_1 representing the *virtual* field of vision. The quotient of the virtual and real fields being also equal to the magnification of the telescope

$$N = \alpha_1 : \alpha .$$

In addition to the focal length of the objective, the real field of vision is determined by the virtual field. Both theoretical and practical considerations induce us to limit the virtual field of vision at 75°. For various reasons, a further increase would be inexpedient. Unlike photolenses, even wide-range telescopes can only cover a limited portion of the object space at one time, in correspondence of geometrical laws. For covering further portions of the object space, one has to turn the head, together with the telescope. The real field of vision for conventional trench telescopes, for example of a magnification of 6 is 7°, covering a field of 140 m diameter at a 1000 m distance. In the case of telescopes of lesser magnification — opera glasses — the covered field is not more than 15° which is still very unsatisfactory in relation to the full 360° field.

The basic idea of simultaneously covering the entire 360° field was first established by MANGIN[1] (Fig. 2).

---

[1] MANGIN, Association française pour l'avancement des sciences 7, Paris 339, 1878.

According to Mangin's theory, the arc BC of a circle of Radius R, if rotated about axis O describes a toroidal surface, reflecting the beams L incident, perpendicularly to the axis O, from all directions of the field. The image thus formed by the concave mirror ring is a real, that is, a receivable annular (panoramic) image. Such a device however, cannot justly be considered a panoramic system, since the telescope will only form annular images of objects situated at small angles.

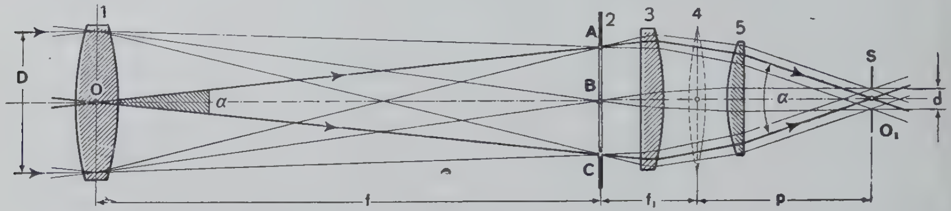

Fig. 1. Determination of the field of vision by means of a simple inverting telescope. Relationship between real and virtual field of vision. The eye-piece consisting of the condensing (field) lens 3 and the eye lens 5 is represented by the resultant lens 4 with a focal distance f_1

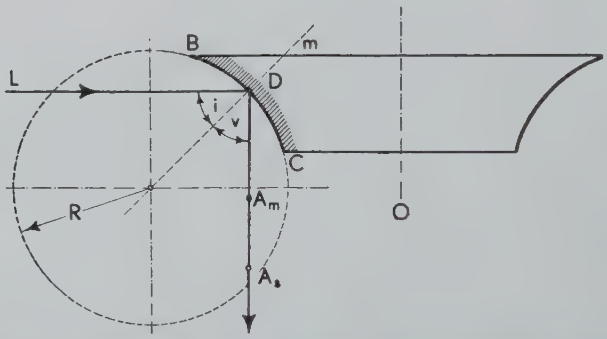

Fig. 2. Creation of the Mangin toric surfaces. Tangential and sagittal image points

The image of a distant point formed by tangential pencils is at A_m, while that formed by sagittal pencils is at A_s. According to the rule of astigmatic image formation

$$C\,A_m = \frac{R \cdot \cos i}{2}$$

and

$$CA_s = \frac{R_1}{2 \cos i}$$

for the sagittal pencils, m representing the normal of incidence, i the angle of incidence and v the angle of reflection. R_1 is the second radius of curvature obtained by rotation in the sagittal section of the toroidal surface. The condition for correcting astigmatism is that

$$CA_m = CA_s$$

Hence it follows that

$$\frac{R}{R_1} = \frac{1}{\cos i^2} \, .$$

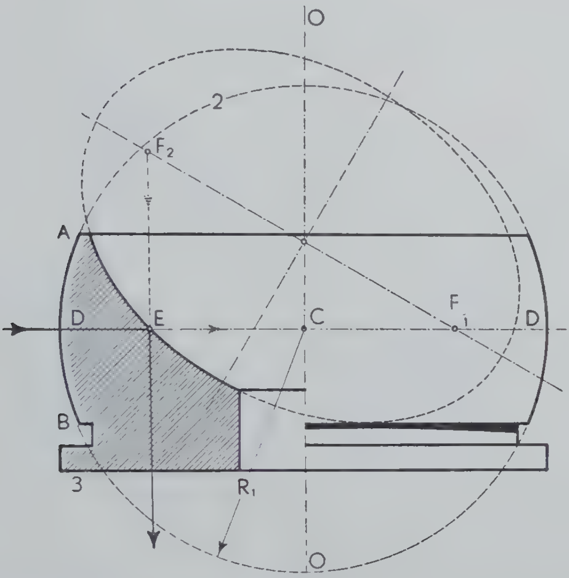

Fig. 3. Lens producing a panoramic image. The surface of incidence is spherical, while the reflecting surface is an ellipsoid and the surface of emergence is plane

Thus, if freedom from astigmatism is obtained by means of such a surface, a certain amount of spherical aberration and deviation from the sine condition must be taken into account. Furthermore, it is impossible to achieve complete freedom from distortion.

Systems forming panoramic images have been designed by using various surfaces of rotation of higher order, and this is how the various kinds of annular lenses were produced. The annular lens represented in Fig. 3 have a spherical entry surface 1 of radius R_1, while the reflecting surface is an ellipsoid. The spherical zone AB is so situated that its diameter D intersects one of the focuses F_1 of the ellipsoid. In order to produce images, the emerging pencils have to be directed to a lens or lens arrangement placed under the annular lens. The horizontal pencil incident upon the spherical zone AB intersects the centre C of the sphere. The ellipsoid 2 is so situated, that the pencil be reflected at point

E as if coming from the other focus F_2 of the ellipsoid. The axis of rotation O intersects the centre C of the sphere and bisects the transverse axis of the ellipsoid. The plane surface 3 is perpendicular to the emerging pencil in order to

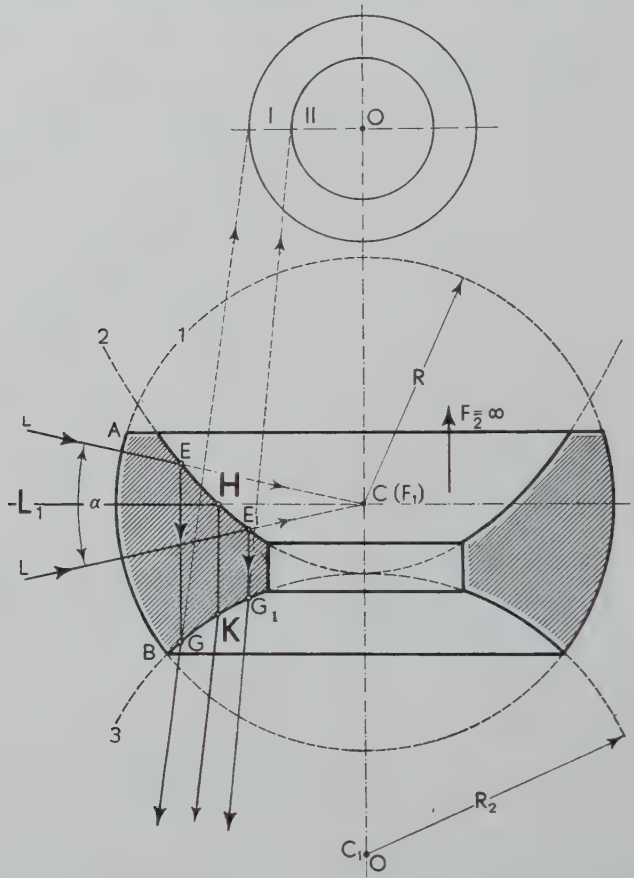

Fig. 4. A lens producing a panoramic image. The surfaces of incidence and emergence are spherical, while the reflecting surface is a paraboloid

ensure its unrefracted emergence. The role of the aperture in the centre of the annular lens will later on be discussed.

Another embodiment of the system is shown in Fig. 4 where the centre C of sphere 1 (radius $= R_1$) is coincident with the focus F_1 of the parabola 2. The pencil of rays from L_1, incident upon the spherical zone AB points towards the centre C, and is reflected at point H of the parabola parallelly to the rotation centre O, as if originating from the other focus F_2 situated at infinity. The pencils travelling from the direction L—L towards C, and subtending an angle α, are reflected at points E and E_1 of the parabola, whereupon they emerge refracted at points G and G_1 of the spherical surface 3 traced by rotating the radius R_2 about point C_1. The locus of the virtual image is above the lens. Part I of the panoramic picture represents the sky whereas part II shows the field.

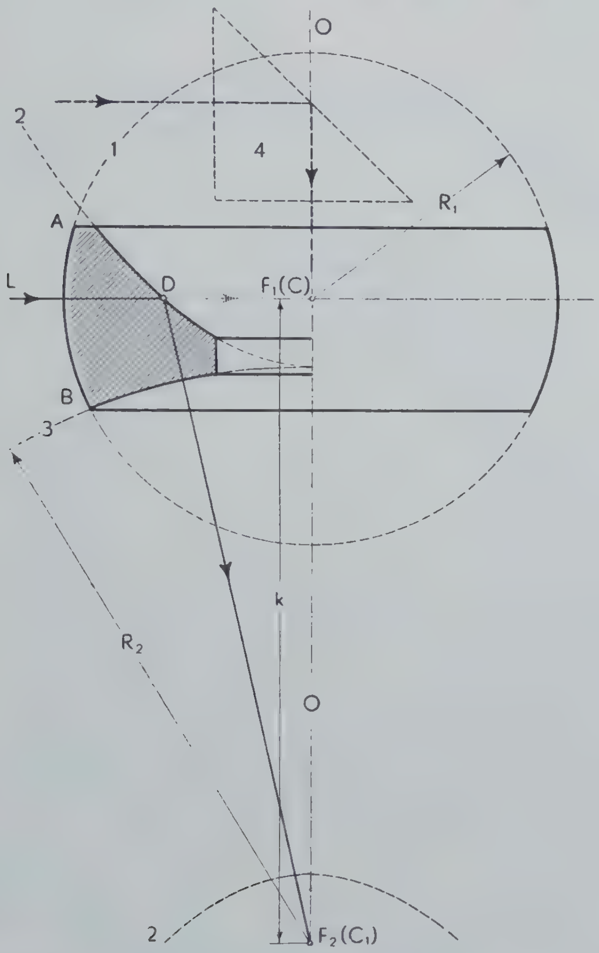

Fig. 5. A lens producing a panoramic image. The surfaces of incidence and emergence are spherical, while the reflecting surface is a hyperboloid

The diagram in Fig. 5 illustrates a system with spheres of radii R_1 and R_2 respectively, as surfaces of incidence of emergence, and with a hyperboloidic surface of reflection. The virtual focuses F_1 and F_2 are so situated that the ray reflected at point D of the spherical zone AB intersects the optical axis O, corresponding to the axis of rotation, at the other focus F_2. For purposes of easier illustration of the distortions of the image formed by the annular lens a rather short distance k was chosen, and the cross-shaped areas 4 to 8 and III to VII of the cross-ruled network in Fig. 6 have been hatched.

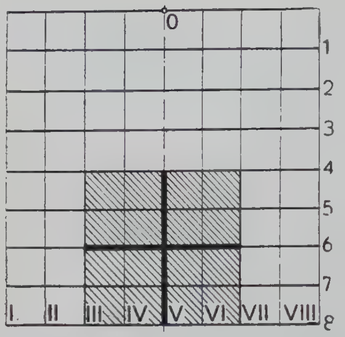

Fig 6. Cross-ruled network for illustrating the distortions associated with panoramic image formation

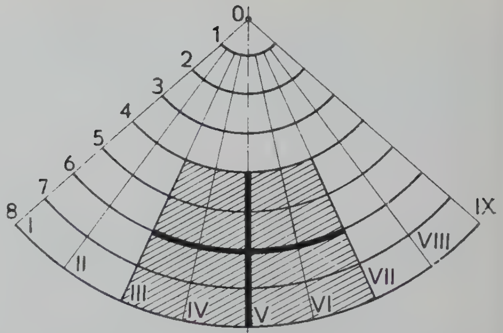

Fig. 7. Distorted image of the network represented in Fig. 6, produced by an annular lens

Fig. 7 shows the image of this network produced by the annular lens. The straight lines 1 to 8 are distorted into arcs around the centre O. Magnification changes radially, but remains constant for the points connected by the arc. Evidently, tangential magnification is also impaired. The centre of projection is at O, thus distorted image satisfies the rules of central projection.

The annular image varies with the type of optical arrangement employed, but the construction of the image closely follows the laws of central projection. In the variations shown in Fig. 8 and 9 the image is viewed at the outer margin of the field of view, and at the inner margin respectively. Thus, their direction is opposed in relation to each other.

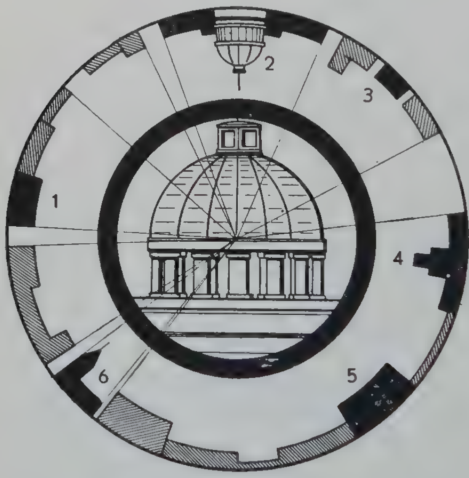

Fig. 8. Panoramic image formed along the outer margin of the field of vision. The centre of projecting lies in the centre of the field of vision

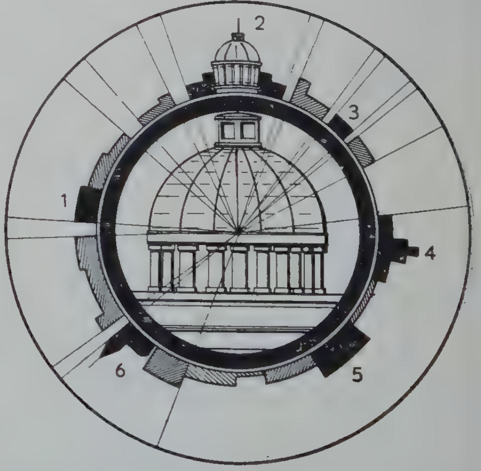

Fig. 9. Panoramic image formed about the inner margin of the field of vision. In both Figures the magnified image of the sighted object in the inner field of vision is produced by pencils of rays directed by another system and passing through the aperture of the annular lens

Ring lenses had to be further improved in order to satisfy the strategic requirements, arising in connection with periscopes, these latter being important equipments of submarines. Periscopes are supposed to enable the personnel to obtain a full view of the entire surface of the sea. The inner part of the annular image, with a magnification of 0,4 to 0,6, presents images of the sighted point or the field respectively, enlarged by a factor 6 (Fig. 10).

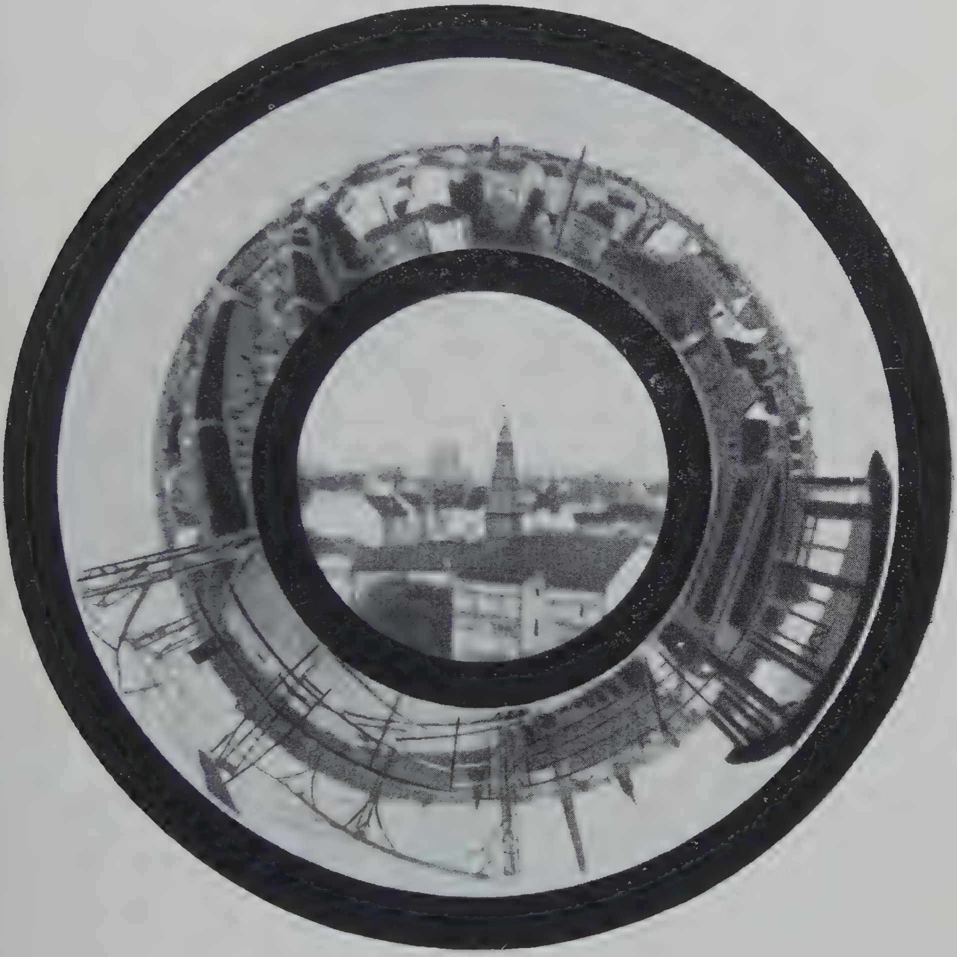

Fig. 10. Panoramic image with the inner part magnified, produced by a Goertz periscope

In 1950 a Hungarian physicist, **Pál Bottka** succeded in designing a lens system representing an annular mirror lens (Fig. 11), as an amalgamation of the Hill lens with the annular lens. The Bottka lens covers an angular field of 200°, and provides satisfactory image formation. After reflection, the rays incident on the front lens arrive to the reflecting surface II of the back lens. Then, after being reflected by the reflecting surface of the front lens, they emerge from the system parallel with the optical axis. The telescopic image is yielded by a lens arrangement mounted behind the mirror lens.

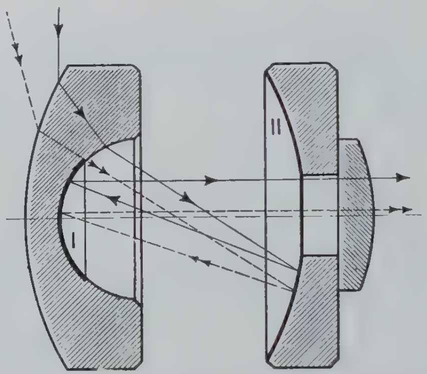

Fig. 11. Panoramic mirror lens arrangement by Pál Bottka

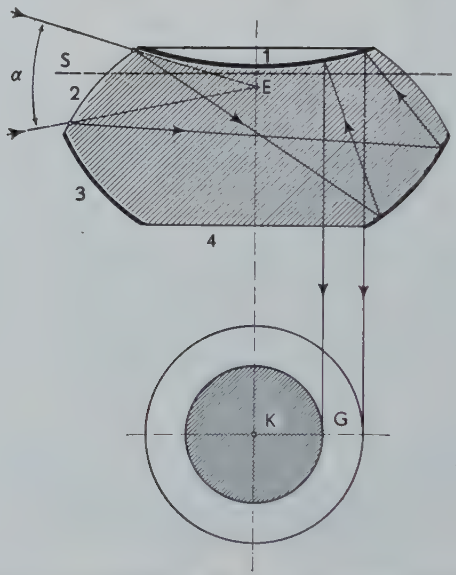

Fig. 12. One-component panoramic lens by Sándor Majoros, comprising both spherical and plane surfaces

Another Hungarian development is an annular lens designed in 1951 by the Hungarian engineer S. Majoros. Fig. 12 presents the one-component lens, solely bounded by spherical surfaces. The annular image *G* is generated in front of the lens.

It is possible to direct pencils of rays emerging from optical systems of varying magnification power through the central opening of the annular lenses.

In the case of the Majoros lens the central image k is produced by the prism and lens arrangements mounted under the lens. The parallel pencils emerging from the lens can, of course, only form images if a system for rendering the pencils convergent is set up behind the lens, as represented in Fig. 13. The lens of diameter D has metal-coated reflective surfaces 2 and 5. The pencils 1 enter the system from all directions under 32° angles and are refracted once, and reflected twice, thus forming an annular path of rays 3 when emerging. The lens arrangement 4 — a triplet in our example — inserted behind the lens form images with the rays at a certain distance.

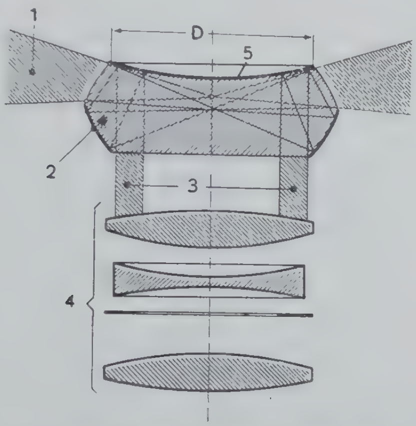

Fig. 13. The path of rays in the Majoros annular lens, together with the positive three-component lens arrangement 4 placed behind the lens

The ring lenses composed of surfaces of rotation of higher order are liable to be easily damaged, they are costly, and in some cases can be produced only in large sizes. Moreover, the annular image is afflicted with heavy distortion, and the maximum enlargement is x0,9. These drawbacks have so limited the usefulness of annular lenses, that the older types are now practically obsolete. With a view to consistency and uniformity, it was nevertheless deemed advisable to give a survey of these lenses, particularly since most of these systems involve ingenious and unexpected solutions.

The so-called multiperiscopes enable representation of the horizon in sections, — if not as a coherent panoramic view. A panoramic picture composed of uniform sections is produced by a number of periscopes pointing in various directions. This solution has the advantage of yielding undistorted, images covering fields of mean size, even for higher magnifying powers, and permitting the simultaneous presence of several observers. Nevertheless, this arrangement proved unsatisfactory owing to its large dimensions.

The periscope was designed with a view to produce a smaller instrument, still admitting several observers. Here, the images are formed by several independent telescopes having one common objective.

P. Triulzi's 1942 patent relates to a multiperiscope. This instrument comprises eight symmetrically arranged panoramic prismatic telescopes and a central air reconnaissance telescope, all of them mounted in a common tube.

Multiperiscopes are rigidly fixed and cannot be rotated about their vertical shaft, whereas simple periscopes are rotated by the observer around the vertical shaft, under constant changes of position, in order to achieve full coverage of the horizon. Another type provides a reflector prism bedded in the upper part of the periscope by whose rotation the succeeding zones of the horizon can be scanned. The first solution is simpler, the second one more convenient. On swinging the reflector prism, the image is laterally displaced in the field, and at the same time suffers tumbling of the image so that observation is almost impossible. It is therefore necessary to provide another optical system with a view to correct image tumbling arising in connection with the lateral displacement.

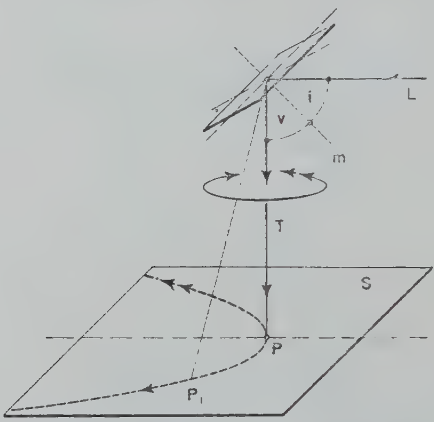

Fig. 14. A plane mirror making a 45⁰ angle with the incident ray, rotated about an axis normal to the optical axis. The trace of the reflected ray describes a curve of fourth degree

Before proceeding to the description of the equipment to be applied in optical systems, let us make an investigation into what happens if a mirror or prism subtending an angle with a ray is rotated about the axis perpendicular to the incident ray. Let us determine the curve described by the trace of the reflected ray on the basic plane (Fig. 14).

The plane mirror 1 makes a 45° angle with the horizontally incident ray *L*. The ray reflected under an angle *v* reaches the plane *S* at *P*. On swinging the mirror about the reflected ray *T* as axis, point *P* will describe the curve indicated by the arrows, in the sense of rotation. The mirror situated at O (Fig. 15) subtends a 45° angle with the vertical. Its normal, rotated about the vertical axis, describes a conical surface of an angular aperture of 45°. Let the normal be situated at say, *O'N*, let the ray directed to *S* have a surface of incidence *SO'N*, let the angle of incidence be φ let the direction of the reflected ray be $O'P$, and, finally, let the angle of reflection be $NOP = SO'N = \varphi$. Let the angle included between the surface of incidente and the perpendicular surface $SO'O$ be α. On swinging the mirror, its normal will travel from $O'N'$ to $O N'$, while the value of α will simultaneously change from 0 to 45°. Let us determine the relation between the coordinates x and y of point P with the angle α.

The first relation to be determined is that between the angles φ and α. Let the radius of the sphere represented in the figure be $R = 1$. In this case,

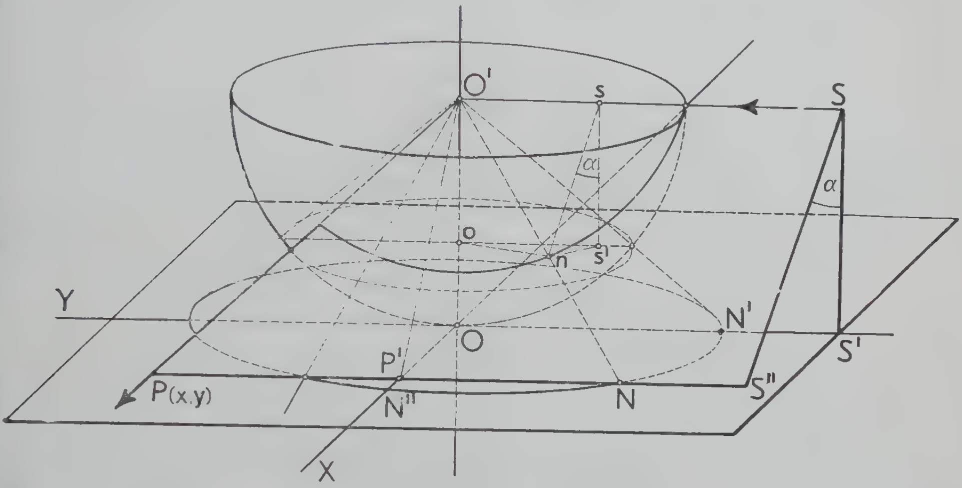

Fig. 15. Geometrical analysis of the ray reflected by the plane mirror represented in Fig. 14

from the triangles nss' and $O'ns$

$$ns = \sin\varphi, \quad ss' = ns \,.\, \cos\alpha = \sin\varphi \,.\, \cos\alpha$$

since

$$O'_0 = O'n \cdot \cos 45°$$

$$s s' = O'_0 ,$$

$$s s' = \sin\varphi \cdot \cos\alpha = \frac{1}{\sqrt{2}}$$

whence

$$\sin\varphi = \frac{1}{\sqrt{2}\cos\alpha} \,. \tag{1}$$

Let us now determine the dependence of $y = PP'$ from φ, that is, from α. In the triangle $PO'P$

$$PO'P' = 2\varphi - \frac{\pi}{2}$$

therefore

$$y = O'P' \operatorname{tg}\left[2\varphi - \frac{\pi}{2}\right] = -O'P' \operatorname{cotg} 2\varphi . \tag{2}$$

The angle at O' in the triangle $OO'P'$ is α, thus

$$O'P' = \frac{OO'}{\cos\alpha} = \frac{1}{\cos\alpha}$$

$$y = -\frac{\operatorname{cotg} 2\varphi}{\cos\alpha} . \tag{3}$$

The $\operatorname{cotg} 2\varphi$ in formula (2) is expressed by angle α. For this end not only formula 1. is needed, but the expression of $\cos\varphi$ by α, too. Using formula (1)

$$\cos\varphi = \sqrt{\frac{2\cos^2\alpha - 1}{2\cos^2\alpha}} \tag{4}$$

$$\cos 2\varphi = \frac{\cos^2\alpha - 1}{\cos^2\alpha} \tag{5}$$

$$\sin 2\varphi = \frac{\sqrt{2\cos^2\alpha - 1}}{\cos^2\alpha} \tag{6}$$

From formula (5) and (6)

$$-\operatorname{cotg} 2\varphi = \frac{1 - \cos^2\alpha}{\sqrt{2\cos^2\alpha - 1}} . \tag{7}$$

Applying formula (7) in formula (3)

$$y = \frac{\sin\alpha \cdot \operatorname{tg}\alpha}{\sqrt{2\cos^2\alpha - 1}} : \tag{8}$$

Let us now examine the dependence of coordinate x of point P from the angle α. In the triangle $OO'P'$ $OP' = x$ and $OO' = 1$. The angle situated at O' is α, whence simply

$$x = \operatorname{tg}\alpha \ldots \tag{9}$$

The equations (8) and (9) produce the parametric set of equations of the curve described by point P. Now eliminating the angle α, $\operatorname{tg}\alpha$, $\sin\alpha$ and $\cos\alpha$ may

be expressed by x, hence $\operatorname{tg} \alpha = x$
From the relation

$$1 + x^2 = \frac{1}{1 - \sin^2 \alpha} \tag{10}$$

thus

$$\cos^2 \alpha = \frac{1}{1 + x^2} . \tag{11}$$

From the same

$$1 - \sin^2 \alpha = \frac{1}{1 + x^2} \tag{12}$$

that is

$$\sin^2 \alpha = 1 - \frac{1}{1 + x^2} = \frac{1}{1 + x^2} \tag{13}$$

From equation (8):

$$y^2 = \frac{\sin^2 \alpha \cdot \operatorname{tg}^2 \alpha}{2 \cos^2 \alpha - 1} . \tag{14}$$

Applying the equations (11) and (13):

$$y^2 = \frac{\dfrac{x^2}{1 + x^2} x^2}{2 - \dfrac{1}{1 + x^2} - 1} = \frac{x^4}{2 - 1 - x^2} = \frac{x^4}{1 - x^2} . \tag{15}$$

Thus, the ray reflected by the mirror describes the curve of fourth degree

$$y = \frac{x^4}{1 - x^2}$$

on the plane at unity distance from the mirror and perpendicular to the axis of rotation of the mirror.

Similar phenomena are experienced on rotating a right-angled 45° prism replacing the plane mirror 1 in Fig. 14. Moreover, the angle of deviation of the reflected ray is twice the angle by which the prism is turned. In the visual field of such telescopes the image is not only laterally displaced but is also tumbling, though not along the arc, but along the curve of fourth degree. The problem to be answered is, to combine the reflector prism with an optical arrangement which will laterally displace the image — upon rotation of the reflector prism — without, however, causing the image to tumble. Such a prism, being able to keep the image erect, in the course of its lateral motion, is, therefore called *erecting prism.*

The first suggestion, as well as, the first practical realization of the erecting prism is due to Chief Engineer Jacob, scientific advisor of the former C. P. Goertz company, in 1905, and has since been in use throughout the world, without any material changes in design.[2]

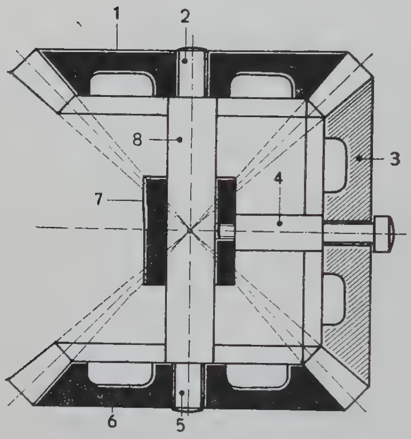

Fig. 16. The general principle of a differential gear

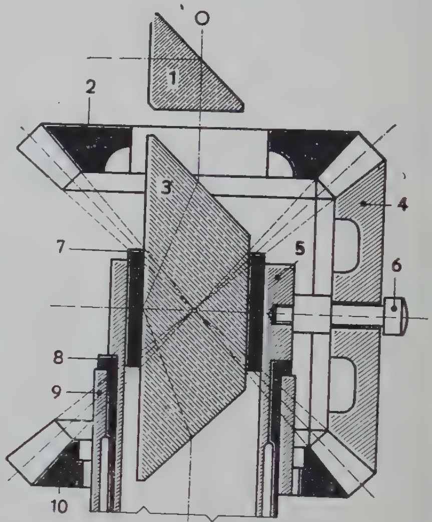

Fig. 17. The Dowe erecting prism controlled by differential gear

These so-called panoramic telescopes allow the observer to sweep the successive sections of the horizon without having to turn the head, by swinging the reflector prism fitted into the top of the instrument. The real field of vision of the telescopes is of 10 to 14°, and the horizon may be observed in the form of a continouos band picture extending over the entire field. In order to obviate tumbling of the image, the right-angled 45° reflector prism rotatable about the vertical optical axis, is so connected with the Dowe erecting prism, that this latter follows the reflector prism with identical sense of rotation, but with half the rotary speed. To fulfill this condition one may introduce a differential gear, too commonly known to be described at all. Nevertheless, it seems advisable to describe its action, as the differential arrangement for telescopes, having two gears less than usual, is somewhat different in construction from conventional differential gears used for motor vehicles.

---

[2] K. Pritschow, Das Rundblickfernrohr. Ztschft. f. Feinmechanik 2, 1915, XIII. 9.

The differential gear represented in Fig. 16 has bevel gears 1 and 6, loosely set on the pins 2 and 5 of shaft 8. They are connected by the bevel gear 3 mounted, free to turn, on the shaft 4 fixed into sleeve 7, freely rotating round the shaft 8. Let us suppose that bevel gear 6 is at a standstill, and the gear 1 is rotated around pin 2. The planet gear 3 connected with gear 1 will also rotate and, revolving along the stationary gear 6, will also take along shaft 4. If the bevel gears 1 and 6 are rotated in opposed direction but with identical rotary speed, planet gear 3 will revolve, while remaining in place, around shaft 4.

Its application for telescopes is represented in Fig. 17. Let prism 1 rotate together with gear 2, this latter will take along planet gear 4, which in turn, revolving along the stationary gear 10 will turn the Dowe prism 3 by means of shaft 6 with a transmission ratio 1 : 2. Prism 3 with its mount 7 is bedded in sleeve 5 which can revolve in the bearing 8 fitted into the telescope tube 9. If the bevel gears 2 and 10, being fixed to the top and to the bottom of the telescope, respectively, are turned in opposed sense, but with an identical angle, planet gear 4, shaft 6 and prism 3 remain stationary.

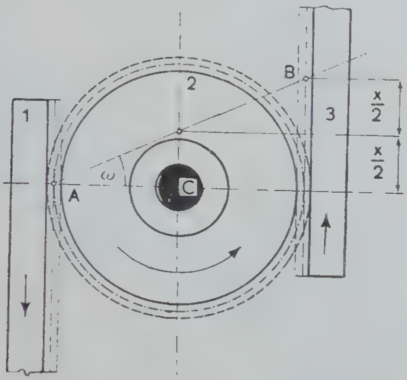

Fig. 18. Relationship between the gears of a differential arrangement

The diameter of the planet gear can be chosen at will, but the diameter and the cog number must be identical for the two driving gears. Fig. 18 shows an arrangement where the bevel gears have been substituted by the ratchets 1 and 3. In case of a displacement in opposed direction but of identical magnitude, shaft *C* of planet gear 2 is independently displaced from the diameter of the planet gear with half the rotary speed ($\omega : 2$).

Fig. 19 represents the Wild panoramic telescope with differential gear and refracted magnifier.

For the vertical adjustement of the reflector prism a separate driving mechanism is provided, to be operated by means of a knob, to be seen on the top right-hand side in Fig. 19. Thus, lateral and vertical adjustement have to be carried out in two separate steps requiring both hands for simultaneous adjustment. There are, however, cases when simultaneous but independent adjustement is imperative.

The telescopes of mechanical construction present ingenious combinations of constructional and optical ideas.

The instrument represented in Fig. 20 designed by the Hungarian engineer Nándor Lippert who died at an early age, is a combination of multiperiscopes and of annular image-formation. This instrument is noteworthy from the point of view of optomechanics, even though it has not found wide popularity, owing to its disadvantages described below.

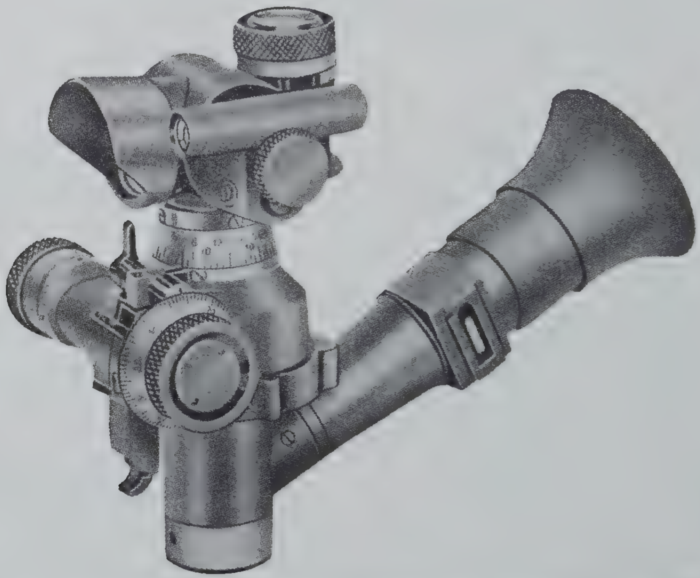

Fig. 19. The Dowe prism rotated by a differential gear, applied in the Wild sighting telescope of refracted sight line

Just as for multiperiscopes, the panoramic image is cut up into sections, with the magnified image of the section just sighted, situated in the centre. On rotating the reflector prism, the central image is shifted, as has been described in connection with panoramic telescopes. The main difference against multiperiscopes is that the images produced by the individual telescopes appear simultaneously in the field of vision, together with the central image. Sighting is done by means of the central image, observation by the panoramic images. The central sighting telescope is surrounded at equal angular distance by eleven telescopes forming image sections. The tumbling of the image occurring in connection with the turning of the reflector prism 1 of the sighting telescope, is corrected by the erecting prism 2. The image formed by means of the objective

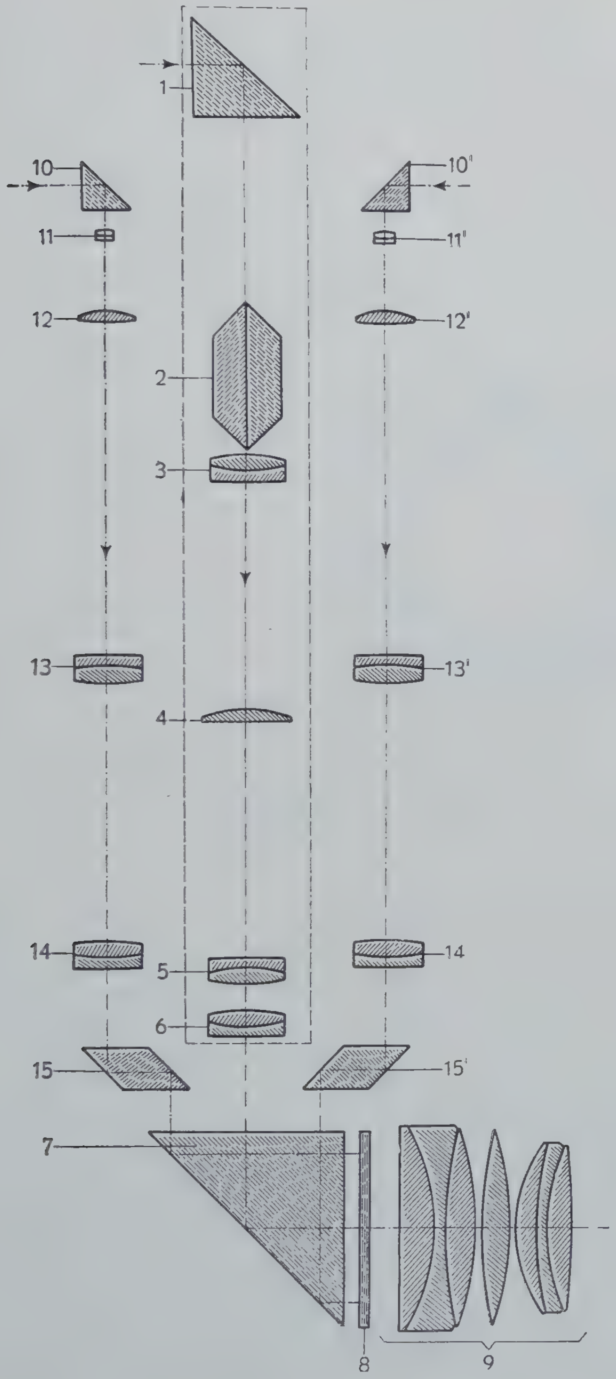

Fig. 20. Multiperiscope by Nándor Lippert, with dual field of vision

3 appears on the plane surface of the lateral field lens 4 of the objective. The inverting system consisting of lenses 5 and 6 form a second image through prism 7 on the cross-hair plate 8 which is observed through an eye-piece covering an unusually wide field. The apparent field of vision of this eye-piece, designed by the Hungarian engineer J. **Barabás**, is 90°. The optical arrangement of the individual telescopes are very similar to the instrument described above, but their magnifying power is lower. The images formed by the wide-angle objectives 11, 11′ . . . of short focal length, situated under the rigidly fixed reflector prisms 10, 10′ . . . arise in the vicinity of the field lenses 12, 12′ . . . . The inverting systems consisting of lenses 13, 13′ . . . and 14, 14′ merge the section images over the rhombic prisms 15, 15′ . . . and the common prism 7 into a fan-shaped panoramic image, visible on the cross hair plate 8. The whole instrument is stationary, except for the rotatable prism 1 of the sighting telescope. With its aid, the enlargement of the images formed by the individual telescopes can be brought to the centre of the field of vision.

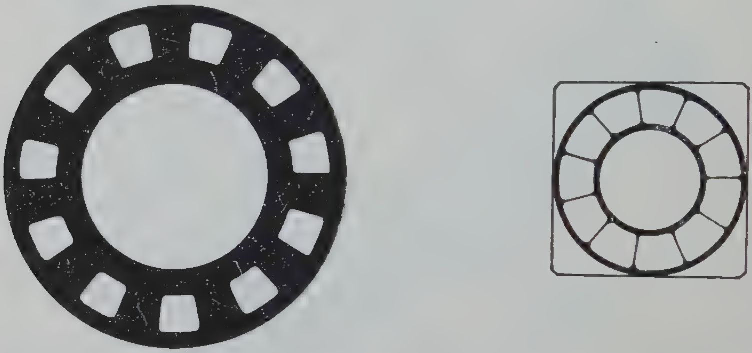

Fig. 21. The screens used in the multiperiscope shown in Fig. 20. The left-hand screen lies in the plane of the condenser lens at the objective side, whereas the right-hand screen is in the field of vision. The images are arranged in fan-shape, separated by thin gaps. The panoramic image obtained, although free from distortion, is incomplete, owing to overlapping at the bottom

The section images are separated by thin spokes or spaces, giving rise to the chief defect of the instrument consisting in that the panoramic image is not continuous and does not altogether satisfy the rules of central projection. The erect images are placed in line without overlapping, but they cannot be arranged in a circle, their continuity being broken on the top. On pushing the images nearer to one another, they will be overlapping below, while a wedge-shaped space will arise on top. An attempt to approach the top part of the images causes the bottom part to overlap to such an extent that serious losses arise. Continuity of the images is further impaired by the spokes or spaces of the screen inserted in the image plane. The section images generate in the spaces left by the spoked screen situated in the vicinity of the field lens 12 (Fig. 21). The optical arrangement of the telescopes is such, that the images may be viewed in sections separated by thin spokes. However thin, the spokes are very inconvenient.

II

The principle of producing undistorted panoramic picture

The principle set forth below for projecting undistorted panoramic pictures or sections thereof, is based on an optico-psychological factor inherent to the human eye, that is, the effect of after-images, a widely, known phenomenon the main field of application which is motion-picture projection.

Motion picture projection consists of the successive and superposed projection of stills separated by short intervals where projection, with a frequency of 28 to 32 of the individual pictures displaced in phase, produces the sensation of continuous motion.

The underlying principle of function, of the instrument to be described below is similar, in so far as the stills are also projected with intervals but juxtaposed instead of superposed. The instrument may be so designed as to allow the projection of a complete panoramic picture or of parts thereof, requiring annular or wide projection screens. In the latter case, the projection screen has to be wider than the kind used for cinematoscopic projection. It should be noted, that projection is effected without the use of anamorphotic lenses.

The principle governing the instrument is diagrammed in Fig. 22. On rotation of the reflector prism 1 about the optical axis *O—O*, the erecting prism 2 revolving in identical sense, but with half speed forms, in the image plane 5, images of each successive point of the horizon, by objective 3, over prism 4. Following the slow rotation of the prism, the image is continuously displaced in the visual field, with a sufficiently slow motion to allow observation of the adjacent sections of the horizon. If one takes photographs of the images, their assembly will yield a coherent panoramic picture of the object space. Incidentally, this can be effected as well by means of panoramic photocameras. For prisms of high revolution per minute, however, the image will be blurred past distinction. (Fig. 23). For periodic projection, the image formed in the focal plane of the objective 3 is periodically interrupted by the slits of a rotary sector disc 5 driven by motor 4 (Fig. 24). At the same time, the axle 6 and the spur gears 7 and 8 drive the reflector prism 1 as well as, by means of a non-represented transmission, the erecting prism 2. This latter is driven with half *R. P. M.* Each position of the prism is associated with a separate picture, but rapid rotation of the prism will give rise to a heavily blurred picture (Fig. 25).

The task set for undistorted panoramic image formation is to juxtapose the successive pictures, in conformity with field position, that is, by bringing into relief that section of visual field falling into the sighting line (Fig. 26).

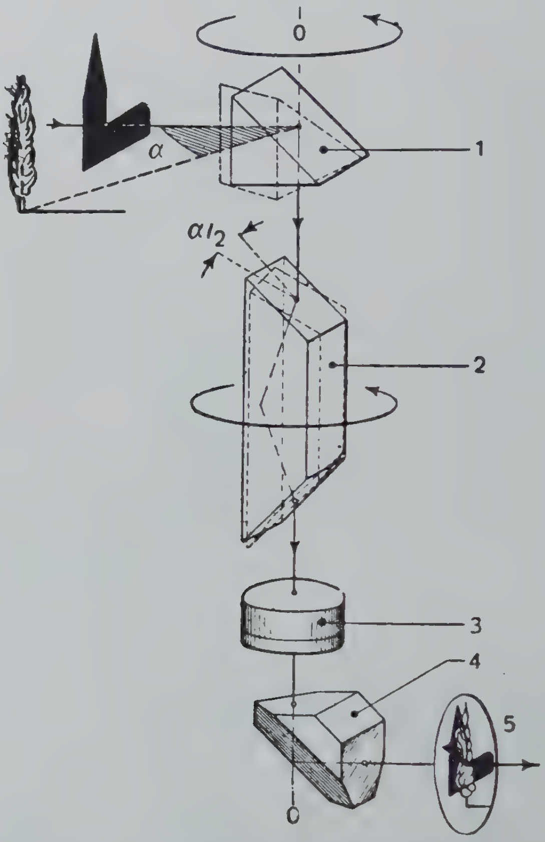

Fig. 22. Conditions arising through rotation of a right-angled 45° prism, in a telescope of refracted sight line

The instrument works in the following manner: the axle 13 of motor 14 drives the rotary sector disc 4, while the spur gears 15 and 16 drive the reflector prism 1. The drive of the erecting prism 2 is again not represented. The objective 3 produces a small-sized wide-angle image I in the plane of the slit of sector disc 4, situated within the focal range of lens 5. The emerging bundle travels parallelly over prism 6 to objective 7 which forms a second image from the first image over prism 8 at point II of the band image plane 9. The objective 7 always receives parallel bundles, so that this lens may be shifted, together with prism 8, into positions 7′ and 8′. In the latter case the image is formed at II′. Mount 12 comprising objective and prism is so directed by the motor-driven

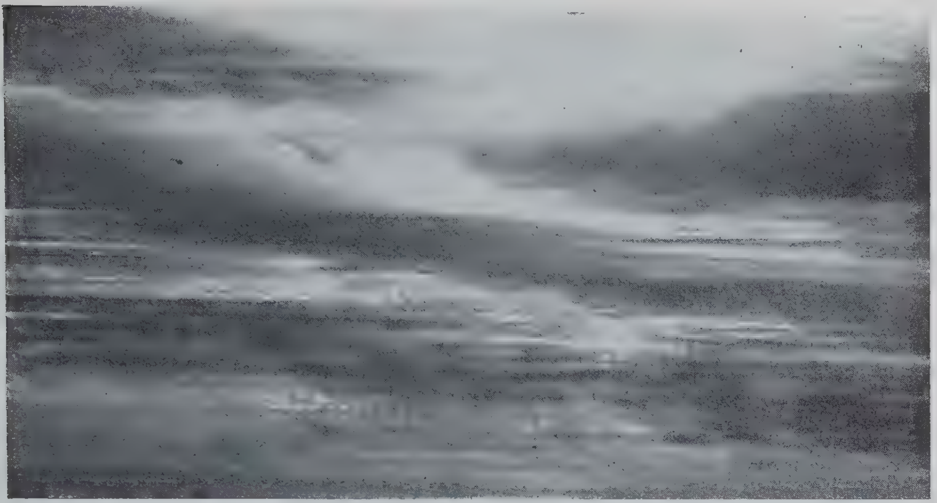

Fig. 23. Image formation by an arrangement diagrammed in Fig. 22, showing the landscape in Fig. 24

heart-cam 11 by means of the arm 10 that the mount will stop the end positions *A* and *A'*, whereas it covers the distance X to and from at a uniform speed.

There is only one slit of the sector disc and one position of the prism corresponding to each individual equidistant section of the image plane 9, that is, the slits of the sector disc are synchronized with the image sections. In the position illustrated in the figure, the slit of the disc 4 exhibits image I so that lens 7 will produce by means of prism 8 the image falling into the direction of the reflector prism 8 at point I. Thereafter, the rotary sector disc will cover

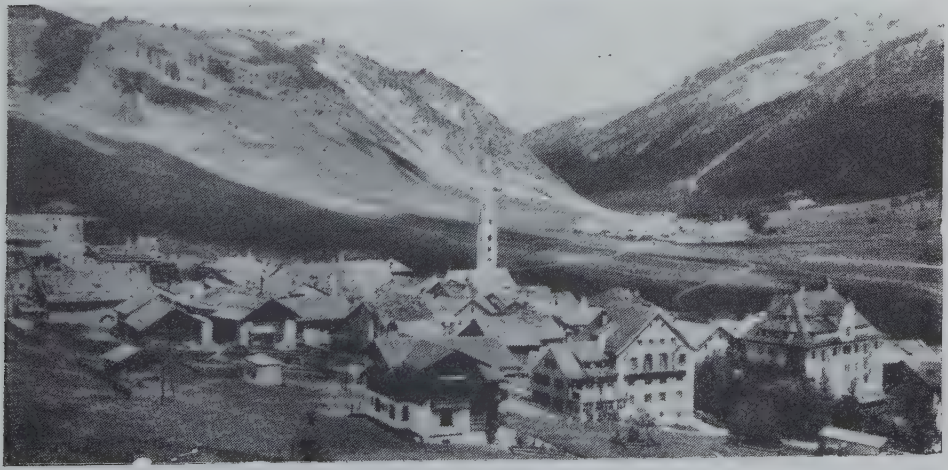

Fig. 24. Landscape selected for illustrating distortion-free image-formation

up the image while the reflector prism 1 continues to revolve, and mount 12 travels to the next field section. Thereupon, the next slit of the sector disc once more exhibits the image. The instrument projects on screen 9 the pictures formed of the successive sections of field by the reflector prism 1. Each picture section appears but for a short time, so that rapid projection produces a coherent panoramic picture band. Fig. 27 represents the procedure of forming a picture band, whereas the picture thus obtained is shown in Fig. 28. However, said picture is not satisfactory as regards definition. It is proposed therefore to modify the system, to work in the manner known for motion picture projectors. The reflector prism will thus revolve intermittently instead of revolving continually. The reflector prism as well as the rotary sector disc and mount 12 will be stopped for a short time during each projection, in the direction of the field of the respective picture section. The systems is either mechanically controlled by means of a maltese cross or a scanning arm arrangement, or it is fitted with optical diffraction elements. These latter optical elements will be treated in a forthcoming paper.

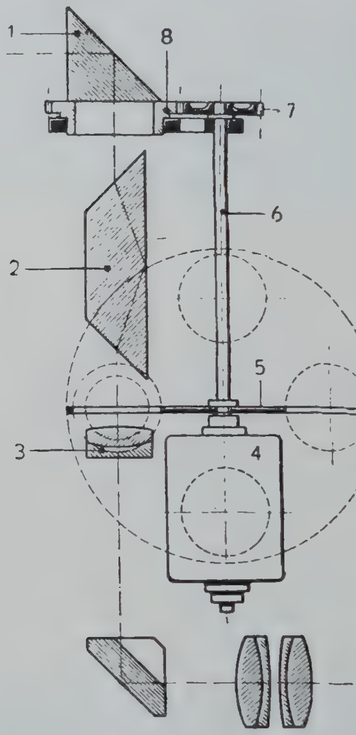

Fig. 25. Rotating-screen arrangement for producing distortion-free panoramic images

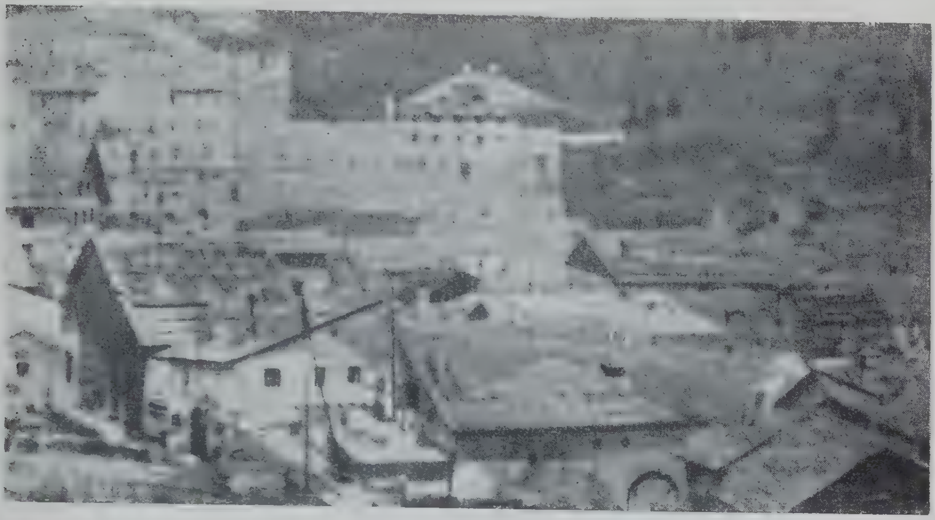

Fig. 26. Image formed by the arrangement shown in Fig. 25

The working of the instrument makes it clear that projection is periodic. It has been found that the human eye, if subjected to continual stimuli of short duration, reacts in an interesting way. The phenomena associated herewith are too complex, and dependent upon too many factors, to be described here in detail. Summarized results, however, offer a basis for computation of image frequency and film speed for panoramic projection which in turn may provide helpful information for the design of the instrument.

Low frequences may bring about the unpleasant sensation of the separation of impressions. For higher frequencies the phenomenon is called flicker, and it is called scintillation for still higher frequencies. High frequency causes the successive stimuli to merge, giving rise to a uniform sensation of light. According to the Talbot—Plateau law a rapid succession of light stimuli induces a sensation equivalent to continual light stimuli over the scintillation limit, if the amount of light prevailing for the periodic stimuli is uniformly distributed overt the whole stretch of time. The sensation of light of short duration being the product of the duration of the sensation with the illumination of the retina or with the luminous flux, respectively, it follows that for the sensation it is the amount of light that matters. For duration of the sensation is independent of the wave length of the radiating energy. The Talbot—Plateau law plays an important part in cinematography and scintillation photometry, thus it is essential, with a view to image projection, to be acquainted with the limit of scintillation and the frequency of merging. This latter for vision has different values by rods and by cones, respectively, and is also dependent on the adaptation of the eye (Ferry—Porter law). For the purposes of the present study we are interested in the minimum value. Assuming similar conditions, this minimum value is reached, if light-dark ranges are equal for frame repetitions. According to this rule, picture frequency is 25 sec. for up-to-date motion-picture-projection. Taking as a basis the general density of luminous flux of the projection screen, 50 light-dark range picture repetitions are required for the frequency of merging. In order to obviate scintillation, a rotary sector disc is provided producing two succeeding obscurations of equal duration.

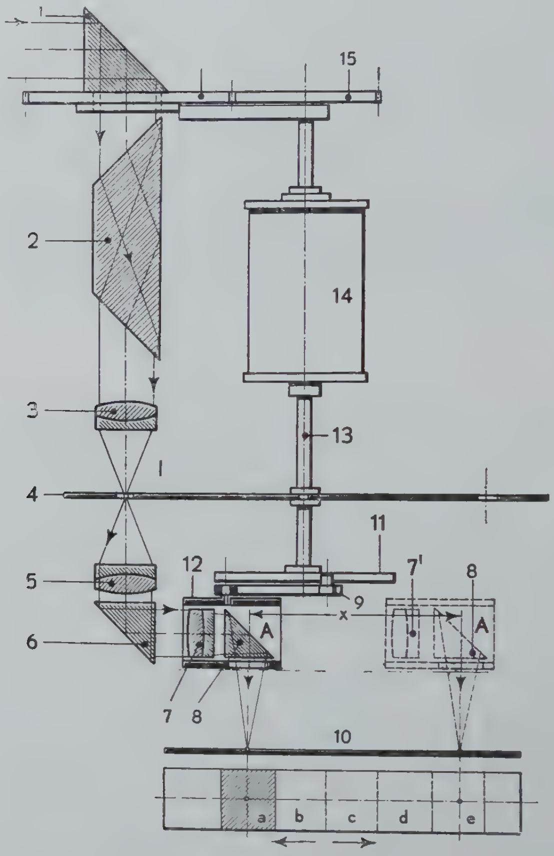

Fig. 27. Formation of a distortion-free panoramic image by the use of a rotating screen and a projector prism of alternating motion

A variation of this procedure is used in connection with panoramic projection. However, frequency of merging should be determined by tests, since the lower this value, the lesser the revolution per minute of the projecting prism, and the speed of the film. With a frequency of 25/sec as starting point, one obtains approximately the following results :

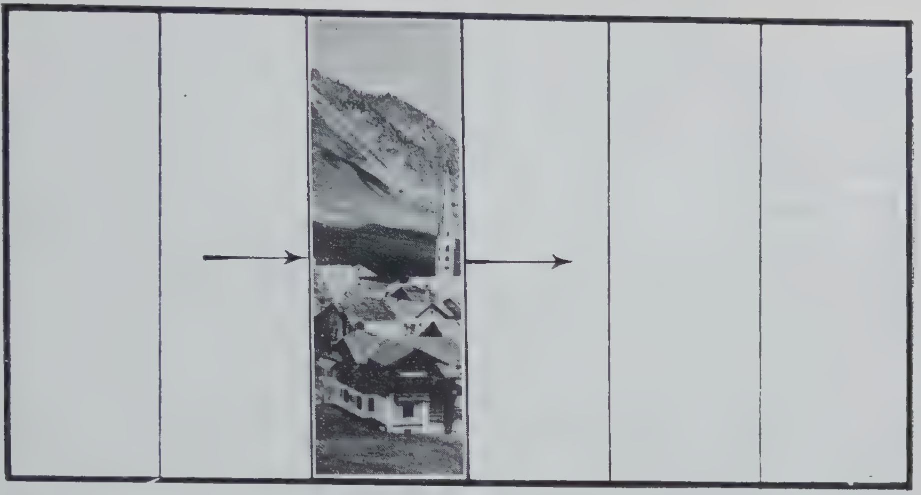

Fig. 28 Explanation of the distortion-free panoramic image obtained by the use of the arrangement diagrammed in Fig. 26

Let the convenient angle of image for the projection be 30°. One picture section is always projected within this angle. The number of picture sections for one revolution of the prism is 360 : 30 = 12. Since each picture section is individually projected on the corresponding spot with the 25/sec frequency assumed, the revolution per minute of the prism is 12 by 25 = 300/sec or 18.000/min. Dividing now one picture frame of the normal cinematographic film into two equal portions, the frame repetition frequency amounts to 150/sec.

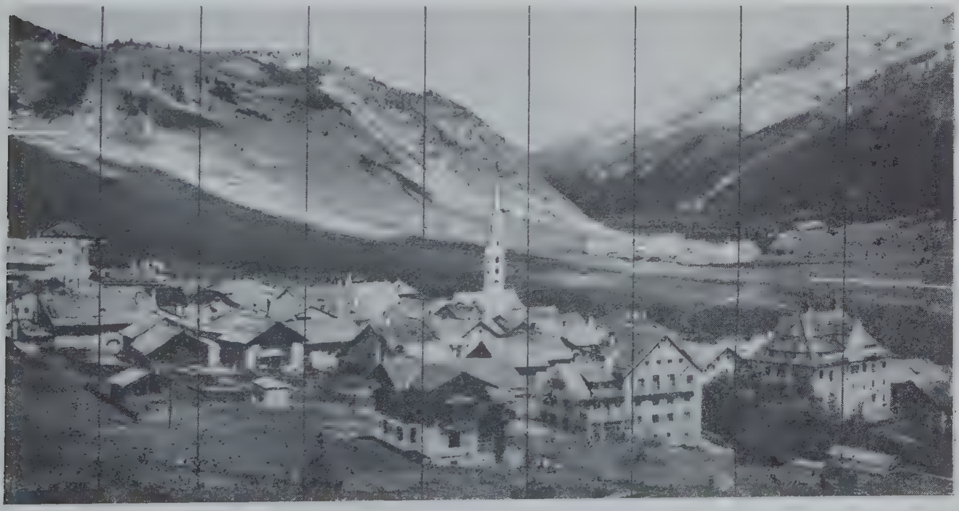

Fig. 29. Distortion-free panoramic image composed of juxtaposed band images

The above figures should be considered as only rough approximations, intended as general information. Only the realization in practice of the instrument may confirm the assumption, that the revolutions per minute of the reflector prism may be still further reduced. Thus, in the event of projection with inverted optical path, the instrument may be so constructed, that the revolving prism scans the picture frames travelling in opposed direction. Another solution envisaged is to use a semicircular projecting screen instead of a circular one. Preference is given to the semicircular arrangement, because the constancy of image distance, and, in consequence, of definition, can only be ensured by placing the projecting apparatus in the centre of the circle.

For the telescopic projection of the whole horizon the length of the picture band is dependent on the real field of vision of the telescope, amounting to 10 to 14° for the telescopes described. The diameter of the circular field of vision is 20 mm, equalling the length of one side of the circumscribed quadrangle. The number of pictures produced during one revolution of the prism is $360 : 12 = 30$ so that the full length of the band picture is 600 mm. This type of panoramic picture reproduces the whole horizon, thus, the right-hand and left-hand ends of the picture belong together. If, for example, the picture represents an automobile passing along the picture band from left to right, the portion of the car disappearing at the right-hand extremity of the picture will appear at the left-hand extremity. Let us mentally bend the band picture into a cylindrical surface, and the observer stationed in the centre will see a full panoramic picture. The size of the picture is, of course, so small that only the unaided eye may view it from a short distance.

It will be noted that a number of unforeseen and sometimes contradictory optical, optomechanical and psychological factors may eventually play an important part in the projection of circular or semicircular distortion-free pictures.

It is assumed that the principle disclosed may be used to advantage in fields of investigation other than the projection of images.

Summary

The common characteristic of the above described image-forming systems is, that they bring about full panoramic (circular) images either by mechanical means, such as systems of rotary prisms or revolving telescopes, or by optical means where the panoramic image is produced by annular lenses, or by a combination of the two methods.

It is clear from the foregoing, that all optical or optomechanical principles have already been applied for producing panoramic images. These principles may be summarized as follows :

1. Image formation is discontinuous for wide-angle photographic lenses. True, the images obtained are free from distortion, yet these instruments are unsuitable for producing telescopic images, owing to their short focal lengths, which do not allow of considerable magnification and, in addition, the relative apertures of such systems are rather small.

2. Speaking of systems of continuous image formation, the panoramic images formed by annular lenses or annular mirror lenses suffer from serious distortions. Moreover, their mag-

nifying power is relatively low from the viewpoint of telescopes, whereas their cost of production are rather high.

3. Images of the entire horizon can only be obtained by means of lenses of the Hill type, but the images are heavily distorted at the margins. These lenses occupy an intermediate position between photographic and ring lenses.

4. Systems forming panoramic images composed of sections have the advantage of yielding undistorted images of satisfactory magnification and visual field. Both the multiple telescopes and the Lippert telescopes produce discontinuous panoramic images, and require a number of telescopes, each to be separately adjusted. Manufacture of these devices are rather elaborate and costly. The following facts must also be noted in regard of observation :

The panoramic image is afflicted with heavy distortion ; unsatisfactory magnifying power and unnatural perspective renders discrimination of the objects difficult.

Whether the scanning of the horizon by means of the swinging reflector prism is continuously or discontinuously, effected slowly or rapidly, a full command over the entire field can only be achieved by taking advantage of the observer's visual memory. In case of a change in the sighting line, determination of the relative position in relation to the basic direction, that is, orientation, is rather cumbersome, even if accessory instruments are employed.

The target is to produce wide-angle, undistorted panoramic images of high magnification, permitting simultaneous coverage of the whole field.

Professor N. BÁRÁNY Budapest XI., Gombocz Zoltán utca 17, Hungary.

EXPLANATION OF THE SO-CALLED “SOUND DETONATION”

By

I. Bihari and M. Kelemen

Department for Mathematics I, Polytechnic University, Budapest

(Received May 31, 1957)

A few months ago a great detonation was heard in the neighbourhood of the Polytechnic University in Budapest. It caused no damage. The explication of this phenomenon given by the newspapers was by no means clear. The explosion was probably effected by a jet engine. The real explanation is as follows.

The question is: What should be the path and speed of a jet plane if there is a point in space to which the sound waves emitted by the jet engine along its course arrive simultaneously (from every point of its path).

First the movement will be assumed to be a two-dimensional one. The following denotations will be used (t. Fig. 1):

equation of the orbit in polar coordinates: $r = r(\varphi)$,
initial position of the airplane (at time $t = 0$) : P_0,
position at time $t : P$,
center of the sound detonation occurring[1] at time $t' > t : A$,
speed of the sound: c,
speed of the airplane (assumed to be constant): v,
length of the arc $\overset{\frown}{P_0P}$: s,
length of the radius vector of P_0 resp. P: r_0 resp. r.

Thus we have

$$r_0 = c\,t', \quad r = c\,(t' - t), \quad t = \frac{s}{v}.$$

Hence

$$r = c\,t' - c\frac{s}{v} = r_0 - \frac{c}{v}s.$$

By derivation[2]

---

[1] A is assumed to be in the plane of the movement.

[2] Equation (1) expresses the fact that the tangent of the path must intersect the radius vector at a constant angle depending on $\frac{c}{v}$.

$$\frac{d\,r}{d\,\varphi} = -\frac{c}{v}\,\frac{d\,s}{d\,\varphi} = -\frac{c}{v}\sqrt{r^2+\left(\frac{d\,r}{d\,\varphi}\right)^2}\,, \tag{1}$$

whence

$$(v^2-c^2)\left(\frac{d\,r}{d\,\varphi}\right)^2 = c^2\,r^2\,.$$

This equation is meaningless unless $v > c$, i. e. the speed of the airplane exceeds the velocity of the sound. — The differential equation (1) is of the simplest type and has the general solution

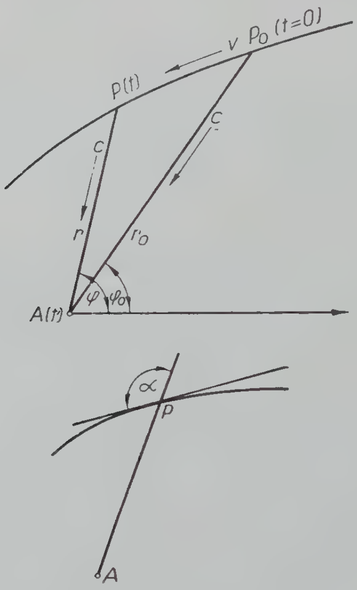

Fig. 1

$$r = k\,e^{\pm\frac{c}{\sqrt{v^2-c^2}}\varphi}\,,$$

(k is an arbitrary positive constant) and thus we come to the conclusion that : in order to cause a sound detonation the airplane must fly on a logarithmical spiral around the point A and the tangent of the path must intersect the radius vector at an angle α for which

$$\operatorname{tg}\alpha = -\frac{\sqrt{v^2-c^2}}{c} \quad \text{or} \quad \cos\alpha = -\frac{c}{v}\,. \tag{2}$$

The airplane must travel along this track toward point A.

An alternative proof[3] may be based on the fact that during a time dt the ways covered by the airplane resp. the sound are $v \cdot dt$ resp. $c \cdot dt$ and that thereafter the sound has the same ways $P'A = QA$ to cover. Hence

$$\cos(\pi - \alpha) = -\cos\alpha = \frac{c}{v}$$

and — as known — a curve intersecting all the radius vectors at a constant angle can be nothing else than a logarithmical spiral. Provided $v = c, \alpha = 0$ or π.

Assuming $\alpha = 0$ the jet plane will move away from A in a straight line and no sound-detonation occurs.

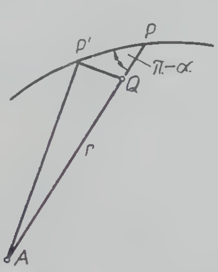

Fig. 2

Supposing $\alpha = \pi$, the airplane approches to point A at the velocity of the sound and causes a sound detonation when reaching A.

Finally, if the airplane is travelling toward point A at a speed $v > c$, no sound-detonation will occur, but it is interesting to note that the sound-signs sent out by the airplane arrive at A in reversed order.

The orbit tends to be a circular one provided $v \to \infty$.

Let the sound energy emitted per second by the airplane be denoted by J. Then the sound energy arriving simultaneously in the immediate neighbourhood of A may be easily computed:

$$E = \frac{J}{4\pi} \int_0^t \frac{dt}{r^2} = \frac{J}{4\pi v} \int_0^s \frac{ds}{r^2} = \frac{J}{4\pi v} \int_{\varphi_0}^{\varphi} \frac{1}{r^2} \frac{ds}{d\varphi} d\varphi$$

and making use of (1)

$$E = \frac{J}{4\pi v} \frac{v}{c} \int_{\varphi_0}^{\varphi} \left(\frac{-\dfrac{dr}{d\varphi}}{r^2} \right) d\varphi = \frac{J}{4\pi c} \left(\frac{1}{r} - \frac{1}{r_0} \right).$$

---

[3] Suggested by P. Sonkoly.

This energy can increase arbitrarily by the decrease of r but a very small r cannot be realised. What is the effect caused by the momentary appearance of the above energy at A? At all events a terrifying one, but the authors know nothing else about it.

Assuming the movement to take place in space let us denote the radius vector of P by $\bar r = \bar r(p)$ and its derivative according to the parameter p by $\dot{\bar r}$, thus we obtain from (1)

$$\frac{d\,|\bar r|}{d\,p} = -\frac{c}{v}\,|\,\dot{\bar r}\,| \tag{3}$$

and we are faced with the problem, wether there are or not — on an arbitrarily prescribed surface — paths satisfying (3) and what should the surface, the constant velocity v and the path be in order to produce a sound detonation.

Assuming the equation of the surface by means of two parameters p, q in the form

$$x = x\,(p, q)\,,\quad y = y\,(p, q)\,,\quad z = z\,(p, q)\ ^{4}$$

and equation of the path to be $q = q(p)$ we have

$$|\,\bar r\,| = \sqrt{x^2 + y^2 + z^2}\ ,\quad |\,\dot{\bar r}\,| = \sqrt{E + 2\,F\,\dot q + G\,\dot q^2}$$

where

$$E = x_p^2 + y_p^2 + z_p^2\,,\quad F = x_p\,x_q + y_p\,y_q + z_p\,z_q,\quad G = x_q^2 + y_q^2 + z_q^2$$

and substituting this in (3)

$$\frac{x\,(x_p + x_q\,\dot q) + y\,(y_p + y_q\,\dot q) + z\,(z_p + z_q\,\dot q)}{\sqrt{x^2 + y^2 + z^2}} = -\frac{c}{v}\sqrt{E + 2\,F\,\dot q + G\,\dot q^2}\ .$$

This equation is an ordinary differential equation of the first order for $q = q(p)$ in the form of $F(p, q, \dot q) = 0$ and always has a solution either real or complex, since it is for $\dot q$ an algebraic equation of the second degree.
This may be written

$$(v^2\,H^2 - c^2\,r^2\,G)\,\dot q^2 + 2\,(v^2\,H\,I - c^2\,r^2\,F)\,\dot q + (v^2\,I^2 - r^2\,c^2\,E) = 0\,, \tag{4}$$

where

$$H = x\,x_q + y\,y_q + z\,z_q\,,\quad I = x\,x_p + y\,y_p + z\,z_p\,.$$

Equation (4) has real solutions provided

$$D = c^2\,r^2\,(F^2 - E\,G) + v^2\,(H^2\,E - 2\,H\,I\,F + I^2\,G) \geqq 0\,.$$

---

[4] Assumed to be continuously derivable in p, q.

Therefore, assuming $D \geqq 0$ in a neighbourhood of P_0 (e. g. $F^2 - EG \geqq 0$, $H^2E - 2\,HIF + I^2G \geqq 0$), this point will be crossed by two (in limit case one) paths existing in the same region of P_0. Flying along these paths the airplane will produce a sound detonation in the origin.

Let us now examine the intuitive geometrical side of the problem.[5] On an arbitrary surface a curve is to be constructed starting from P_0 and intersecting all the radius vectors at an angle α for which $\cos\alpha = \dfrac{c}{v}$. Supposing that the normal vector $\bar{n}$ of the surface forms an angle β with the radius vector,

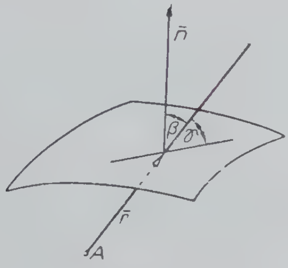

Fig. 3

all the tangents of the surface in P_0 form with the radius vector an angle γ for which $90° - \beta \leqq \gamma \leqq 90° + \beta$. Since P_0 has a neighbourhood where the condition $90° - \beta < \gamma < 90° + \beta$ is satisfied, we can construct step by step a polygonal path and from this by a limit passage a path starting from P_0 and intersecting all the radius vectors at the angle α, provided $90° - \beta < \alpha < 90° + \beta$.

An example. Let us determine the resp. paths on a circular cone. Let the axis of the cone be the axis z and the cylindrical coordinates of P be p, q and z. Since

$$x = q\cos p\,,\ y = q\sin p\,,\ z = z(p)\,,\ q = q(p)\,,\ |\bar{r}| = \sqrt{q^2 + z^2}\,,\ |\dot{r}| = \sqrt{q^2 + \dot{q}^2 + \dot{z}^2}$$

we obtain from (3)

$$\frac{q\,\dot{q} + z\,\dot{z}}{\sqrt{q^2 + z^2}} = -\frac{c}{v}\sqrt{q^2 + \dot{q}^2 + \dot{z}^2} \quad \text{or} \quad v^2\,(q\,\dot{q} + z\,\dot{z})^2 = c^2\,(q^2 + \dot{q}^2 + \dot{z}^2)\,(q^2 + z^2).$$

The surface will be a cone with its vertex in the origin, provided $z = \lambda q$, where λ is a constant. Then from the last equation

$$(\lambda^2 + 1)\,(v^2 - c^2)\,\dot{q}^2 = c^2\,q^2\,,$$

---

[5] Suggested by E. MAKAI.

whence again $v > c$, and

$$q = k\,e^{\mu p} \quad \left(\mu = \frac{1}{\sqrt{\lambda^2+1}}\,\frac{c}{\sqrt{v^2-c^2}} \quad \text{and} \quad k > 0\right).$$

The equation of the orbit is

$$x = k\,e^{\mu p}\cos p\,, \quad y = k\,e^{\mu p}\sin p\,, \quad z = \lambda\,k\,e^{\mu p}\,,$$

i. e. the path is a helix on the cone and the tangent of the path intersects the radiusvector at a constant angle. Reversely, given this angle the cone will be determined. The only place of the sound detonation can be the vertex of the cone.

Case of variable velocity

I. *Movement in a plane*

1. Let the velocity be given a function of the way covered (i. e. of the length of the arc of the path) : $v = v(s)$. Then from equation

$$d\,r = -\,c\,\frac{d\,s}{v\,(s)} = -\,c\,d\,t$$

we have

$$r - r_0 = -\,c\int\limits_0^s \frac{d\,s}{v\,(s)} = F\,(s) = -\,c\,t\,, \tag{1}$$

hence $s = \Phi(t)$. Since

$$\sqrt{v^2-c^2}\,\frac{d\,r}{d\,t} = c\,r\,\frac{d\,\varphi}{d\,t} \quad \text{and} \quad \frac{d\,r}{d\,t} = -\,c$$

we get

$$\frac{d\,\varphi}{d\,t} = -\,\frac{\sqrt{v^2-c^2}}{r} = -\,\frac{\sqrt{\bar{v}^2-c^2}}{r_0-c\,t}\,,$$

where

$$\bar{v} = v\,(t) = v\left(\Phi\,(t)\right).$$

Finally,

$$\varphi - \varphi_0 = -\int_0^t \frac{\sqrt{\bar{v}^2 - c^2}}{r_0 - c\,t}\,d\,t \qquad \left(t < \frac{r_0}{c}\right). \tag{2}$$

Equations (1) and (2) yield φ and r as functions of t. Eliminating t we obtain the polar equation of the path. r depends always linearly on t.

2. Let the velocity be a prescribed function of the time : $v = v\,(t)$. Then we obtain in the same manner

$$r - r_0 = -\,c\,t \tag{1'}$$

$$\varphi - \varphi_0 = -\int_0^t \frac{\sqrt{v^2 - c^2}}{r_0 - c\,t}\,d\,t\,. \qquad \left(t < \frac{r_0}{c}\right) \tag{2'}$$

Let us prove the following statement :

In order to cause a sound detonation in the origin an arbitrary path may be chosen.

This can be seen very easily.

Let the path be given in the form of $r = r(\varphi)$. From equations

$$\frac{d\,r}{d\,\varphi} = -\,\frac{c}{v\,(\varphi)}\,\frac{d\,s}{d\,\varphi}\,, \quad s = s\,(\varphi)\,, \quad \varphi = S\,(s)$$

$v\,(s)$ may be determined since $\dfrac{d\,r}{d\,\varphi}$, $\dfrac{d\,s}{d\,\varphi} = \sqrt{r^2 + \left(\dfrac{d\,r}{d\,\varphi}\right)^2}$ are known quantities. Then by $s = \Phi\,(t)$

$$v = v\,(s) = v\,(\Phi\,(t)) = \bar{v}\,(t)\,.$$

A sound detonation will occur provided the path will be run at this speed. Giving the path by a parameter τ in the form

$$r = r\,(\tau)\,, \quad \varphi = \varphi\,(\tau)$$

we obtain

$$r\,(\tau) = r\,(t) = r_0 - c\,t$$

whence

$$\tau = f(t) \quad \text{and} \quad \varphi = \varphi\,(f(t)) = \psi\,(t)$$

and comparing this to (2′)

$$\varphi = \varphi_0 - \int_0^t \frac{\sqrt{v^2 - c^2}}{r_0 - c\,t}\,d\,t = \psi\,(t)$$

and by derivation

$$-\frac{\sqrt{v^2 - c^2}}{r_0 - c\,t} = \psi'(t)\,,$$

whence we find

$$v = v(t) = \sqrt{c^2 + (r_0 - c\,t)^2\,\psi'(t)^2}\,.$$

II. *Movement in the space*

1. Let us prescribe a surface and the velocity for the movement in all points:

$$x = x(p, q)\,,\ y = y(p, q)\,,\ z = z(p, q)\,,\quad v = v(x, y, z) = \bar{v}(p, q)\,,$$

then for the determination of the path on the surface we obtain the same differential equation as in case of a constant velocity. Only v should be replaced by $v(p, q(p))$. The equation will be

$$\dot{q}^2(v^2 H^2 - c^2 r^2 G) + 2\,\dot{q}\,(H\,I\,v^2 - c^2 r^2 F) + (I^2 v^2 - c^2 r^2 E) = 0\,. \tag{3}$$

Every point P_0 of the surface will be crossed by two (in limit case by one) paths provided

$$D = c^2 r^2(F^2 - G\,E) + v^2(H^2 E - 2\,H\,I\,F + G\,I^2) \geqq 0 \tag{4}$$

in some neighbourhood of P_0.
Inversely, given the curve $q = q(p)$ on the surface, $v = v(p)$ may be computed from (3) provided $D \geqq 0$ in some region of P_0.

2. Let us take now an arbitrary curve of the space:
Prescribing the speed arbitrarily no sound detonation will occur. In order to produce the phenomenon, equation

$$\frac{d\,|\bar{r}|}{d\,\tau} = -\frac{c}{v(\tau)}\,|\dot{\bar{r}}| \qquad \left(\dot{\bar{r}} = \frac{d\,\bar{r}}{d\,\tau}\right)$$

must be satisfied. $v(\tau)$ may be determined herefrom since $\dfrac{d\,|\bar{r}|}{d\,\tau}$ and $|\dot{\bar{r}}|$ are known quantities. By means of the equations

$$t = \int\limits_{\tau_0}^{\tau} \frac{1}{v(\tau)}\,\frac{d\,s}{d\,\tau}\,d\,\tau = \int\limits_{\tau_0}^{\tau} \frac{1}{v(\tau)}\,|\dot{\bar{r}}|\,d\,\tau = F(\tau)\,,\ \tau = \Phi(t)$$

we obtain

$$v = v(\tau) = v(\Phi(t)) = \bar{v}(t)$$

and thus

$$x = x(\Phi(t)) = \bar{x}(t)\,.$$

$y = \bar{y}(t)$, $z = \bar{z}(t)$ may be computed similarly.

Summary

This paper gives the explanation of the so called „sound detonation”. It is proved here that a jet engine can produce a sound detonation covering an arbitrary path in the space and the speed depending on the path and necessary for this end is determined too.

I. Bihari
M. Kelemen
Budapest XI. Budafoki út 4—6, Hungary.

NEW ACOUSTICAL METHOD OF VACUUM MEASUREMENT

By

J. ANTAL and A. KŐNIG

Physical Institute, Polytechnic University, Budapest

(Received June 10, 1957)

1. Introduction

In vacuumtechnique pressures to be measured most frequently are in the region a few times 10^2 mmHg to 10^{-5} mmHg. There are several kinds of meters which are capable of measuring the actual pressure in this interval, but none of them can be used in the whole region. The different kinds of meters can be practically devided into two groups, one of them measuring the region above 10^{-3} mmHg, while the other operates below 10^{-3} mmHg.

It is to be noted that instruments belonging to the first group have a limited range of measurement lying between 1 and 10^{-3} mmHg, and there are only a very few of them whose upper limit of measurement can be extended as far as the atmosphere. However it is quite possible to construct meters for the interval 1—760 mmHg e. g. a simple U-type mercury manometer should be used.

Some types of vacuummeters can be regarded as absolute ones, while the rest must be calibrated against an absolute meter. The most common absolute manometer for this purpose is the so-called McLoad gauge.

2. Acoustical method for determining pressures

To explain the method let us place, for the sake of simplicity, a loudspeaker and a microphone in a chamber in which a certain given pressure exists. Connect the loudspeaker to an audio frequency generator set to a proper frequency. Then the loudspeaker will radiate sound energy in the chamber. Let the microphone be connected to a suitable vacuumtube voltmeter, then this will indicate the *ac* voltage generated by the sound energy received by it.

The energy is chiefly transferred from loudspeaker to microphone by the aid of the medium existing in the chamber i. e. by the air molecules (neglecting the conduction through the rigid parts of the system), therefore the voltage output of the microphone will vary with pressure in a definite way, supposing constant loudspeaker input and absence of any other noise in the chamber.

It can be easily seen that by this simple method it is possible to determine pressures to such a low value below atmosphere, at which the radiated energy is comparable to that one picked-up by conduction.

3. A first-order theory of the method

A simple approximate theory will be given for the proposed method. Only the ideal case is treated, supposing a tube with movable membranes on its both ends (Fig. 1) and neglecting any conduction, reflexion (interference) and noise.

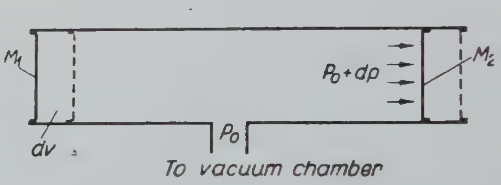

Fig. 1

Let us suppose that in this tube a given pressure p_0 exists, and let the membrane M_1 move to a distance dx so, that the volume v of the tube will be smaller by dv. Then the pressure in the immediate vicinity of the membrane M_1 will increase, and this increase of pressure will extend through the tube till it reaches the other end of the tube, where it will act on the membrane M_2 and causes it to move outwards, resulting in some increase of volume.

Let us suppose that the whole process will be adiabatic, then for ideal gases, and so in good approximation for air, too

$$p_0 \cdot v^{\varkappa} = \text{const}\,.$$

So

$$dp \cdot v^{\varkappa} + \varkappa \cdot p_0 \cdot v^{\varkappa-1} \cdot dv = 0$$

and finally:

$$dp = -\varkappa \cdot p_0 \cdot dv/v\,.$$

It can be seen, that with constant loudspeaker input (i. e. $dv = \text{const.}$) the change of pressure at the microphone, dp, will linearly vary with the existing pressure p_0, that is the instrument will have a linear scale.

It must be emphasized that this simple explanation is only a very first-order theory, neglecting for example, reflections from the walls of the tube, which result in a strange response regarding the applied frequency, because of the possibility of interference. The applied frequency should not be too low, because noises are always present.

As is mentioned above there is energy transfer, not only by radiation, but also by the aid of conduction. This will determine practically the lower end of the measurable region.

4. Experimental results and remarks

Several measurements were made and the mentioned linearity was found through a region ranging from atmosphere to a few times 10^{-2} mmHg. In these measurements carried out a various pressure, care was taken, to the change in acoustical impedance of the loudspeaker and microphone.

The measurements were made by crystal loudspeakers and microphones and also in some cases with dynamic loudspeakers. The applied frequency varied from 500—10 000 c/s, and sometimes a highpass filter was used at the microphone-end to prevent of undesirable response caused by noises.

It was found, that in all cases this simple measuring arrangement could be used for pressure measurements from atmosphere till $5 \cdot 10^{-2}$ mmHg. However, it is possible to extend the lower end by diminishing conduction with the aid of suitable acoustically damping materials.

An instrument based on this principle can be regarded as an absolute meter, or at least as a semi-absolute one, having a linear scale and can be calibrated at atmospheric pressure.

An absolute meter, however, should not need any calibration, as its geometrical dimensions are quite enough to calculate the pressure. The discribed method above gives a linear relation which enables us to calculate the scale till a numerical factor which is to be determined by calibration for example at atmospheric pressure.

For a more accurate treament of the theory of this method as well as for the realization of the instrument including the possibility of the application of pulsed sources to prevent conduction we refer to our next article to be published in the near future.

Acknowledgement

We are indebted to Professor P. Gombás for the kind permission to perform this work in the Institute, as well as to Mr. E. Fazekas for his valuable assistance in the measurements.

Summary

A new acoustical method is presented for measuring pressures lower, than atmosphere. Based on this principle it is possible to construct an absolute vacuumeter, the usuable range of measurement of which extends from atmosphere, to below the micron-mercury region. Some practical remarks are also given for the actual construction of such instruments, and for the possibilities to extend the lower limit of measurement.

J. Antal
A. Kőnig
Budapest XI. Budafoki út 8. Hungary.

BOOK REVIEW — BUCHBESPRECHUNG

Electric Machinery Vol. III. Synchronous Machines

by J. Liska, with the co-operation of A. Mándi. Tankönyvkiadó, Budapest 1955. 332 pp. 320 figs.

The present book written by Professor J. Liska, as the third volume of his comprehensive work on Electric Machinery, was preceeded by the publication of Vols. I and II on transformers and d. c. motors, respectively, and Vol. V, written together with several co-authors describing the design principles of electric machinery. The present volume is an excellent textbook dealing with the theory and practical designing of synchronous machines.

As regards the structure of the book three main parts may be distinguished. Chapters I to VIII contain the necessary basic information on the operation of synchronous machines including a detailed treatment on the theory and practical applications of the work diagram and vector diagram, respectively.

The second main part comprises Chapters IX to XIII devoted to winding and wiring problems of synchronous machines. Corollary to this subject matter a discussion on the magnetic circuit is given.

The last part including Chapters XIV to XXIV provides detailed information on characteristic curves of the machine, as well as on the determination of data required for the computation of several characteristics, such as the necessary excitation values, reactances and losses. Chapters on the parallel operation of synchronous generators, on synchronous motors, on hunting phenomena of synchronous machinery as well as on sudden changes in operating conditions (the problem of short-circuits) as well as a detailed description of the testing methods of synchronous machines, together the full design computations of two of them have also been included in this part. Besides the computation procedure the reader becomes familiar with observed data of these actually constructed machines. Values obtained by computation may thus directly be compared with results of these actually conducted.

Chapter XXV. contributed by A. Mándi, presents original and theoretically well substantiated ideas on the heating problems of synchronous machines including turbo-generators.

The careful selection of subject matter from the very wide and divergent material minute distinction between essential and non-essential topics, between important subjects and subjects less interesting in the practical sense make this outstanding even among foreign publications of similar nature. We refer hereby in the first place to the great comprehensive monographies by Arnold, Richter and Liwschitz. As will be revealed by a closer study of the book, Professor Liska includes, with the accuracy and modesty of an excellent teacher, only such chapters as are essential for satisfying the needs of education and introduces the subject in an advanced form meeting the approval of the practical engineer as well. The omittance of obscuring details contributes to the clearness and at the same time to the unsefulness of this handbook. The essential chapters of the comprehensive material have been written by Professor Liska in a systematic, coherent and clear fashion. A new, excellent book of reference of the highest technical standard has thereby been made available to Hungarian electrical engineers.

K. P. Kovács

THE IMPACT OF ELECTRONICS ON MODERN INSTRUMENTATION

By

G. Striker

Electronic Instruments' Branch, Dept. of Electrical Engineering, Polytechnic University, Budapest

The application of the newest achievements of physical sciences to the field of measurement and instrumentation has in recent years gained more and more recognition as an independent science of its own. [1, 2, 3, 4.] The wide range of new measureables and the complexity in applying the recent technical achievements to the design of technical and scientific instruments amply justify such a view. Few will disagree with the renowned scientist Dr. Wildhack of the US Bureau of Standards, when he writes [2] :

"It is easy to foresee an increased recognition for the science of instrumentation. Expect for atomic energy, the development and application of instrumentation probably have greater potential material significance for our age and our civilization than any other factor on the contemporary scene. This seems valid militarily, industrially, and scientifically."

The significance of the new science of "instrumentation" has increased with particular rapidity since the spectacular growth of electronics during the past decade. A row of ingenious scientific devices came into being as a result of combining modern physics with the newest technique of electronic circuitry. With the help of the achievements attained in the field of instrumentation, entire new branches of science were established in some cases. This in itself is not new in the history of natural sciences — let us only remember the tremendous impact given to the science of geophysics by the discovery of the gravitational torsion balance by Roland Eötvös. Or, has the simple device known as the Wilson-chamber not revolutionized our knowledge of the nucleus and started an entirely new branch of atomic science? The same may be said of the effect of such instruments as the X-ray powder spectrograph, the mass-spectrograph of Niehr or the n. m. r.-spectrometer — all of which have opened up new chapters in physics and physical chemistry.

Electronics, however, seem to hold an especially valued place in up-to-date development of scientific and industrial instruments. The ratio of devices employing some application of electronics is continuously growing, even in such "conservative" fields as that of spectroscopy, with spectrophotometry and quantometry taking an ever greater share. Knowing the numerous shortcomings and complexities of electronic components and circuits, due in part to the relatively large manufacturing tolerances and limited service life of electronic tubes and other components, as well as the not too exact methods of eletronic circuit design — one may wonder about the factors which justify the wide use of electronics in modern instrumentation, despite these shortcomings. It is the aim of this short study to systematically expose some of these factors.

What does electronics offer to instrumentation?

The electron tube — or, as the British usage more figuratively says : the electron valve — constitutes a current-valve of exceedingly small inertia, requiring minute controlling power. These two properties determine its great value for the instrument designer whose primary aim is to interfere as little as possible with the process under measurement (i. e. not to draw any power from it) and to obtain practically momentary response. Three further characteristic features offered by electron tubes: large amplification, high input impedance and the ability to generate high-frequency voltages or short pulses, are closely connected with the two basic properties mentioned and the combination of these characteristics cannot be found at present in any other device. Let us see how these properties are applied to the measurement of various data.

a) The *amplification* obtainable with electron tubes enables us to measure *voltages* down to a *few microvolts* or — in the case of a very restricted frequency range — voltages as low as *10^{-8} Volt.* Such an amplification is usefully employed in certain magnetometers for the precise measurement of the earth's magnetic field, in radiation detectors for infrared spectrophotometers, and in such special devices as the microwave power-levelmeter developed by the Hungarian Telecommunication Institute. This instrument, using a thermistor to transform the microwave energy of a few microwatts into a resistance variation, uses a bridge-detector amplifier with a gain of 10 million and a sensitivity limit of 10^{-7} Volt. Obviously, only the application of electronic tubes can serve to solve such a problem.

b) The *lack of inertia*, inherent to electron tubes, enabled us to follow events of extremely short duration, such as those associated with nuclear fission. The "piece-meal" counting of hundred thousand pulses per second — accomplished in up-to-date high-speed scalers, as those manufactured by the Hungarian industry, as well as the observation of milli-microsecond (10^{-9}sec) fission processes, a daily routine in our Central Physics Research Institute, are good examples for the use of electron tubes as switching and amplifying devices, almost free of inertia. Another application of the fast-action feature of electron tubes is to be found in the field of microwave technique where precision signal generators are used for producing billions and ten billions of oscillations per second. The 10cm ORION—EMG Signal Generator is another good example of how this feature of modern electronics can be applied to scientific instrumentation.

c) The possibility of a *high input impedance* as mentioned above further adds to the versatile application of electronics in scientific measurement. The well-known glass electrodes for pH measurement were of as little use to the chemist, as the photo-tubes to the physicist, were it not for the ability of electron tubes to amplify voltages with almost no power drawn from the circuit under measurement. A voltage measuring circuit with an input resistance of ten billion ohm is now a matter of industrial routine, as for instance in the ORION electronic pH-meter. Moreover, in the continuous radiation meter Model GK—4 using a GM tube, an electrometer-tube circuit having an input resistance of 10^{14} ohm, enables, the measurement of currents as low as 10^{-14} ampère. No other non-electronic device can accomplish this with such simplicity, ruggedness and speed.

d) The *ease of data-transmission* over long distances is another merit of electronic measuring circuits. A combination of high-frequency technique with the inherently high sensitivity of these circuits has very recently rendered a splendid performance of electronic telemetry in combination with the IGY satellite program. A less spectacular, but more practical example of "wired" electronic telemetering is the radioactive prospecting equipment developed by our Geophysical Institute, which is capable of measuring minute traces of radioactivity (as well as a number of other data) at a depth of 2—3000 meters. It is possible by means of minute electronic components to sense only these variables in a bore hole 2 miles deep and of a diameter not over 5", and to transmit them with the accuracy of a precision measurement to the amplifying and recording mechanism above. A similar accomplishment can be seen in the famous "Laterolog" enabling the specific resistance measurement of a soil-layer not more than 20 cm in thickness at a depth of 2000 meters below the surface (shaded area of Fig. 1). This is achieved by setting up a current and potential pattern as shown in Fig. 2, and electronically stabilizing this distribution against wide variations in the resistivity of the surrounding material. The shown potential distribution assures an accurate measurement of the resistivity of the lateral earth sheet, with the unshaded areas bearing no influence on the measurement. Recent improvements made by our Geophysical Institute in the electronic amplifying and stabilizing circuitry have further added to the simplicity and accuracy of this ingenious method; a simplified reproduction of the results is shown in Fig. 3. As against the "averaged" data obtained by classical resistance measuring methods(left-hand) curve, the electronic logging system yields accurate data of the resistivity of a layer one tenthousandth as thick as its depth below the point of measurement — with the probe often being surrounded by a mud of high electric conductivity (right-hand curve) [5].

In the many different geophysical instruments produced by our industry for the accurate mapping of mineral resources, electronics is widely used for the telemetered scanning of bore holes and for the registration of artificial shock-waves in the well-known seismic investigations. Again, the fast-acting electron tube comes as an aid to accomplish what no other device can do for the prospector — the divining rod of bygone days has found its more reliable successor in the complex electronic equipment of our seismometric geophysical field laboratories (Fig. 4).

e) An entirely new aspect of instrumentation is the great increase in accuracy, accomplished through the *digital technique of data processing*. In the past, the accuracy of measurement was greatly limited by the use of scales and dials, which permit an accuracy of reading around 1% in industial devices and 1‰ by the most accurate laboratory methods, requiring laborious precaution and much time. To-day, with the use of binary and decade switching and counting circuits and special indicating tubes (decatrons, etc.), this limit no longer exists. The measurement of time-intervals and frequencies to an accuracy of *one part in a million* can now be achieved in a fast and direct way, the result being presented within a second's time on appropriate meter scales or counter tubes. The same holds true in the counting of swift events — such as cosmic showers of high-energy particles — or the revolutionary method of counting millions of red blood cells in the viewing field of a microscope — all within a matter of seconds. The so-called "cycle counter" or digital frequency meter, shown at a Hungarian Instruments Exhibition last year, is a good example of such a type of equipment. Thanks to the unique speed and versatility of electronics, the results of such digitalized precision measurements can now be further processed without loss in accuracy by the most advanced electronic tool, the *digital computing machine*, capable of handling a million binary digits per second.

In this manner the *high amplification* at almost no input power, *speed of action*, high input impedance, ease of *data transmission* and the possibility for fast *digitalized data processing*, add up to a combination of features which evidently can hardly be matched by any other means known to instrument-physicists. No wonder then, that despite its apparent drawbacks and complexity, electronics are constantly gaining space in up-to-date instrumentation.

New data-transducers for electronics

The characteristics of electronic circuitry opened up entirely new possibilities for measuring certain variables, too small, too fast changing, or otherwise not accessible to "classical" measuring methods.

Certain fundamental physical phenomena such as the changing of a wire's resistance to its physical dimensions, or the electrolytic semiconductivity of glass, suddenly find their "renaissance" in the strain gauge, using an electronic bridge indicator for measuring a dimensional change of 0,0001% — or in the glass electrode of an electronic pH meter having an input resistance of over ten thousand megohms. Minute voltages raised in a conductor moving by a few microns through a magnetic field suffice to detect and measure —

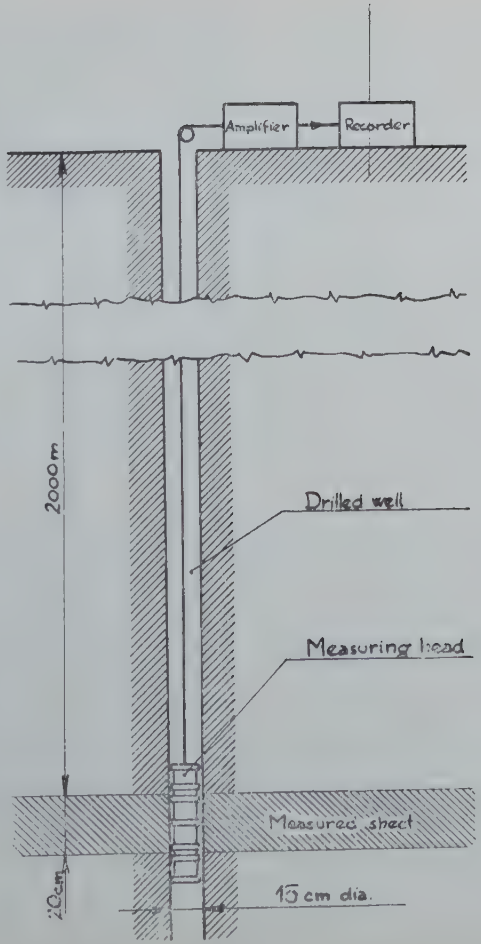
Amplifier
Recorder
2000 m
Drilled well
Measuring head
Measured sheet
20cm
15 cm dia.

Fig. 1

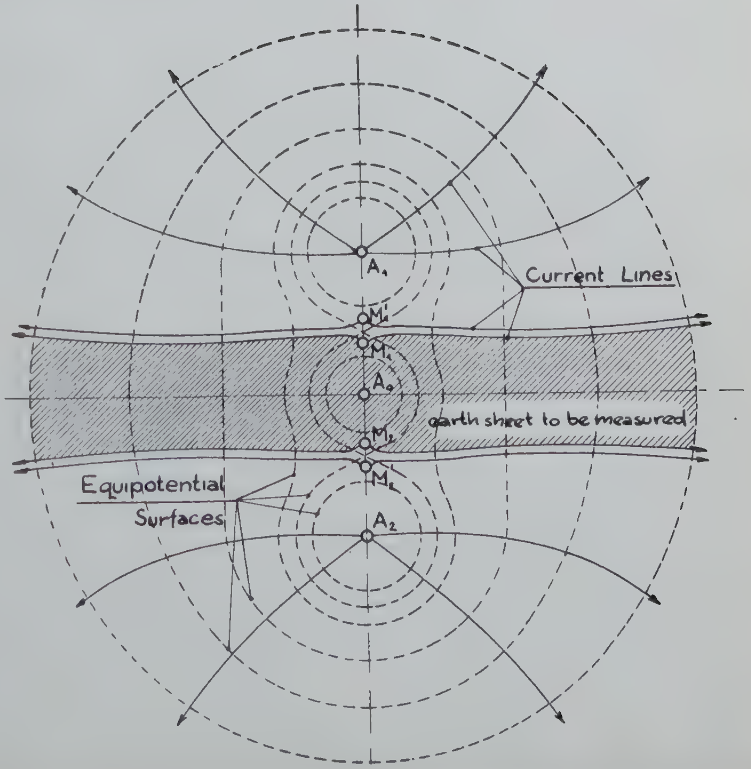
A₁
M₁'
M₁
A₀
M₂
M₂'
A₂
Current Lines
earth sheet to be measured
Equipotential Surfaces

Fig. 2

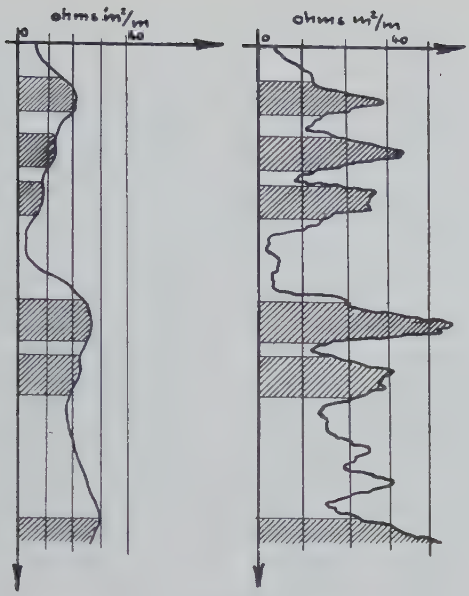

Fig. 3

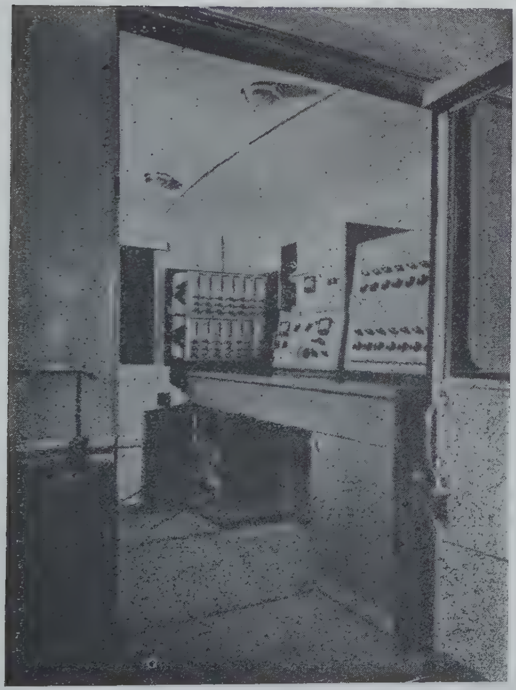

Fig. 4

with the aid of electronic amplifiers — seismic shockwaves propagating through miles of geological strata.

Beyond the revival, however, of classical physical phenomena, a number of new and characteristic *electronic transducers* have become widely used for measuring purposes. Among these are the *photomultiplier* in optics, the *GM-counters* in nuclear physics, new semiconductor-type transducers as *thermistors*, *photo-resistors* and *photo-transistors* as sensing elements for visible and thermal radiation, to mention but a few. Most of these transducers show a startling feature over the older ones, that is : they combine the sensing and amplifying function into one and the same element, thereby working at a great *power-gain* as against most "old-time" transducers which emparted a *power-loss* upon the quantity to be measured. The "efficiency" of ,,classic' transducers is always a quantity smaller than one, while these most recent electronic transducers operate at a considerable gain even before an additional amplifier is employed. Electron-multipliers with a sensitivy of 60 ampère pro lumen or thermistors and phototransistors, having only slightly smaller figures of merit — not to speak of the G-M tube with an inherent amplification of 10^6 — are good examples of how some of these electronic transducing elements perform.

The examples mentioned clearly show that electronics not only opened up a new perspective by its speed and sensitivity in conjunction with conservative sensing elements, but it also created new transducers which by themselves out-perform any of their "classical" predecessors by many orders of magnitude. It now remains for the scientists of our days to combine the stability and reliability of those older devices with the sensitivity and speed of action of their electronic successors. It is no secret that much has yet to be done in this direction in the interest of lasting precision and reliability of measurement.

Certain results are scored in this respect by the development staff of our instrument industry, which is steadily growing more "electronics-conscious". In addition to the large size electronic instruments' factory ORION, the Geophysical Instruments' Factory and a score of smaller specialized manufacturers are engaged exclusively in the advancement of the electronic art. Electronics is also at the same time rapidly infiltrating into most other instrument factories — be it in the shape of automatic electronic potentiometers or of electronic surface roughness testers. The greater part of our *Industrial Institute of Instrument Research* is engaged in electronic circuit development and their work is complemented by electronic instrument research made at the *Telecommunication Research Institute*, the *Geophysical Institute* and the *Central Physical Research Institute* of our Academy[6]. The development and research of new transducers for electronics is the primary task of the Academic *Institute for Measurement and Instrumentation*, and certain results in the field of thermistors[7] magnetostrictive torque-transducers and new photomultiplier applications[8] can here be registered.

With so great an effort to keep abreast with the pace of world progress in electronic instrumentation, the training of specialists, obviously, becomes a central problem. It was with this in mind that a special *Electronic Instruments' Branch* was set up within the Instrument Department of our Electrical Faculty. The coming years will show how well the training in general instrumentation and the specialized courses and projects in instrument electronics will be combined to furnish the highly qualified yet universally trained specialists fit for one of the various diverse tasks to be done.

Electron-optical instruments

Without in any way attempting completeness, another important class of electronic instruments should not escape our attention. Beyond the application of circuit-technique and electronic transducers, modern scientific instrumenation is coming to use an ever greater variety of large measuring devices in which the *wave-nature* of accelerated electrons play an important role. We refer here to the wide application of electron optics in such devices as the *electron microscope*, the *electron-diffractograph* or the *microfocus X-ray tube* — instruments yielding data on the submicroscopic structure of materials not obtainable by any other method. Intramolecular spacing of crystal lattices in the order of one angström-unit can, for example, be measured to four decimals. Let us not forget, furthermore, that various kinds of electron accelerators for generating high energy radiation — the *betatron*, *synchrotron* and *synchro-cyclotron* — are also special cases of applied electron optics. Briefly mentioning a few representatives of this important class of electronic instrumentation only serves to round out the picture aimed at by the present review and to prove — should such a proof still be required — how universal a research tool electronics has become in modern science.

Conclusions

The appearance of electron tubes and semiconductors in experimental physics marks — as we have shown — an important milestone in the development of new tools for nvestigating the processes of nature and of technology, as well as for influencing and controlling them. The revolutionary impact of electronics on modern instrumentation has caused a quite sudden „discontinuity" in the orders of magnitude in which man to-day can conveniently obtain data, not only of unbelievably small values of voltage or current, but also those of time and space as well as of most other variables known to physics. The exact scientist whose task it is: "To measure everything measurable and to render measurable all that cannot yet be measured" — has truly received a powerful new tool and it can be safely predicted that electronics will in its daily progress hardly leave any part of experimental science untouched by its magic wand.

In order to meet this challenge, instrument engineers have to join hands with electronic specialits everywhere — and this is also true in our country where a healthy start has been made both in industry and scientific research. Our great traditions of some outstanding past accomplishments in instrumentation and in electronics commit us to a forward looking, high level educational program for training young engineers capable of keeping abreast with world progress.

LITERATURE

1. Condon, E. U.: Is there a science of instrumentation? *Science* **110**. 339. (1949).
2. Wildhack, W. A.: Instrumentation in perspective. *Science* **112**. 515. (1950).
3. Trimmer, J. D.: Instrumentation and cybernetics. *Sci. Mon.* **69**. 328. (1949).
4. Striker, G.: The place of instrumentation in the system of sciences. (In Hungarian.) *Mérés és Automatika* **4**. 289. (1956).
5. Doll, H. G.: The Laterolog: a new resistivity logging method with electrodes using an automatic focusing system. *Petroleum Trans. AIME* **192**. 305. (1951).
6. Náray, Zs.: On the reduction of the dark current of photomultipliers. *J. Sci. Instr.* **33**. 476. (1956).
7. Haas A.: Analytische Untersuchung einer automatischen Temperaturkompensationsmethode bei Messdosen, die in unausgeglichenen Wheatstone'schen Brücken angewendet werden. *ATM* 260. (1957) P. R 89—R 92.
8. Striker, G.: Ultra-photometer using magnetically modulated photo-multiplier. *Acta Technica Hung.* under print.

A kiadásért felel az Akadémiai Kiadó igazgatója
Műszaki felelős: Farkas Sándor
A kézirat nyomdába érkezett: 1957. IX. 16. — Terjedelem: 8,50 (A/5) ív, 57 ábra

43399/57 — Akadémiai Nyomda, Budapest. V., Gerlóczy u. 2. — Felelős vezető: Bernát György

Instruments for laboratories and research institutes
Measuring instruments for the textile industry
Instruments for power-plant control
Medical and surgical instruments
Medical and surgical apparatus
Electric measuring instruments
Medical and dental furniture
Electro-medical apparatus
Electronic instruments
Veterinary instruments
Geodetic instruments
Dental supplies
Ampoules

Exporters :

METRIMPEX

Hungarian Trading Company
for Instruments
Letters : Budapest 62.
P. O. B. 202
Telegrams : Instrument
Budapest

Metrimpex

M

Electronic measuring instruments
for all branches of science and industry

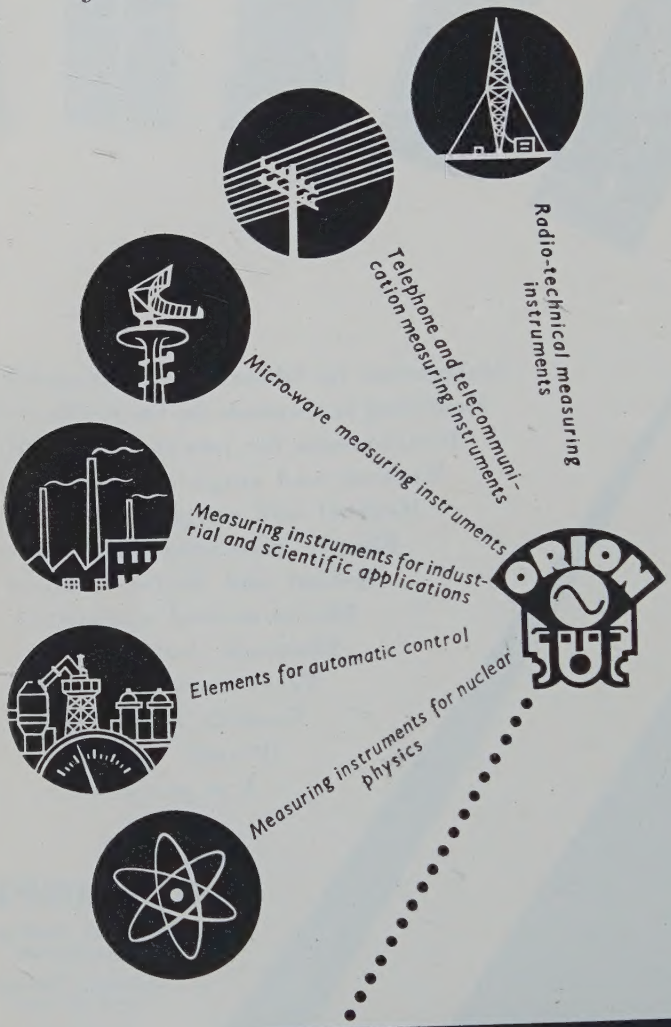
Radio-technical measuring instruments
Telephone and telecommunication measuring instruments
Micro-wave measuring instruments
Measuring instruments for industrial and scientific applications
Elements for automatic control
Measuring instruments for nuclear physics
ORION

EXPORTERS:

METRIMPEX

HUNGARIAN TRADING COMPANY FOR INSTRUMENTS
LETTERS: BUDAPEST 62, P. O. B. 202.
TELEGRAMS: INSTRUMENT BUDAPEST

A Budapesti Műszaki Egyetem Periodica Polytechnica címen idegen nyelvű tudományos folyóiratot indított. A folyóirat három sorozatban — vegyészeti, villamossági, valamint gépész- és általános mérnöki sorozatban — jelenik meg, évente négyszer, sorozatonként egy-egy kötetben. Az egyes kötetek terjedelme 14—18 ív.

A Periodica Polytechnicában megjelenő tanulmányok szerzői az Egyetem tanári karából és tudományos dolgozóiból kerülnek ki. Főszerkesztő Dr. Csűrös Zoltán egyetemi tanár, akadémikus.

A folyóirat előfizetési ára sorozatonként és kötetenként 50,— Ft. Megrendelhető az Akadémiai Kiadónál (Budapest 62, Postafiók 440. NB. egyszámlaszám: 05-915-111-44), a külföld számára pedig a Kultúra Könyv és Hírlap Külkereskedelmi Vállalatnál (Bp. 62, Postafiók 149. NB. egyszámlaszám: 43-790-057-181), illetve a vállalat külföldi képviseleteinél és bizományosainál.

INDEX

RÁCZ, I.: Transiente Vorgänge in Doppelkäfigmotoren, I. 215

CSÁKI, F.: Effect of the Spark-gap Working Time upon the Short-circuit Currents in Circuits Containing Series Capacitor 233

SIMONYI, K. and UZSOKY, M.: About the Star-like Fusion Reactor 243

BÁRÁNY, N.: Continuous Image-forming Systems of Large Field of Vision (Telescopes) 259

BIHARI, I. and KELEMEN, M.: Explanation of the so-called "Sound Detonation" 287

ANTAL, J. and KŐNIG, A.: New Acoustical Method of Vacuum Measurement 297

Book Review — Buchbesprechung 301

Industrial Review — Aus der Industrie 303